leti
innovation for industry

Annual Research Report 2013

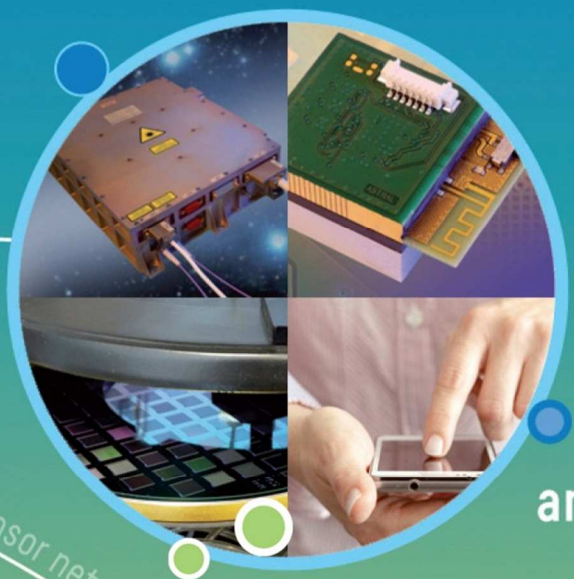

Power electronics

Energy

Electronic systems

Sensing

Wireless sensor networks

Systems and Solutions Integration

Signal processing

Security

Wireless communications

Telecom

DE LA RECHERCHE À L'INDUSTRIE
cea

Annual Research Report 2013

Systems and Solutions Integration

Leti is an institute of **CEA**, a French research-and-technology organization with activities in energy, IT, healthcare, defence and security.

By creating innovation and transferring it to industry, Leti is the bridge between basic research and production of micro- and nanotechnologies that improve the lives of people around the world.
Backed by its portfolio of 2,200 patents, Leti partners with large industrials, SMEs and startups to tailor advanced solutions that strengthen their competitive positions. It has launched more than 50 startups. Its 8,000m² of new-generation cleanroom space feature 200mm and 300mm wafer processing of micro and nano solutions for applications ranging from space to smart devices. Leti's staff of more than 1,700 includes 200 assignees from partner companies. Leti is based in Grenoble, France, and has offices in Silicon Valley, Calif., and Tokyo.

Visit www.leti.fr for more information

Systems and Solutions Integration research activities are mainly devoted to Telecommunications, Internet of Things and Power Management Systems. These activities include the design and development of fixed or nomadic devices and sensor networks with embedded power management, energy harvesting, sensors, data and information processing, RF communications and security functions. The R&D works are performed with academic or industrial partners with the strategic objective to improve the next generation of industrial products thanks to the integration of emerging nanotechnology techniques. Industrial partners range from SME to large international companies. Typical internal equipments are available to partnership R&D works such as RF Anechoic Chamber, Information Technology Security Evaluation Facility, Magnetometers Test Facility, and a Students Platform for Industrial Innovation.

Contents

Edito

Roland Blanpain
Head of Systems and Solutions
Integration Division

Few years ago, CEA-LETI decided to focus drastically on SMI/SME support for innovation and technological transfer. The objective was, when relevant, to enrich or to upgrade future industrial products with advanced electronic functions to boost industry. DSIS Division was created at CEA-LETI to coordinate this action in the field of Technologies for Information and Communication and Energy Management.

Based on MINATEC Campus in the Laboratory for Electronics & Information Technology (CEA-LETI), the Systems and Solutions Integration Division is today offering a large spectrum of technological solutions to foster the industry competitiveness. To propose such innovative capabilities, relevant research projects have to be raised and achieved. This document will introduce you on basic technological bricks investigated in the DSIS Division, sometimes in collaboration with other Leti or CEA laboratories or with external partnership.

Of course, a large part of research in Information and Communication technologies is devoted to new wireless transmission techniques. These works cover a large spectrum of our future daily life such as cellular networks, indoor communications, short range high data rate radio links but also contactless systems and more recently new relevant and efficient use of the old analog TV frequency bands.

A second key point is to provide technologies for miniaturized, efficient and smart sensors. This domain includes both conceptual physical approach and smart integrated interface chips in order to deliver solutions close to industrial requirements.

Finally, the most emerging and promising works are dedicated to energy management, including improvement of global efficiency and environmental preserving aspects. Beyond the mandatory energy management for both the future electrical vehicle and the smart grid, this strategic area unveils new energy harvesting solutions for nomadic devices.

Key Figures

136 permanent researchers
27 PhD students and post-docs
38 short-term contracts

21 M€ budget
90% external funding

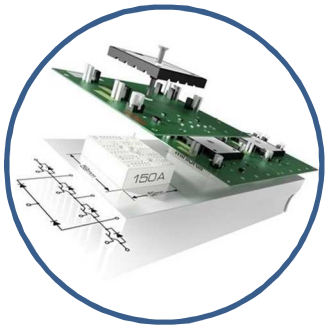

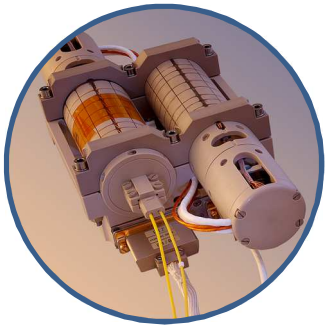

46 patents granted in 2013
350 patents portfolio
24 book chapters and journals
99 conferences and workshops

Technical facilities:
3 anechoic chambers
Magnetometer test ground
Information Technology Security Evaluation Facility (ITSEF).

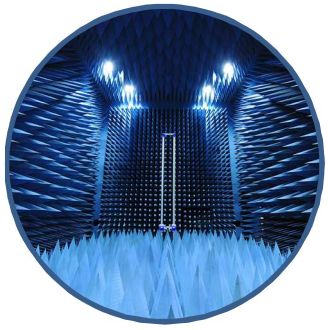

3 new common laboratories
2 start-ups created in 2013 (Primo1D, ISKN)

Scientific activity

Publications

123 publications in 2013, including book chapters, journals and top conferences like GLOBECOM, TRANSDUCERS, NEWCAS, POWERMEMS, VTC, ESSCIRC, PIMRC, FuNEMS.

Prize and Awards

Best paper award: B. Mawlawi, "*Les formes d'ondes avancées de signaux, la prise de décision et la mise en œuvre des systèmes de radio cognitive", COST action IC0902, Feb. 2013.*

C. Godin, FIEEC 2013 3rd prize for her work on motion capture.

Experts

20 CEA experts.
6 researchers with habilitation qualification (to independently supervise doctoral candidates).

Scientific Committees

Participation to Technical Programs and Steering Committees in major conferences and international bodies: JNM, COSADE, ICUWB, BodyNETS, ICCVE, Globecom, ICC, GreenCOM, CrownCom, VTC, Winncom, PIMRC, IEEE RFID, COST IC1004, MEMSWAVE, ICT, IEEE DYSPAN-SC, IEEE P1900.6, IEEE P1900.7, White Space Summit.

Conferences and Workshops organizations

i-RISC Workshop on Innovative Reliable Chip Designs from Unreliable Components, CLEEN 2013, WDN-CN 2013, EuroMicro DSD special session on Flexible Digital Radio, TV White Space Summit.

International Collaborations

Univ. La Sapienza (Italy), Univ. Di Bologna (Italy), Univ. Milano (Italy), Univ. Catholique de Louvain (Belgium), VTT (Finland), IISB Fraunhofer (Germany), CSEM (Switzerland), SupCom Tunis (Tunisia).

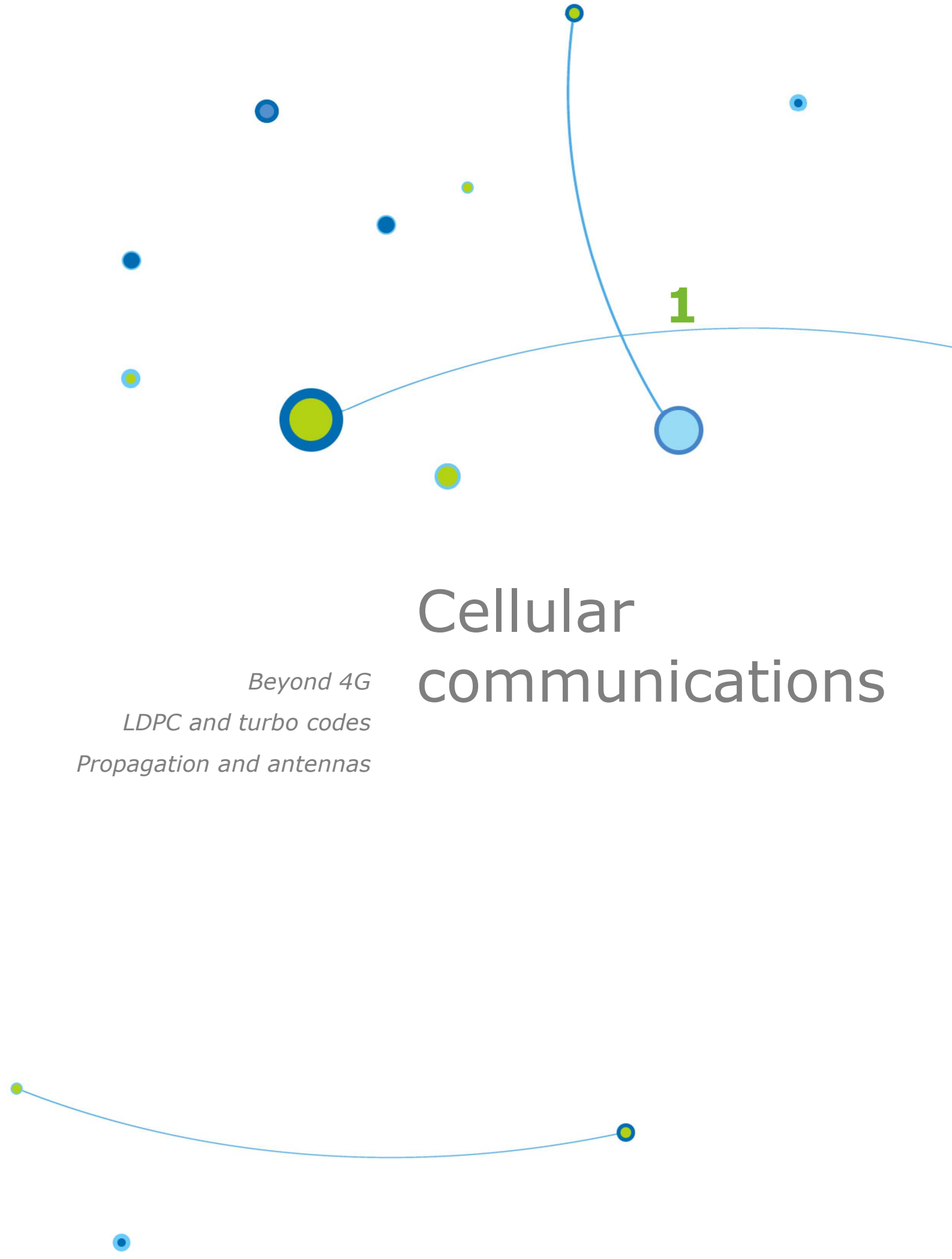

1

Cellular communications

Beyond 4G

LDPC and turbo codes

Propagation and antennas

Blind identification of the uplink scrambling code index of a WCDMA transmission and application to femtocell networks

Research topics : mobile communications, detection, decoding

M. des Noes, V. Savin, L. Ros, J.M. Brossier

ABSTRACT: Interference between macro and femtocells is an important issue for the development of WCDMA femtocell networks. More specifically, the uplink signal of a macro User Equipment may generate an unacceptable level of interference at the femto Base Station. An algorithm which performs a blind identification of the uplink scrambling code index of a WCDMA transmission is proposed in this article. This gives the possibility to implement interference cancellation algorithm at the femto BS.

The development of femtocell networks is an important perspective for increasing cellular systems capacity. A femtocell is covered by a small Base Station (BS), designed for typical indoor environments (home, business) which do not require a coordinated deployment. In this paper, an algorithm which estimates blindly the uplink scrambling code index of a User Equipment (UE) is proposed. It offers the perspective of implementing interference mitigation techniques at a femto Base Station (BS), and hence providing a solution to the problem of uplink macro to femto interference issue in WCDMA femtocell networks.

A macro UE transmits at high power because it is either at the cell edge or inside a building. Since the power control procedure concerns only the uplink with the macro BS, it will be received at the femto BS with a power much larger than the power of a femto UE. This is the well-known near-far effect in CDMA systems. If the power of this interferer is too large, the femto BS may not be able to demodulate any communication with its attached UEs. This creates a "dead zone" in the network coverage. In order to avoid this situation, it is required to implement interference mitigation techniques. All the proposed techniques exploit the knowledge of the UE's scrambling code, which is chosen from a set of scrambling codes identified by their index.

The scrambling code index of the macro UE is allocated by the macro BS and is signaled to the UE in a dedicated control channel. Unfortunately, in a closed access mode, there is no signaling link between the macro and femto BSs. Hence, a femto BS has no knowledge of the scrambling code index of an interfering macro UE. It has to estimate this index blindly. Given the signal transmitted in the UL (Fig.1), the objective is thus to estimate the scrambling code Sn.

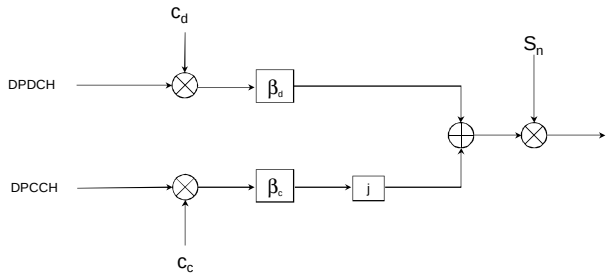

Figure 1: Uplink spreading and modulation.

It is generated using 2 m-sequences y and x. The index is given by the state of the registers of sequence x at the beginning of each frame.

In order to identify this index, the proposed algorithm exploits the a-priori knowledge of the initial state of the sequence y at the beginning of each frame (all '1').

The algorithm is split in 3 steps:

1. Chip level processing which results in a direct observation of a modified version of the sequence x.
2. Estimation of the initial shift registers state of this sequence with an iterative message-passing decoder.
3. Determination of the initial state of the sequence x with the use of a transposition matrix. This exploits the decimation and "add and shift" properties of m-sequences.

Figure 2 shows the probability of missed detection as a function of the input SNR, for different length of the vector entering the decoder. The ability to estimate the scrambling at a SNR as small as -6 dB is sufficient to detect a strong interferer and cancel its destructive influence. It was also found that the algorithm is also almost insensitive to false alarm. Simulations over 10^7 frames did not produce any false alarm. This means that $P_{FA} < 10^{-6}$ with a good confidence level. This kind of processing has also been applied to the uplink of the CDMA2000 system [2].

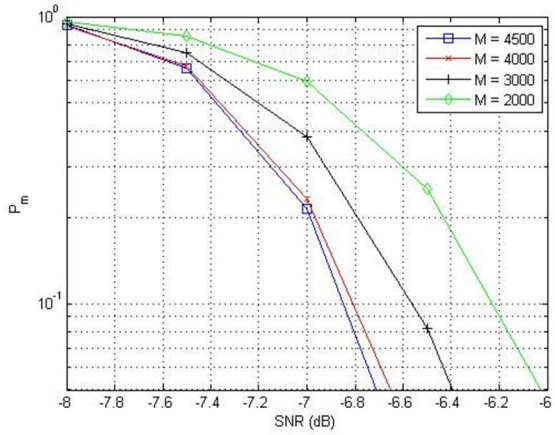

Figure 2: Probability of missed detection- influence of the decoding vector size (AWGN channel).

Related publications:
[1] M. des Noes, V. Savin, L. Ros, J.M. Brossier, "Blind Identification of the Uplink Scrambling Code Index of a WCDMA Transmission and Application to Femtocell Networks", IEEE Int. Conf. on Communications (ICC), Budapest, Hungary, 9-13 June 2013.
[2] M. des Noes, V. Savin, L. Ros, J.M. Brossier, "Blind Identification of the Scrambling Code of a Reverse Link CDMA 2000 Transmission", IEEE Int. Conf. on Communications (ICC), Budapest, Hungary, 9-13 June 2013.

Time and frequency synchronization for cooperative multipoint transmission with filter bank multicarrier

Research topics : mobile communications, 5G, non-orthogonal waveforms

N. Cassiau, J.-B. Doré, D. Kténas

ABSTRACT: Filter Bank Multicarrier (FBMC) is a multicarrier modulation technique characterized by a prototype filter that can be optimized either in time or in frequency. FBMC is often referred as a non-orthogonal modulation technique as symbols overlap in the time domain and as adjacent subcarriers overlap in the frequency domain. In cellular systems, Multi-User (MU) downlink cooperation between cells (CoMP) enables to provide a good quality of service to cell edge users while maintaining a high spectral efficiency in the system. For MU-CoMP, time and frequency synchronization between cooperating Base Stations (BSs) and the User Equipment (UE) is a crucial mandatory step. In this study, where synchronization for CoMP with FBMC is considered, it is demonstrated that the UE can robustly estimate very large delays and arbitrarily high carrier frequency offsets. The correction of the delays requires only few bits of feedback and the correction of the frequency offset can be entirely realized at the UE side. These results demonstrate that FBMC is a suitable technique for DL CoMP cellular systems.

FBMC is a multicarrier modulation technique that was first investigated in the 1960s, prior to OFDM. Today FBMC, which computational complexity is higher than OFDM, is experiencing renewed interest, due to a significant increase in the processing capacity of electronic devices. The FBMC prototype filter can be designed with great flexibility to match time or frequency dispersive channels or to cope with implementation constraints related to standards (e.g. frequency mask). Subcarrier filters can be for example designed with arbitrarily low secondary lobes, making FBMC a good candidate for multiple access communications or opportunistic spectrum access (TV White Space applications). Furthermore, contrarily to OFDM, FBMC symbols and subcarriers are structurally non orthogonal, inherently bringing some advantages to this technique: there is no need for a Cyclic Prefix (CP) - the spectral efficiency of the system is hence greatly improved - and synchronization processes are somewhat relaxed.

There has been a significant interest towards Multi-User cooperative MultiPoint (MU-CoMP) techniques for fourth generation cellular systems and beyond [1] where UEs on the edge of cells are served by several BSs. In such cooperative schemes, a crucial issue is the synchronization between the UE and the serving BSs.

Time and frequency synchronizations for Downlink CoMP with FBMC were investigated in this study [2]. The system model is described in Figure 1.

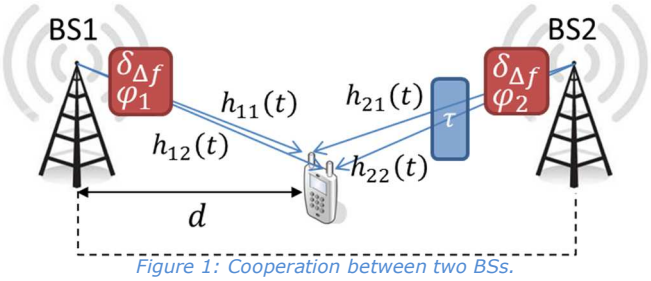

Figure 1: Cooperation between two BSs.

The whole system forms a virtual 2x2 MIMO transceiver. The two BSs transmit in the same time and frequency resources. The signal from BS2 is received at the UE with a delay τ compared to the signal from BS1, reflecting the over-the-air propagation delay. The UE is assumed synchronized in time with BS1. BS1 and BS2 are assumed synchronized in frequency but not in phase. The Carrier Frequency Offset (CFO) $\delta_{\Delta f}$ between the BSs and the UE is normalized to the carrier spacing Δ_f.

A method with low computational complexity was derived for estimation of CFO values lower than $0.5\delta_{\Delta f}$. Simulations run with the system presented on figure 1, with a delay $\tau > 0$ and $\varphi_1 \neq \varphi_2$ showed that the proposed estimation is very accurate and robust.

A complementary method for estimating the 'entire part' of CFOs higher than $0.5\Delta_f$ in the frequency domain has also been developed. Given a well-designed preamble, any CFO can then be estimated and corrected at the receiver.

Concerning time synchronization, an algorithm for the estimation of the delay at the UE was proposed. It is based on the estimation of the time response of the channel. Performance results show that delays up to 230 time samples (more than 4400 ms) can be estimated with almost both null false alarm and miss detection probabilities. The proposed algorithm requires only few bits of feedback from the UE to the BSs for correction.

Figure 2 shows the proposed chronology of operations to be realized for the synchronization of the BSs and the UE.

Figure 2: Chronology of the synchronization process.

This study has proven that FBMC, thanks to the very good frequency localization of its carriers and to its overlapping structure, is well suited for downlink CoMP transmissions.

Related publications:
[1] G. Wunder et al., "5GNOW: Challenging the LTE Design Paradigms of Orthogonality and Synchronicity", 2013 IEEE 77th Vehicular Technology Conference (VTC 2013 Spring), June 2-5, 2013, Dresden, Germany.
[2] N. Cassiau, J.-B. Doré, D. Kténas, "Time and frequency synchronization for Cooperative Multipoint with Filter Bank MultiCarrier", 10th Int. Symp. on Wireless Communication Systems (ISWCS 2013), August 27–30, 2013, Ilmenau, Germany.

Enabling green cellular networks: a survey and outlook

Research topics : mobile communications, green IT

A. De Domenico, E. Calvanese Strinati, A. Capone

ABSTRACT: Today, green communication is one of the main design goal of future mobile networks and current research aims to enable sustainable growth of broadband wireless infrastructure. This paper has provided an analysis of the models proposed in literature to evaluate the energy efficiency of current wireless architectures. We have presented green metrics that have been used and theoretical trade-offs that have been investigated. Finally, following a proposed classification, we have presented and critically discussed energy efficiency enablers recently proposed by the wireless research community.

Traditionally, in cellular systems a quite remarkable research effort has been devoted to the improvement of energy efficiency of User Equipments (UEs), in order to enhance their battery lifetime. The mobile communications research community has recently extended its attention towards energy efficient operation at the Base Station (BS) side. Actually, while mobile terminals consume around 10% of the energy consumed by BSs, BSs contribute for around 60% to 80% of the whole cellular network energy consumption. By deploying low-power access nodes, such as small cells and relays, Mobile Networks Operators (MNOs) aim at satisfying the ever-growing demand for data traffic and reducing the energy consumption by shortening the distance between the end-users and the serving Access Point (AP).

From one side, to evaluate the effects of novel enabling mechanisms and architecture for energy saving, it is important to understand the impact of the BS components on the aggregate energy consumption. The Energy Efficiency Evaluation Framework described in [1] can be used to map the radiated RF power to the power supply of a BS site and underlines the relationship between the BS load and its power consumption.

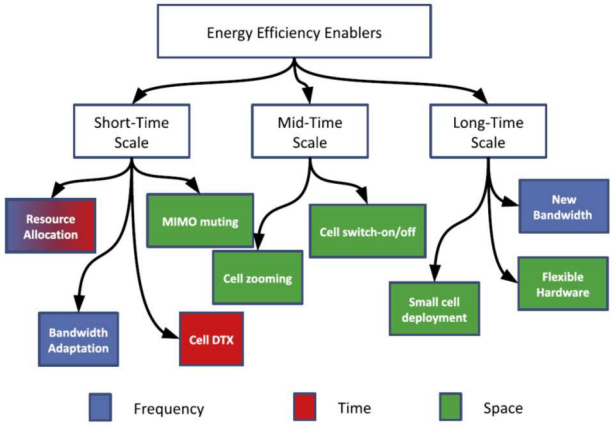

Figure 1: Energy efficiency enablers classification.

From the other side, it is necessary to evaluate the fundamental trade-offs that are the theoretical basis for optimizing the wireless system performance with respect to the energy consumption. Future wireless networks require enabling mechanisms/hardware, which exploit the green trade-offs to improve the network sustainability (Fig. 1). These approaches allow the cellular network to adapt its characteristics to load variations and avoid energy wastage while ensuring end-users quality of service (QoS). Then, a first classification of such enabling technologies can be made by observing the timescale, in which they operate.

Fast adaptation mechanisms are implemented in short-time scales (from milliseconds to seconds) to reply to fast changes due to mobility, cell load, and wireless channel conditions. Slower schemes operate on a per-hour basis in order to adapt the network characteristics to the traffic daily variations (Fig. 2). Moreover, additional flexible hardware/software can be integrated in the system in a longer time scale (weeks to months) to improve the network capacity in a more sustainable way.

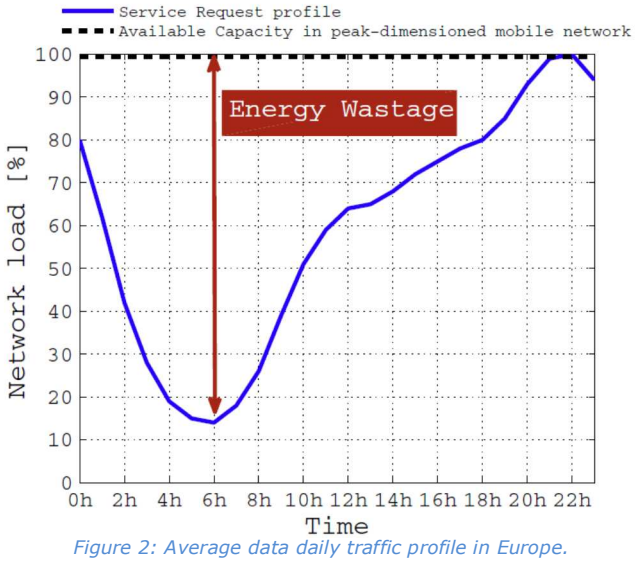

Figure 2: Average data daily traffic profile in Europe.

Related publications:
[1] A. De Domenico, E. Calvanese Strinati, A. Capone, "Enabling Green cellular networks: A survey and outlook", Computer Communications, Volume 37, December 2013, Pages 5-24.

A backhaul-aware cell selection algorithm for heterogeneous cellular networks

Research topics : mobile communications, heterogeneous networks, small cells

A. De Domenico, V. Savin, D. Kténas

ABSTRACT: This paper considers heterogeneous cellular networks, where cluster of small cells are deployed to create local hot spots inside the macro cell. In the past, most of the research in this topic has focused on mitigating inter-cell interferences; however, wireless backhaul has recently emerged as an urgent challenge to enable ubiquitous broadband wireless services at small cells. Hence, we propose a novel cell selection framework, which associates users and heterogeneous access nodes to improve the efficiency in the overall radio and backhaul resource utilization while at the same time avoiding load congestions.

Small cell eNBs (SCeNBs) will likely be deployed at about 3-6 meters above the street level (on street furnitures and building facades) to improve the system coverage. At these locations, installing fixed broadband access for backhaul or Line-Of-Sight (LOS) based microwave links may be too expensive. Hence, in a given area, different small cells will be characterized by heterogeneous backhaul connections, with respect to physical design (wired/wireless), capacity, latency, and topology. Solutions that jointly optimize the Radio Access Network (RAN) and the backhaul network are required to offer ubiquitous support for broadband mobile services [1]. In this paper, we have focused on backhaul-aware cell selection mechanisms for Heterogeneous Networks (HetNets). In current systems, a User Equipment (UE) selects the eNB associated to the strongest Received Power (i.e., SINR) [2].

Recently, researchers have investigated joint cell association and resource allocation to achieve fair load balancing in HetNets. To the best of our knowledge, there is a lack of solutions that investigate cell selection in scenario where the Radio Access Network (RAN) can be constrained by the backhaul network.

In this paper, we first propose load-aware cell selection mechanisms that jointly take into account the radio access and backhaul characteristics. Second, we analyze the joint impact of cell load, backhaul constraints, and resource allocation in the overall network capacity. Finally, we present and evaluate an innovative mechanism characterized by limited complexity and latency to enhance the HetNet performance by improving radio and backhaul utilization efficiency. Evaluation of the proposed scheme is provided through analytical derivations.

In particular, we have proposed and assessed an iterative algorithm characterized by limited complexity, which aims at enhancing the overall network capacity by optimizing the cell selection process.

This algorithm, named Evolve, starts from a given simple solution of the cell selection problem, and evolves towards a more beneficial association. At each step, it evaluates the possible changes in the current association, and then selects the strategy which increases the most the selected optimization metric (Fig. 1). As we will show in the following, the algorithm converges after a limited number of iterations.

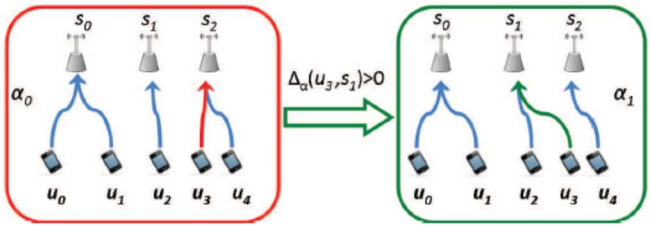

Figure 1: Evolve paradigm for managing UE-eNB association.

Figure 2 shows the CDF of capacity achieved by using Evolve and the classical approach with respect to different backhaul constraints. Simulation results show that Evolve results in 25% of gain (measured at the median value of the CDF) in all the investigated scenarios.

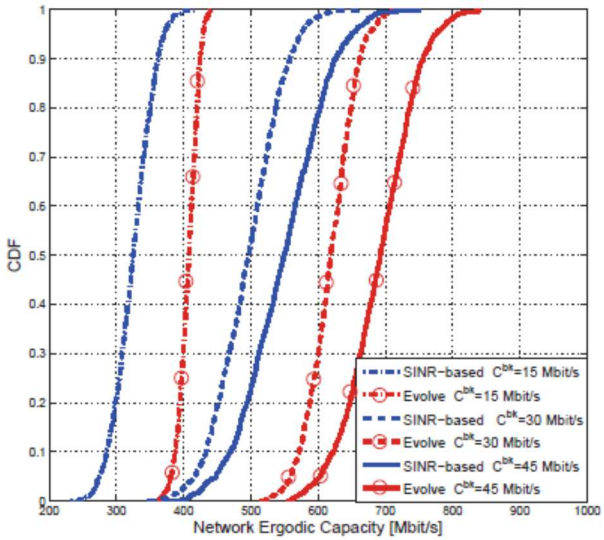

Figure 2: Cumulative distribution function of the Network Ergodic Capacity achieved by Evolve and the SINR-based algorithm with respect to different backhaul constraints.

Related Publications :
[1] P. Rost, CJ. Bernardos, A. De Domenico, M. Di Girolamo, M. Lalam, A. Maeder, D. Sabella, and D. Wübben "Cloud Technologies for Flexible 5G Radio Access Networks," IEEE Communications Magazine, vol. 52, no. 5, pp. 68-76, May 2014.
[2] A. De Domenico, V. Savin, and, D. Ktenas, "A backhaul-aware cell selection algorithm for heterogeneous cellular networks," 2013 IEEE 24th Int. Symp. on Personal Indoor and Mobile Radio Communications (PIMRC), pp.1688,1693, Sept. 8-11, 2013, London, UK.

Dynamic selection of cooperative links in location-enabled heterogeneous networks

Research topics : mobile communications, cooperative networks, wireless localization

S. Zirari, B. Denis

ABSTRACT: Modern wireless contexts comprise fixed heterogeneous resources and cooperative multi-standard Mobile Terminals (MT). One open challenge is thus to select in a decentralized way only the most informative and reliable peer-to-peer links to localize the latter MTs, while minimizing power consumption, latency and over-the-air traffic. Here, we consider improving existing selection criteria based on conditional theoretical performance bounds (but formerly suitable to static scenarios), by taking into account the velocity and the asynchronous location estimates of neighboring terminals. At each MT, one can predict in a reasonably short-term future the most relevant combinations of available range measurements with respect to neighbors over short-range links. We further couple the selection scheme with a decentralized and cooperative tracking filter.

Most indoor environments are endowed with heterogeneous wireless resources, such as WiFi Access Points (AP), Long Term Evolution (LTE) Femto-Base Stations (BS) and Wireless Sensor Networks (WSN). They are also contextually crowded by end-users, who are equipped with multi-standard Mobile Terminals (MT) with unprecedented short-range cooperation capabilities. In such environments, the location information has been identified as a key enabling feature for improved users' connectivity experience or personal navigation services. However, one challenge is to optimally combine those available sources of information in a parsimonious way, so as to limit power consumption, traffic, latency and computational complexity.

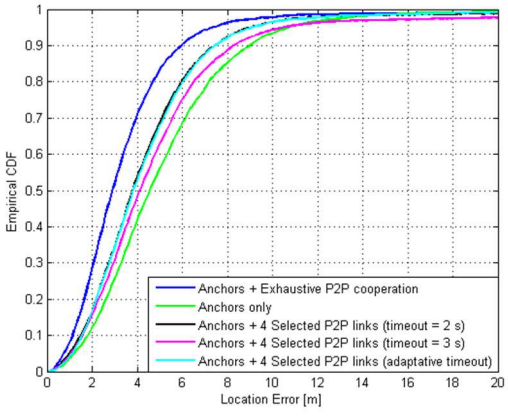

Figure 1: CDF of estimated location errors through distributed EKF with 4 selected neighboring MTs and various timeouts before refreshing neighborhood and selected links (incl. adaptive strategy).

In [1] for instance, cooperative localization has been investigated in a heterogeneous WiFi/Zigbee indoor context, where located MTs could broadcast their own estimated positions to help non-located MTs during the steady-state positioning stage. Different link selection strategies have been compared in dynamic simulated scenarios, but still relying on static criteria (i.e. conditional Cramer Rao Lower Bounds (CRLB) characterizing positioning accuracy). The obtained results have shown unexpected degradations through cooperation, mostly due to the wrong static assumption. One main reason is that the exchanged coordinates integrated in the performance indicator can vary significantly between the time when they are estimated and the time when they are asynchronously transmitted.

In [2], a novel intuitive solution has thus been figured out so as to integrate the estimated locations and velocities of cooperative neighboring MTs, relying on a time-dependent CRLB formulation. This new dynamic indicator can be used also to predict the life-time of optimal sets of peer-to-peer links. Accordingly, the sounding of MT's neighborhood can be adaptively and contextually refreshed, depending only on the targeted application accuracy and on the instantaneous connectivity conditions (see Fig. 1). This selection scheme has been coupled with a decentralized tracking filter (EKF) at each MT, showing reasonable sensitivity to the real velocity errors integrated in the time-dependent CRLB predictions (see Fig. 2). Even more recently, these algorithms have been also validated in a jointly cooperative and heterogeneous context involving real Impulse Radio - Ultra Wideband (IR-UWB) and Zigbee radio platforms [3].

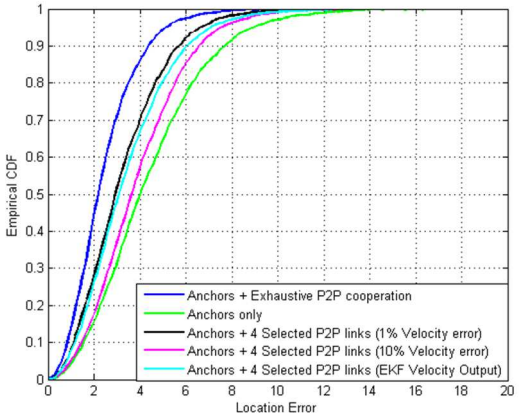

Figure 2: CDF of estimated location errors through distributed EKF with 4 selected neighboring MTs vs. relative velocity errors integrated in CRLB prediction.

Related Publications:
[1] S. Zirari, B. Denis, "Comparison of Links Selection Criteria for Mobile Terminal Positioning in Cooperative Heterogeneous Networks", in 20th Int. Conf. on Software, Telecommunications and Computer Networks (IEEE SoftCOM'12), Split, Croatia, Sept. 11-13, 2012.
[2] S. Zirari, B. Denis, "Velocity-Based CRLB Predictions for Enhanced Cooperative Links Selection in Location-Enabled Mobile Heterogeneous Networks", 10th Workshop on Positioning, Navigation and Communication (WPNC'13), Dresden, Germany, March 2013.
[3] B. Denis, et al., "Assessment of Cooperative and Heterogeneous Indoor Localization Algorithms with Real Radio Devices", to appear in 2014 IEEE Int. Conf. on Communications (ICC'14), Advances in Network Localization and Navigation (ANLN) workshop, Sydney, Australia, June 10-14, 2014.

Design of min-sum-based LDPC decoders using imprecise arithmetic

Research topics : LDPC codes, low-power decoders, imprecise arithmetic

C. L. Kameni Ngassa, V. Savin, D. Declercq

ABSTRACT: This work evaluates the robustness of Low-Density Parity-Check decoders against errors due to imprecise arithmetic. While the use of imprecise arithmetic is motivated by savings in energy, delay and area, it also causes errors during the decoding process. We design imprecise arithmetic operators and investigate their use within several Min-Sum-based decoders. We show that all decoders are able to provide error protection, but most of them suffer a performance penalty compared to the exact arithmetic implementation. Remarkably, the Self-Corrected Min-Sum decoder incurs no performance penalty when imprecise arithmetic is used.

In order to support the sustainable development of future communication systems, energy efficiency became one of the most important issues to be addressed. Forward error correction (FEC) codes have been key components to design reliable communication systems. Nowadays, there is an increased interest in shorter range communications, from a few meters to a few millimeters. In this context, power consumption of the FEC decoder module is often a bottleneck, as it can require an important part of the processing power, or even more power than the receiver can supply.

To trade the accuracy of the circuit for the power consumption, imprecise circuits, obtained by pruning the exact circuit, are used. This amounts to removing a certain number of logic gates from the circuit, which may result in significant savings in energy, delay and area. Imprecise arithmetic proved to be particularly useful for applications from the domain of image and video processing. This work [1] investigates the robustness of FEC decoders against errors due to imprecise arithmetic. This is a new paradigm in coding theory, which traditionally assumes that the operations of FEC decoders are exact, and errors can only be introduced by the channel. While the use of imprecise arithmetic is motivated by savings in energy, delay and area, the first question we have to answer is whether or not FEC decoders are able to provide reliable error protection when they operate on imprecise hardware. We focus on Low-Density Parity-Check (LDPC) codes and evaluate the performance of several Min-Sum-based LDPC decoders using imprecise arithmetic operators. While the performance penalty due to imprecise arithmetic depends on the considered decoder, we show that the Self-Corrected Min-Sum decoder is inherently robust, and does not suffer any performance penalty due to imprecise arithmetic.

To design imprecise arithmetic components, we suppress several logic gates from all the adders and in the comparators of the circuit. However, the objective is to control the errors introduced by pruning the circuit, hence some constraints might be defined according to the desired level of errors.

For adders, first we require that the changes to the exact circuit do not impact the most significant (sign) bit. Protecting the sign of each addition from errors reduces the impact of the inexact circuit. Secondly, we require that for operands x and y, such that the value of the exact addition x + y is small, the error made by the imprecise adder when computing x + y must also be small (close to 0).

For comparators, for any two operands x and y, we allowed the output of the imprecise comparator to be in error only if x and y have relatively close values. The comparator's output is 1 if x < y.

For both arithmetic components, logic gates are suppressed starting from the LSB to the MSB until the suppression of any of the remainder logic gates will fail to comply with the requirements. Table I provides examples of imprecise additions and comparisons.

Table I: Example of arithmetic operations.

A	-29	-21	7	-31		A	-7	-1	-5	3
B	-27	-19	9	7		B	7	-3	-7	2
A+B	-24	-8	48	-56		A<B	1	1	1	1

Figure 1 shows the performance of Min-Sum-based decoders for the (2304, 1152) irregular quasi-cyclic LDPC code specify by the IEEE 802.16e (WiMAX) standard.

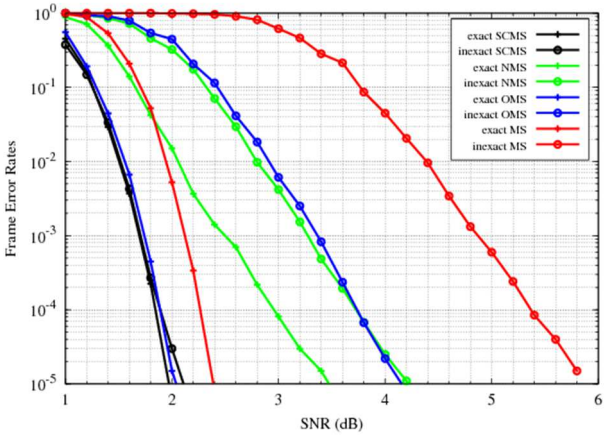

Figure 1: Frame Error Rate for the IEEE 802.16e code.

The simulation results show that all Min Sum (MS)-based decoders manage to provide error protection, but the imprecise arithmetic circuits significantly degrade their performance. On the contrary, the imprecise Self-Corrected Min-Sum proved to be robust to imprecise arithmetic circuits, due to its ability to detect unreliable messages during the decoding process. Hence, this work demonstrated that the SCMS decoder provides efficient error protection on devices with imprecise arithmetic circuits.

Related Publications :
[1] C.L. Kameni Ngassa, V. Savin, D. Declercq, "Design of Min-Sum-based LDPC decoders using imprecise arithmetic," IEEE Int. Conf. on Computer as a Tool (EUROCON 2013) pp.375-382, July 1-4, 2013, Zagreb, Croatia.

Min-sum-based decoders running on noisy hardware

Research topics : LDPC codes, low-power decoders

C. L. Kameni Ngassa, V. Savin, D. Declercq

ABSTRACT: This work investigates the behavior of the noisy Min-Sum decoder. We show that in some particular cases, the noise introduced by the device can actually result in an increased correction capacity with respect to the noiseless decoder. We also reveal the existence of a specific threshold phenomenon, referred to as functional threshold. To demonstrate the behavior of the noisy decoder, we first introduce a new error model approach and carry out the "noisy" density evolution analysis of the fixed-point Min-Sum decoding. Then, we determine the range of the signal-to-noise ratio values for which the decoder is able to achieve a target bit error rate performance. Finally, we evaluate the finite-length performance by Monte-Carlo simulation.

With the advent of nano-electronics, the reliability of the forthcoming circuits and computation devices is becoming questionable. It is then becoming crucial to design and analyze error correcting decoders able to provide reliable error correction even if made of unreliable components. Very recently, the characterization of the effect of noisy logic components on standard iterative LDPC decoders has been proposed but using only very simple error models, which emulate the noisy implementation of the decoder, by passing each of the exchanged messages through a noisy channel. In this work, we introduce new error models and focus on the Min Sum (MS)-based decoders, which are widely implemented in real communication systems.

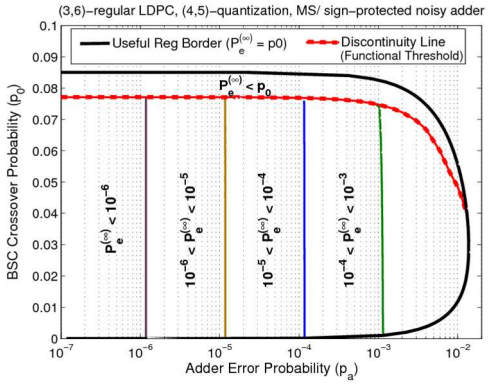

Figure 1: Asymptotic results over BSC channel.

In [1], we describe the probabilistic models for noisy adders, comparators and xor-operator, which are used to emulate the noisy implementation of the finite-precision MS decoder. The density evolution technique is performed under the independence assumption of exchanged messages, holding in the asymptotic limit of the code length, in which case the decoding performance converges to the cycle-free case. Due to the symmetry of the decoder, the analysis can be further simplified by assuming that the all-zero codeword is transmitted through the channel. In [2], we carry out the asymptotic analysis of the noisy MS decoder and provide the density evolution equations. We show that the decoder performance can be significantly improved by using an appropriate choice of the channel-output scale factor and provide the optimum values.

Noiseless decoders exhibit a threshold phenomenon, separating the region where the decoding error probability goes to zero, from that where it is bounded above zero. In case of noisy decoders, the decoding error probability does not always converge and may become periodic when the number of iterations goes to infinity. Besides, the decoding error probability is always bounded above zero if the adder is noisy since there is a non-zero probability of fault injection at any decoding iteration. Hence, a decoding threshold, similar to the noiseless case, cannot be defined anymore but we consider instead the notions of functional threshold, useful decoder and target error rate threshold [1]. The impact of each noisy component on the MS decoder performance are studied for the Gaussian channel [2] and for the binary symmetric channel [1,3]. Fig. 1 shows the asymptotic results obtained for a (3,6)-regular LDPC decoder over the BSC channel with only noisy adders.

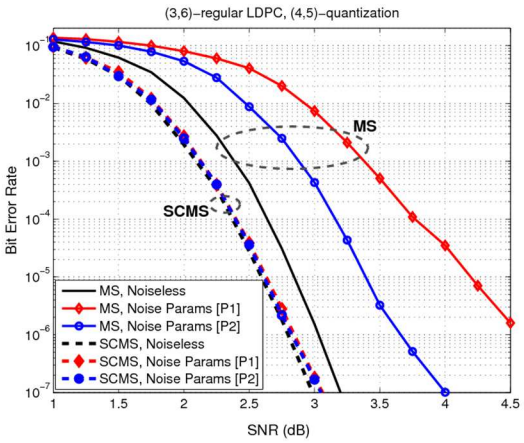

Figure 2: Bit Error Rate (BER) comparison between noisy MS and noisy Self-Corrected Min-Sum (SCMS) decoders over AWGN channel.

We corroborate the asymptotic analysis, through finite-length simulations using (3, 6)-regular LDPC codes. It can be seen (Fig. 2) that while the hardware noise alters the performance of the MS decoder, the noisy SCMS decoder exhibits very good performance. Therefore, one can think of the self-correction circuit as a noisy patch applied to the noisy MS decoder, in order to improve its robustness to hardware noise. The robustness of the SCMS decoder to hardware noise is explained by its intrinsic capability to detect and discard unreliable messages.

Related Publications:
[1] C.L. Kameni Ngassa, V. Savin, D. Declercq, "Analysis of Min-Sum based Decoders Implemented on Noisy Hardware", IEEE Information Theory and Applications Workshop, San Diego, CA, February 10-15, 2014.
[2] C.L. Kameni Ngassa, V. Savin, D. Declercq, "Min-Sum-based decoders running on noisy hardware," IEEE Global Communications Conference (GLOBECOM), Atlanta, GA, December 9-13, 2013.
[3] C.L. Kameni Ngassa, V. Savin, D. Declercq, "Analysis of Min-Sum based Decoders Implemented on Noisy Hardware", Asilomar Conference on Signals, Systems and Computers (Asilomar), Monterey, CA, USA, November 3-6, 2013.

Distributed turbo coding techniques with HARQ at relays for LTE-A

Research topics : turbo-codes, relay, LTE-A

L. Maret, D. Kténas

ABSTRACT: Advanced relaying concepts that enhance capacity on top of coverage need to be investigated in future releases of LTE-Advanced. In this context, the challenge of our work is to design novel distributed HARQ (Hybrid Automatic-Repeat-on-Request) protocols for cooperative transmissions. The analysis focuses on a relay channel in which source and relay cooperatively construct a distributed turbo code. Outage probability is considered to evaluate the link quality between relay and destination and to estimate if retransmission will fail. Simulation results show that the proposed distributed HARQ protocols can significantly enhance the User Equipment (UE) throughput and the residual Packet Error Rate (PER).

Cellular networks are facing a constant growth of traffic due to an increasing number of subscribers and new services requiring high throughput for handling Internet and multimedia services. In the LTE-Advanced Study Item, ways to extend LTE were being explored in order to reach very high data rates up to 1Gb/s and a spectral efficiency equal to 30 b/s/Hz in peak and 2.6b/s/Hz in average. However, some of the adopted techniques are complex and significant research efforts are needed to bring these techniques to reality. Therefore, advanced relaying concepts that provide higher capacity on top of coverage need to be investigated in order to offer ubiquitous user experience.

In our work, cooperative distributed turbo coding techniques coupled with cooperative HARQ are investigated in order to enhance the transmission robustness while limiting spectral/energy efficiency degradation. The question we address is how to efficiently select which agent(s) (eNodeB or Relay Node) of the cooperation scheme has to retransmit when a packet decoding error is detected at destination and possibly at relay(s). We propose a novel approach based on the exploitation of the instantaneous mutual information knowledge at the receiver location.

The general proposal is as follows. Source (S) always broadcasts CC1 convolutional encoder, which is the first constituent of the turbo-encoder. Then, the destination (D) decodes CC1. If the decoding is unsuccessful (NACK at UE), there are two possibilities. First, if there is also a NACK at relay (R), then the source proceeds with CC1 broadcast and chase combining is done at CC1 decoder inputs of UE and relay. Second, if there is an ACK at relay, the relay interleaves and transmits CC2 (second constituent of the distributed turbo-encoder) to UE. Then Turbo decoding is performed at destination with chase-combined CC1 and CC2. If there is still a NACK at destination, then several retransmission schemes are envisaged considering either persistent retransmissions at both S and R nodes or only the necessary/best one(s) (R first only, S only or both R and S) based on outage detection.

In [1], performance of these algorithms in the case of a perfect S-R link was evaluated with only one retransmission. The two most promising schemes were the following. In the first one (Retx both – partner info), both nodes retransmit their complementary codeword. With this scheme, better performances are achieved due to the increased maximum diversity order experienced by the system. With the second scheme (Retx outage – partner info), the decision on which node(s) (R only, S only or both R and S) retransmits is decided based on channel outage detection. In this case, the retransmitting node sends to the destination its partner codeword trying to increase the reliability of the turbo code and to improve the overall system performance through the spatial diversity. The former scheme achieves the lowest PER while the latter offers the best average coding rate and achieves the highest link throughput.

In [2], a step further was done by taking into account non error free decoding at relay, non-truncated HARQ and bringing a new outage forecast step after the first transmission (immediate stop). In that latter case, if outage of the relay channel is forecasted even after Nmax retransmissions, then there is an immediate stop directly after the first transmission.

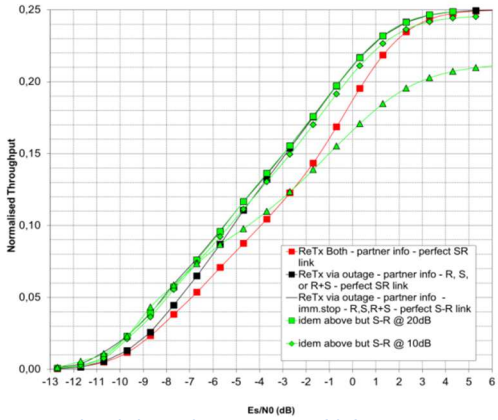

Figure 1: Normalized throughput vs. SNR (dB), asymmetric scenario.

In Figure 1, we compare the performance of the different proposals in terms of normalized link throughput in the asymmetric scenario. Solution based on outage check combined with immediate stop seems to be very efficient in term of achieved throughput even in the case of non-perfect decoding at relays while improving the energy efficiency of the cooperative scheme. Our technique based on outage forecast is performing well up to an S-R link equal to 10dB. This new HARQ algorithm even performs better in a real S-R link context than the solution consisting in always retransmitting from both source and relays in a perfect S-R link context. Indeed, the former scheme offers the best average coding rate and achieves the highest link throughput. This study will be extended to more complex scenarios, increasing the number of available relays and allowing turbo-code transmission directly at the source.

Related publications:
[1] A. De Domenico, E. Calvanese Strinati and D. Kténas, "Distributed Turbo Coding Techniques with HARQ Relays for Future Mobile Generations", in Proceedings of Future Networks Mobile Summit 2011, Warsaw, Poland, June 2011.
[2] L. Maret and D. Kténas, "Distributed Turbo Coding Techniques with HARQ at Relays for LTE-A", IEEE Vehicular Technology Conference spring 2013 (VTC spring 2013), 2-5 June 2013, Dresden, Germany.

OTA test for system performance evaluation

Research topics : Over-The-Air test, radio channel

L. Rudant, R. D'Errico

ABSTRACT: Over-The-Air (OTA) tests allow wireless system performance evaluation in realistic propagation environments. Power amplifier nonlinearity compensation based on nonlinearity estimation at the receiver was tested by means of an OTA test-bed in anechoic chamber.

The Over-The-Air (OTA) test in an anechoic chamber consists in emulating multipath propagation with multiple source antennas distributed all around a test zone and coupled to an RF channel emulator. The term OTA is widely used for many applications and may embrace non-conducted tests, such as test of compliance with regulation limits, conformance and interoperability tests based on a specific wireless standard and performance tests beyond the minimal specifications.

CEA-LETI is working on OTA tests for different applications, e.g mobile networks, wireless sensor networks, vehicular communications. A technique to mitigate Power Amplifier (PA) nonlinearity was tested in an OTA system [1].

Indeed, in mobile applications, the PA within a transmitter (Tx) must guarantee a linear response. Consequently, the PA is often used in a power range with reduced power efficiency to back off from its nonlinear regime. A classical technique to improve PA power efficiency is nonlinearity compensation with pre-distortion of transmitted signals. Nonlinearity is usually estimated with a local loop (adaptive pre-distortion) at the Tx. An innovative technique for direct estimation of nonlinearity at the receiver (Rx) was previously studied at CEA-LETI. Then, nonlinearity information is transmitted together with a software feedback to Tx for compensation. In the multi-users scenario illustrated, the PA nonlinearity of Tx at transceiver side of a femtocell or a relay is estimated by one user. Then, all users benefit from nonlinearity compensation without Tx local loop implementation.

However, the propagation channel can affect the nonlinearity estimation since the received power depends on multipath fading conditions. This estimation bias introduced by the radio channel must be investigated experimentally. Measurement campaigns in real environments are often not allowed in licensed frequency bands, and can be expensive and time-consuming.

We tested non linearity compensation based on nonlinearity estimation at the receiver, considering 802.16e specifications with a 10 MHz bandwidth around 3.5 GHz, and Orthogonal Frequency Division Multiplexing (OFDM) with 1024 sub-carriers 64QAM. The PA and the small antenna of a typical femtocell or relay were put in anechoic chamber and the downlink multipath channel was emulated. A realistic multipath propagation channel was emulated in the anechoic chamber with OTA two-paths test-bed. Different fading depths were generated in the signal bandwidth. The reliability of nonlinearity estimation in multipath channel was demonstrated with back-to-back validation. Moreover, a direct assessment of nonlinearity compensation benefits for multi-users scenarios was given through OTA test by emulating different channels for the estimation and the transmission. From OTA tests, it was observed that nonlinearity compensation allows better performances in terms of Error Vector Magnitude (EVM), thus a possible 3 dB drop of Input Back-Off with respect to EVM=3%.

This OTA test was performed with a simplified two paths channel model. CEA-LETI is now working on the OTA test-bed evolution thanks to a Multiple Input Multiple Output (MIMO) 8x8 channel emulator in the scope of the IRT Nanoelec program.

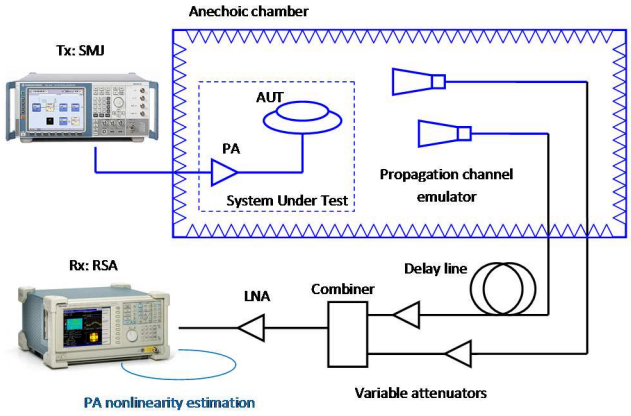

Figure 1: OTA test-bed for a power amplifier non-linearity estimation [1].

Related publications:
[1] L. Rudant, R. D'Errico, M. Robin, J. Zeleny, P. Rosson, C. Dehos, A. Kaiser "Over-the-air validation of PA nonlinearity estimation at the receiver," 7th European Conference on Antennas and Propagation (EuCAP), 8-12 April 2013, Gothenburg, Sweden.

Transmit-arrays in X- and V-band with beam synthesis capability and multiple feeds

Research topics : reconfigurable antennas, antenna arrays

A. Clemente, L. Dussopt, R. Sauleau (IETR) P. Potier (DGA), P. Pouliguen (DGA)

ABSTRACT: This paper presents two 20×20 elements transmit-arrays at X- and V-band based on 1-bit phase-shifting unit-cells. The X-band antenna is an electronically-reconfigurable transmit-array with beam steering and beam synthesis capability; the V-band antenna is a fixed beam transmit-array. In the two cases, the unit-cell is composed of two rectangular patch antennas printed on the top and bottom layers of the dielectric stack-up and connected by a metallized via hole. The phase shift of the X-band antenna is obtained by PIN diodes integrated in each unit-cell. Multiple-feed configurations have been investigated in V-band to reduce the focal distance.

High-gain electronically reconfigurable antenna arrays are needed in many emerging applications at microwaves and millimeter waves. Transmit-arrays have excellent capabilities for real-time beam steering and beam synthesis in these frequency bands and may be employed in a number of military and civil telecommunication and radar systems. A transmit-array consists of a focal source illuminating a first antenna array operating in receive mode and connected through phase-shifting elements to a second antenna array operating in transmit mode. Our work in this domain is focused on the development of fully-reconfigurable antennas in the 5-40 GHz range and fixed-beam or switched-beam high-directivity antennas in the millimeter-wave range (50-90 GHz).

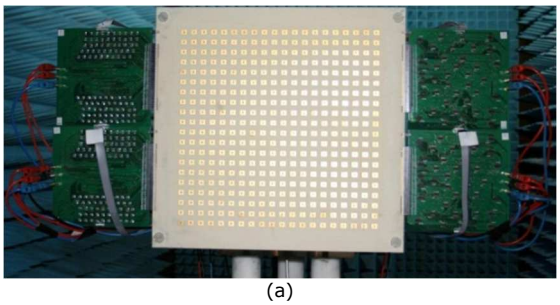

(a)

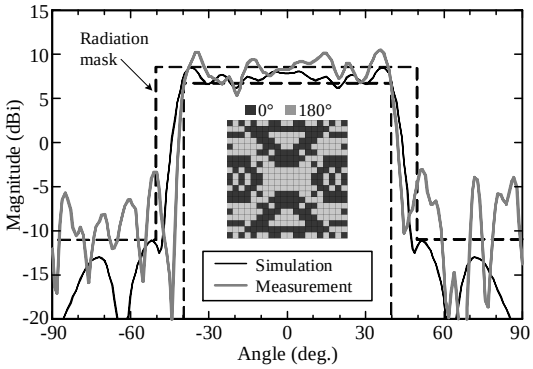

(b)

Figure 1: 20×20 unit-cells 9.8-GHz electronically-reconfigurable transmit-array prototype with the steering-logic boards (a), Measured and simulated radiation patterns for a flat-top beam synthesis (b).

An X-band (10 GHz) electronically reconfigurable transmit-array with beam-steering and beam-forming capabilities has been demonstrated (Fig. 1a) [1]. This array is composed of 400 reconfigurable unit-cells [2] and a 10-dBi horn focal source. 800 p-i-n diodes are integrated on the array in order to independently control the transmission phase of each element by a 1-bit phase-shift (0/180°). This array has been experimentally characterized and showed a maximum gain of 22.7 dBi, a 3-dB fractional bandwidth of 15.8%, and pencil-beam scanning over a 140×80-degree window [1]. Since each unit-cell of the transmitarray is controlled independently, any arbitrary phase distribution can be synthesized. In order to demonstrate the beam forming capabilities of this antenna, a flat-top beam pattern has been synthesized with a mask power template defined by a beamwidth of 80–90°, a ripple level less than 2 dB in the main beam, and a side-lobe level below 20 dB. The measured and simulated results are presented in Fig. 1b.

An important design parameter of transmit-arrays is the focal ratio (F/D, where F is the focal distance and D the array diameter) since it defines the total volume of the antenna and plays a key role for the integration and mounting of the antenna on the host platform (vehicle, building, aircraft, etc.). Multiple feed transmit-arrays are investigated as a solution to reduce the focal distance, thus leading to lower antenna profiles [3].

A theoretical study was performed for medium-size arrays (10λ in diameter) with dual or quadruple feeds. This study was validated through the full-wave simulations of a single- and a quadruple-feed linearly-polarized square transmit array in V-band (60 GHz) (Fig. 2). The optimal focal ratios are 0.54 and 0.34 for the single- and quadruple-feed cases, respectively, showing a reduction of the antenna volume by 37% at nearly constant radioelectrical performances. These results offer the perspective to design lower-profile transmit-array antenna systems, thus enabling an easier integration onto vehicles, buildings, or other platforms.

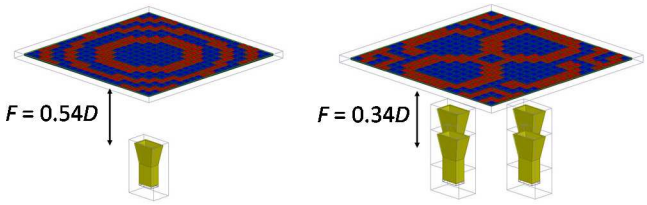

Figure 2: 20×20 unit-cells transmit-array at V band in single- and quadruple-feed configuration.

Related Publications :
[1] A. Clemente, L. Dussopt, R. Sauleau, P. Potier, and P. Pouliguen, "Wideband 400-element electronically reconfigurable transmitarray in X Band," IEEE Transaction on Antennas and Propag., vol. 61, no. 10, pp. 5017-5027, Oct. 2013.
[2] A. Clemente, L. Dussopt, R. Sauleau, P. Potier, and P. Pouliguen, "Reconfigurable unit-cells for beam-scanning transmitarrays in X band," 7th European Conference on Antennas and Propagation (EuCAP 2013), 8-12 April 2013, Gothenburg, Sweden.
[3] A. Clemente, L. Dussopt, R. Sauleau, P. Potier, and P. Pouliguen, "Focal distance reduction of transmit-array antennas using multiple feeds," IEEE Antennas and Wireless Propag. Letters, vol. 11, Nov. 2012.

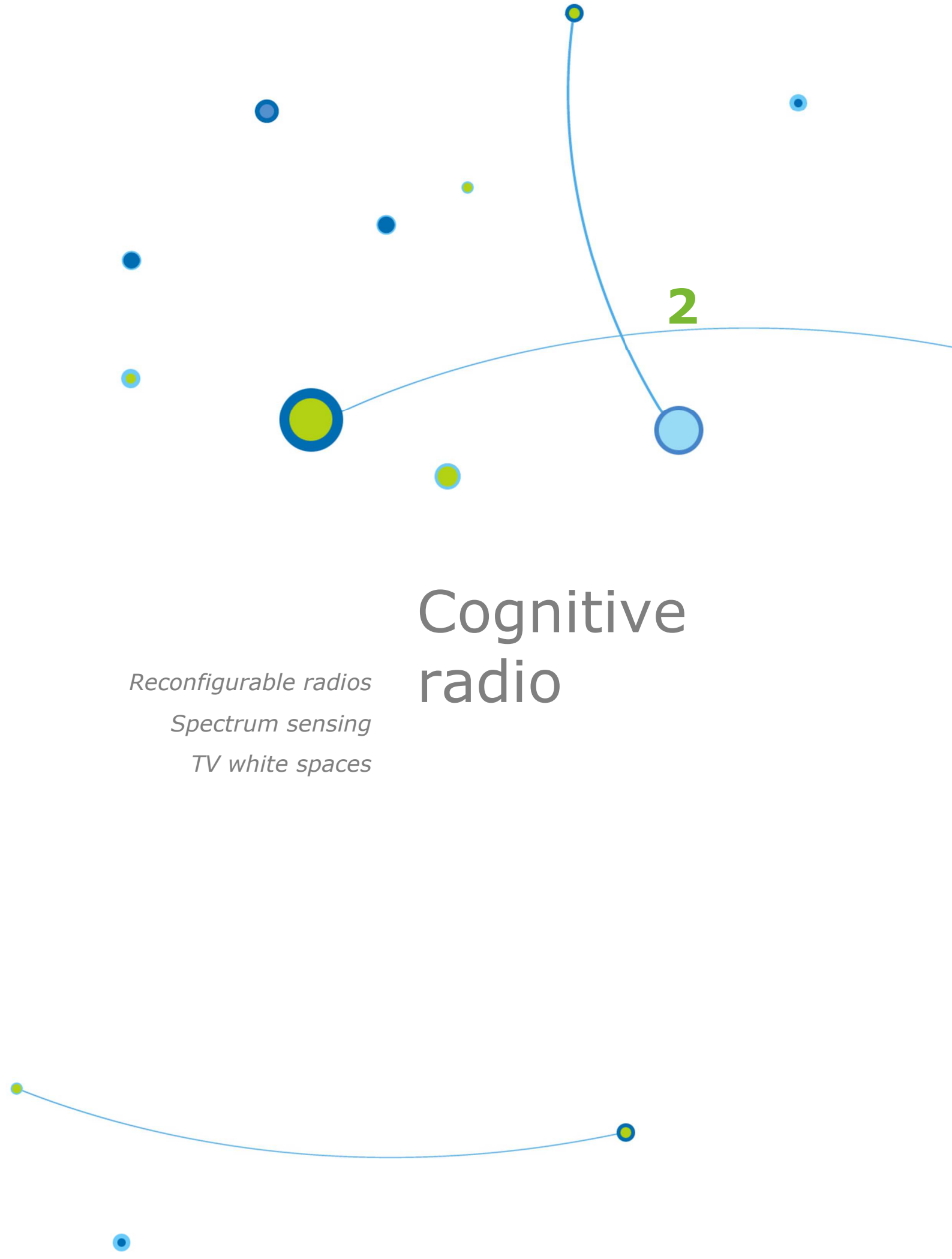

2

Cognitive radio

Reconfigurable radios

Spectrum sensing

TV white spaces

A flexible radio transmitter for TVWS based on FBMC

Research topics : cognitive radio, flexible digital radio, TV white spaces

V. Berg, J.-B. Doré, D. Noguet

ABSTRACT: A flexible radio approach for opportunistic access to the television white space (TVWS) is presented. Opportunistic transmission and TV broadcast signals imposes a high adjacent channel leakage power ratio (ACLR). Flexibility is required to address the vacant channels in the TVWS spectrum but difficult to obtain simultaneously with large ACLR levels. The approach proposed in this paper is based on filter bank multi-carrier modulation (FBMC) scheme and a flexible hardware platform that combines RF agility and the digital filtering capability of FBMC. An experimental setup validates the coexistence with a TV broadcast signal and a comparison with a classical approach shows 9dB gain in performance.

In 2009, the US radio regulator authorized opportunistic unlicensed operation in the TV bands. Such systems have to coexist with TV broadcast signals and wireless microphones. A priority mechanism must guarantee that opportunistic systems cause no harmful interference to the incumbents. Co-channel communication is prohibited and adjacent channel leakage ratio (ACLR) is limited in order to prevent an opportunistic system from interfering with an incumbent operating in an adjacent channel.

From these requirements, it can be concluded that an opportunistic system must be agile in frequency and ACLR must be large enough to meet 55dB. Unfortunately when considering standard Orthogonal Frequency Division Multiplexing (OFDM) waveforms, high ACLR values are usually obtained with SAW or BAW filters. Frequency agility is therefore very limited.

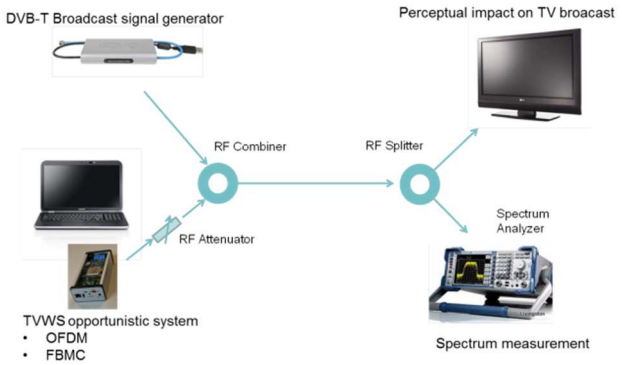

Figure 1: FBMC validation testbed setup.

Filterbank multicarrier modulation (FBMC) has been considered as a promising alternative. However, the strict ACLR and flexible requirements of the TVWS bands require experimental implementation to further assess feasibility. It has been shown that the filtering scheme embedded in the modulation itself guarantees high ACLR and relaxes the constraints of the analog filtering [1]. A first attempt to implement a FBMC transmitter on the TVWS platform T-FleX [2] is presented and ACLR performance level is evaluated. The ACLR performance is validated through spectrum profile measurements and by observing the impact of adjacent opportunistic communication on a TV broadcast signal. The setup of the testbed involves the TVWS transmitter and a DVB-T modulator, which signals are combined to share the same medium. Then, the signal is split to be visualized on a spectrum analyzer on one hand and to a TV demodulator on the other hand. This setup is illustrated in Figure 1.

An attenuator is placed at the output of the RF transmitter in order to adjust the TVWS vs DVB-T relative power. An interesting setup consists of adjusting the TVWS transmission power in order to be on the limit of the DVB-T receiver performance. It also enables to compare the respective impact of OFDM and FBMC on the DVB-T television demodulator.

The ACLR performance of the FBMC transmitter is significantly better than the one of the CP-OFDM. Then, the coexistence with incumbent TV signal is improved by an additional 9dB with the FBMC modulator [3] (Fig. 2).

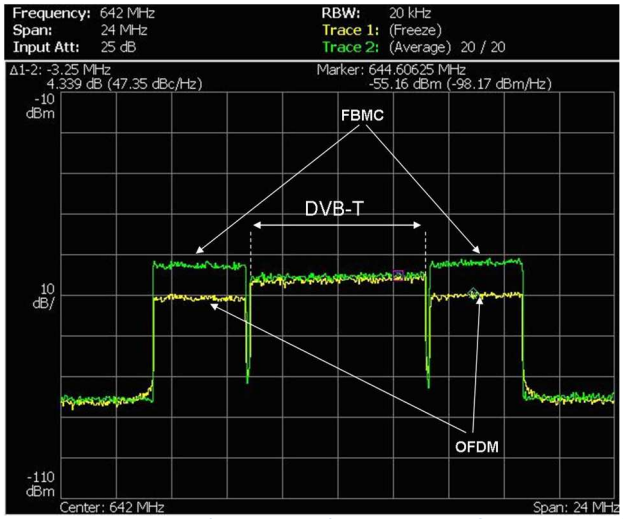

Figure 2: CP-OFDM and FBMC signals in presence of a DVB-T signal.

This performance was measured with an actual RF implementation, therefore accounting for all the impairments of the transmission chain. Besides, as the FBMC modulated signal is shaped digitally at the baseband, no compromise on the transmitter frequency agility is required.

Related publications:
[1] D. Noguet, M. Gautier, V. Berg, "Advances in opportunistic radio technologies for TVWS", EURASIP Journal on Wireless Communications and Networking 2011, 2011:170.
[2] V. Berg, D. Noguet, X. Popon, "A Flexible Hardware Platform for Mobile Cognitive Radio Applications," 15th Euromicro Conference on Digital System Design (DSD), pp.459-462, 5-8 Sept. 2012, Cesme, Turkey.
[3] V. Berg, J-B. Dore, D. Noguet, "A Flexible Radio Transmitter for TVWS Based on FBMC," 16th Euromicro Conference on Digital System Design (DSD), pp.163¬-167, Sept. 4-6, 2013, Santander, Spain.

Signal detection using watermark insertion

Research topics : cognitive radio, RF sensing

M. Gautier, D. Noguet

ABSTRACT: Signal detection using watermark insertion is presented. The watermark is artificially embedded into the digital modulated signal. When a signal has a weak cyclostationnarity signature, its detection is hard to achieve using blind detectors. For that kind of signals, we propose to insert a low-power watermark that will be detected by a matched filter based detector. The analysis addresses the trade-off between the watermark insertion strength (i.e. reducing the transmission quality) and the detection sensitivity. This trade-off is discussed in this study and simulations results show the advantage of the watermark insertion.

Cognitive radio systems can use different approaches to determine spectrum occupancy. The first is to query a database of the positions of the radio transmitters and their parameters (power, frequency) in order to deduce a map of the spectrum occupation. Another approach is to directly detect the signal using spectrum sensing techniques. If the first can protect perfectly the incumbents, it cannot help the management of resource allocation among opportunistic users. Detection techniques must be specifically adapted to the opportunistic users. Many detection techniques have been proposed in the literature [1]. Those offering the highest levels of sensitivity for a given detection time are those that use a-priori informations on the signal. However, some signals do not contain intrinsic signatures. In that case, only blind algorithms can be applied, such as the energy detector, but these algorithms have limited sensitivity.

The solution proposed herein [2] relies on the following: the detection can be assisted by the explicit introduction of a specific signature (or watermark) into the transmitted signal. In our approach, the watermark is inserted with a very low power in order not to alter the signal significantly. Thus, a receiver must be able to demodulate the signal without any knowledge on the watermark, and only the sensor uses the watermark to detect the signal.

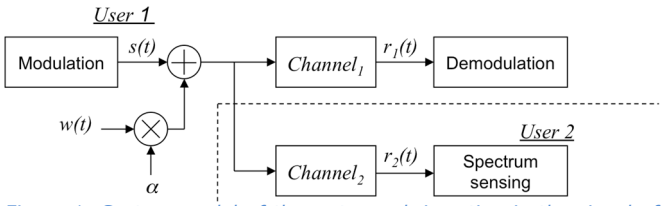

Figure 1: System model of the watermark insertion in the signal of User 1 and its detection by User 2.

The proposed watermarking scheme is inspired from the watermarking of audio signals where the hidden information is embedded inside an audio signal. The watermarking consists in adding the signal w(t) with the signal s(t) as shown in Fig 1.

The watermark inserted into User 1 should improve its detection by other users. The aim of the detector is to detect the presence of the watermark, not to detect the signal itself. Thus, the detection can be stated as the following hypothesis (in the case of an AWGN noise n2(t)):

$$\begin{cases} H_0 : r_2(t) = n_2(t) \\ H_1 : r_2(t) = s(t) + \alpha w(t) + n_2(t) \end{cases}$$

Fig. 2 shows the impact of the watermark on signal demodulation for several values of Watermark to Signal Ratio (WSR). For instance, the degradation is lower than 1 dB @BER=10-3 for WSR < -15 dB.

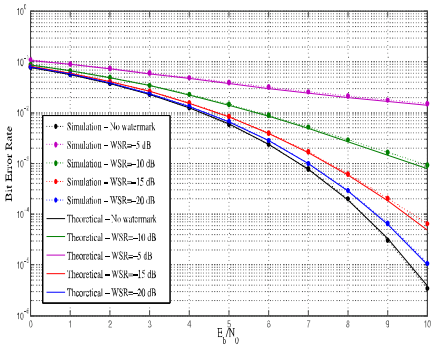

Figure 2: Impact of the watermark on the receiver performance.

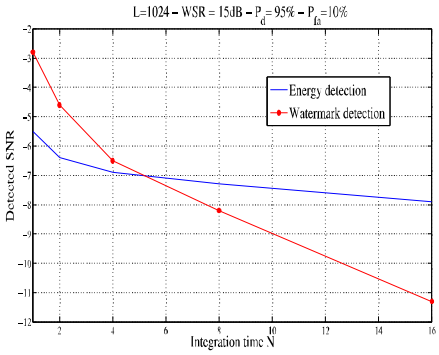

Figure 3: Comparison of watermark vs energy detection, WSR=-15dB.

On the other hand the presence of the watermark enables to significantly increase the sensitivity compared to energy detection as illustrated in Fig. 3.

It can be concluded that watermark insertion even at a very low power (low WSR) improves detection capability significantly, while the interference incurred by the watermark only slightly impacts signal demodulation. Thus, watermarking is an effective technique to improve signal detection with limited cyclostationarity signature, such as FBMC modulations.

Related Publications:
[1] D. Noguet, et al. "Sensing techniques for Cognitive Radio - State of the Art and Trends", IEEE P1900.6, April 2009.
[2] M. Gautier, D. Noguet, "Signal detection using watermark insertion", IEEE 77th Vehicular Technology Conference (VTC Spring), June 2-5, 2013, Dresden, Germany.

Mapping cognitive radio system scenarios into the TVWS context

Research topics : cognitive radio, TV white spaces

P. H. Lehne, D. Noguet, V. Berg, O. Grondalen (Telenor), R. MacKenzie (BT Tech.)

ABSTRACT: Cognitive Radio has been one of the key research topics in the wireless community for about 10 years. The digital switch-over in the TV bands provides opportunities for Cognitive Radio Systems (CRS) to operate in the 470-790MHz spectrum under incumbent protection restrictions. Regulatory bodies, in particular the US Federal Communications Commission and OFCOM in the UK, have specified parameters under which CRS shall operate. This paper considers link budget and expected capacity when using TVWS for a variety of scenarios. Indoor WLAN-like scenarios and fixed rural broadband are identified as the most promising scenarios.

A growing regulatory trend to allow for license-exempt users in licensed bands is emerging and the TV Band (TVWS) has been identified as the first band to be used for opportunistic channel access in many areas of the world. In this context, some usage scenarios have been particularly under consideration during the FP7 QoSMOS project - Quality of Service and Mobility driven cognitive radio Systems. These scenarios include private access solutions from device to device similar to today's WiFi, rural broadband involving the provision of wireless internet connectivity to homes in rural locations, emergency ad-hoc networks for first respondents and finally cellular extension in whitespaces for improved capacity. The usage scenarios have been mapped to three propagation scenarios to derive range expectations using current US Federal Communications Commission (FCC) and foreseen Ofcom recommendations, e.g. in terms of transmit power levels: portable personal device (PPD) to PPD indoor and indoor-to-outdoor propagation, fixed device (FD) long range propagation and mobile cellular propagation [1]. The results are summarized in Table 1 to Table 3.

Table 1: Range estimates for indoor PPD (WiFi-like access and ad-hoc networks in device to device).

Carrier Frequency	**630 MHz**		
TX EIRP	20 dBm	17 dBm	4 dBm
Cell Range:	Best case (0 dBi Rx antenna)		
Same floor	220 m	180 m	75 m
One Floor	120 m	100 m	40 m
Cell Range:	Worst case (-7 dBi antenna)		
Same floor	140 m	115 m	50 m
One Floor	75 m	65 m	25 m

The propagation models given in recommendation ITU-R P.1238 are extended from the range above 900MHz to the TV Band (470MHz to 790MHz). For indoor PPD-to-PPD propagations, range up to a few hundred of meters may be considered. The range is dramatically reduced as propagation through multiple floors is considered.

For the fixed long range propagation scenario, the models proposed by ITU-R P.1546 and the Okumura-Hata method produce similar results. Ranges of up to almost 10km may be achieved assuming a roof-top antenna reception in a suburban environment.

Table 2: Range estimates for Fixed Long Range (Rural Broadband).

Carrier Frequency	**630 MHz**
TX EIRP	36 dBm
ITU-R P.1546 Urban	4.72 km
ITU-R P.1546 Suburban	8.27 km

Finally, for the cellular extension scenario, two models give quite different results. The P.1546 model gives a maximum cell range of 600-1700m while the P.1411 estimates much shorter ranges from 250m to 600m. The P.1411 model is assumed too pessimistic in this scenario as the base station antenna is generally located at a height above roof level (15m).

Table 3: Range estimates for mobile cellular extension.

Carrier Frequency	**630 MHz**	
TX EIRP	36 dBm	
Rx Antenna Gain	-7 dBi	0 dBi
ITU-R P.1546 Urban	0.6 km	1.0 km
ITU-R P.1546 Suburban	1.1 km	1.7km
ITU-R P.1411 Urban	260 m	390 m
ITU-R P.1411 Suburban	385 m	580 m

Under these assumptions cellular extension in the TVWS may only be considered for rather small cells such as for instance in congested areas where TVWS could be used as a tool to offload part of the cellular traffic.

Assuming a single LTE base station with 3 sectors, capacity offloading has also been estimated in this latter scenario using Spectrum Engineering Advanced Monte Carlo Analysis Tool (SEMCAT) simulator. Without any TV interferer, up to 26.1 Mbit/s offloading may be achieved per 8 MHz channel. However, when a DVB-T SFN urban scenario is considered, the capacity offloading in the TVWS is reduced to less than 5 Mbit/s.

Finally, cognitive femtocells have been analyzed in terms of density requirement to provide full coverage in a city equally divided between urban and suburban areas. It is estimated that an average of 10% of households with an active TVWS femtocell uniformly distributed in the city would guarantee a full coverage of the femtocell service.

Related publication:
[1] P. H. Lehne, O. Grondalen, R. MacKenzie, D. Noguet, V. Berg, "Mapping Cognitive Radio System Scenarios into the TVWS Context", Journal of Signal Processing Systems, Vol. 73, No 3, pp. 227-242, Dec. 2013, Springer Science, New York.

Wireless short-range communications

Millimeter-waves

Miniature antennas

RFID

Body Area Networks

Security

Hybrid on-chip/in-package integrated antennas for millimeter-wave short-range communications

Research topics : millimeter-wave antennas, integrated antennas

J.A. Zevallos Luna, L. Dussopt, A. Siligaris

ABSTRACT: A hybrid on-chip/in-package integrated antenna is designed and demonstrated for the first time in a QFN (Quad Flat No Lead)-packaged 60-GHz Ultra-Wide-Band (UWB) low-power transceiver. The on-chip radiating element is a folded dipole antenna realized on the transceiver high-resistivity silicon chip (CMOS-SOI technology). It is coupled electromagnetically to a patch antenna embedded under the package lid. The experimental radiation patterns and gain values are in agreement with the simulations, they show an antenna gain up to 4.6–8 dBi at 60 GHz and a 3-dB beamwidth of 43°×72°, suitable for short-range low-power Gbps communications.

On-chip antennas integrated on CMOS technologies have been investigated for many years in order to provide highly-integrated and low-cost solutions for short-range and high data-rate communications in the 60 GHz band. The main benefit of the on-chip integration is to avoid any complex and expensive interconnection for millimeter-wave signals between the antennas and the RF front-end. The main difficulty comes from the poor antenna performances obtained with CMOS integrated antennas, even on high-resistivity silicon due to the substrate loss. In this work a low-cost solution is proposed to improve the radiation performances of an integrated on-chip folded dipole antenna using a patch radiating element placed under the removable lid of a standard QFN (Quad Flat No Lead) pre-molded cavity package [1].

The folded dipole is fabricated with the transceiver chip in 65-nm CMOS-SOI (Silicon-on-Insulator) technology with a high-resistivity silicon substrate. The chip size is 3.1×1.9×0.3 mm3 (Fig. 1a), it is mounted in a QFN pre-molded cavity package (Fig. 1b) soldered on a test board with connections to power supplies and input/output digital signals. The QFN48L package size is 7×7×1.75 mm3, the walls and lid of the package are made of LCP (Liquid Crystal Polymer). The chip is bonded in the package with 25-µm aluminum wires.

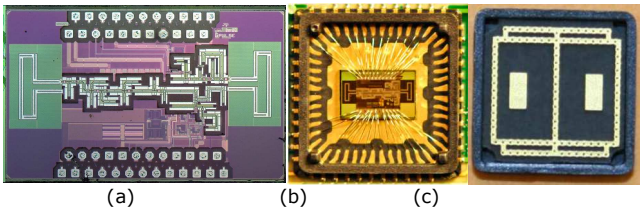

(a) (b) (c)

Figure 1: Photographs of the 60-GHz transceiver chip (a) the same chip in a QFN package (without lid) (b) and the patchs under the lid (c).

The patch radiating elements are printed on a 381 µm-thick RT-Duroid 5880 substrate from Rogers Corp. This thickness results in a distance of 419 µm between the integrated folded dipoles and the patch antennas, allowing a good coupling level while still large enough to avoid any contact of the substrate with the bond-wires. Each patch has a length of 1.45 mm and a width of 0.7 mm; they are placed above the on-chip folded dipoles. The patch substrate is cut to the inner dimensions (5.7×5.7 mm2) of the package lid and glued to it. A minimum quantity of glue was used in order to minimize the uncertainty at the interface between the substrate and the lid. In order to improve the antenna gain in the broadside direction and the shape of the radiation pattern, rings of metallic vias were drilled in the superstrate and around the patchs (Fig. 1c) [2],[3].

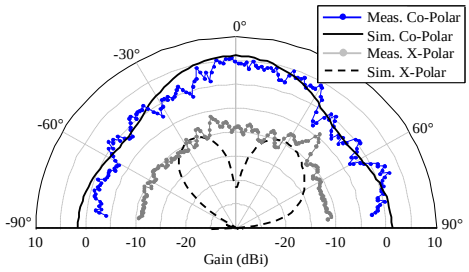

(a)

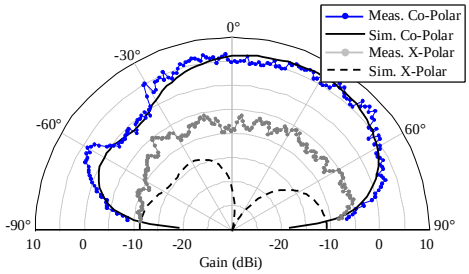

(b)

Figure 2: Simulated and measured gain radiation patterns at 60 GHz in the E-plane (a) and H-plane (b).

The measured radiation patterns are in good agreement with the simulations (Fig. 2a,b). In the E-plane, the radiation pattern exhibits a maximum gain of 4.6 dBi in the broadside direction; the 3-dB beamwidth is about 43°. In the H-plane, the pattern exhibits a maximum gain of 8 dBi at 50° with a wide 3-dB beamwidth from about -18° to 54°, and only a minor local minimum of about -2.3 dBi at -44°. The cross-polarization level is about -10 dB below the main polarization and could not be measured accurately due to the limited sensitivity of the measurement set-up. The simulated radiation efficiency is 73%.

Related publications:
[1] J.A. Zevallos Luna, L. Dussopt, A. Siligaris, "A 60 GHz CMOS-SOI Integrated Antenna with Coupled Patch in a QFN Package", 7th European Conference on Antennas and Propagation (EUCAP), Gothenburg, Sweden, April 2013.
[2] J.A. Zevallos Luna, L. Dussopt, A. Siligaris, "Packaged integrated transceiver for short-range high data rate communications at 60 GHz", Antennas and Propagation Society International Symposium (APSURSI), Orlando, Florida, USA, July 2013.
[3] J.A. Zevallos Luna, L. Dussopt, A. Siligaris, ''Hybrid On-Chip/In-Package Integrated Antennas for Millimeter-Wave Short-Range Communications'', IEEE Transactions on Antennas and Propagation, vol. 61, no. 11, Nov. 2013, pp. 5377-5384.

Reconfigurable 60-GHz on-chip CMOS-SOI antenna array for radiation pattern diversity

Research topics : millimeter-wave antennas, integrated antennas

Shynu S.V. Nair, J.A. Zevallos Luna, L. Dussopt, A. Siligaris

ABSTRACT: A beam-switched parasitic antenna array on CMOS-SOI (Silicon-on-Insulator) technology at 60 GHz is studied. The three-element reconfigurable array along with the NMOS transistor switches are fabricated on 130-nm CMOS technology occupying a mere 1.2×2.65 mm2 chip size and providing a simulated gain up to 5.5 dBi with beam switching at ±56°. The fully integrated antenna provides a low-cost diversity solution for the emerging gigabytes per second (GBps) short-range communication systems in the 60 GHz band.

On-chip silicon CMOS antennas exhibit a moderate gain level due to their small size and silicon substrate losses. Moreover, their radiation pattern is significantly perturbed by reflections and scattering on nearby objects (package, casing). Radiation-pattern diversity may be a good strategy to mitigate these effects in high data-rate short-range (<3 m) 60-GHz wireless applications by providing a few dBs of diversity gain. This reconfigurability shall be obtained for a minor additional complexity and power consumption to preserve the benefits of on-chip antenna integration with respect to in-package antenna solutions.

In order to provide this additional antenna gain without additional complexity in the front-end, a switched parasitic antenna array is investigated in this work because of its simple structure and ease of implementation with semiconductor switches [1]. A novel design of a reconfigurable three-element parasitic antenna array at 60 GHz on a 130-nm CMOS-SOI technology is presented.

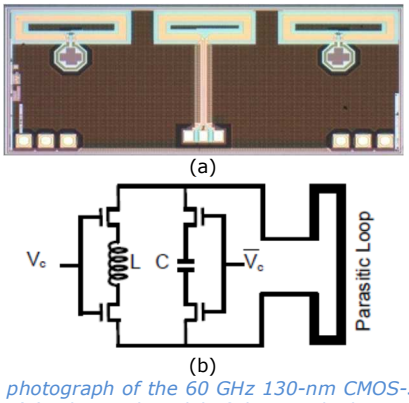

Figure 1: Die photograph of the 60 GHz 130-nm CMOS-SOI parasitic antenna array (a). Electrical model of the switched reactive load (b).

The array consists of a microstrip loop antenna as a driven element with parasitic loops operating near resonance and connected to switchable reactive loads with NMOS transistor switches (Fig. 1a) [2]. The CMOS-SOI technology was chosen to benefit from the high-resistivity substrate leading to reduced losses. The switched reactive loads are modeled as L (octagon inductor) and C (MIM capacitor) pairs with NMOS transistor switches (Fig. 1b).

The proposed antenna can provide 16 possible reactive load combinations and four different radiation patterns by selecting the bias conditions of the eight NMOS transistors. The switchable directions of the beam lie in the E plane. The maximum realized gain of the antenna varies between 4.2–5.5 dBi. Its operational bandwidth (reflection coefficient lower than -10 dB) is 2.35 GHz wide, centered around 59.1 GHz.

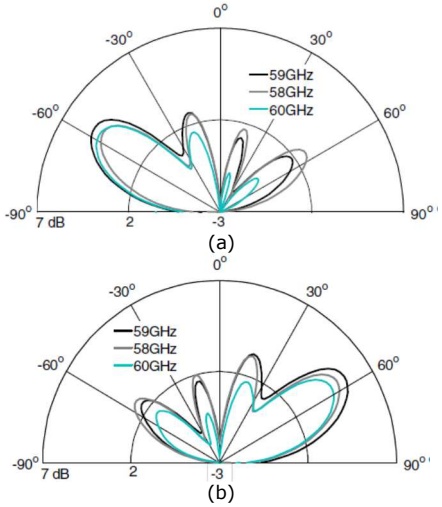

Figure 2: Simulated radiation patterns of the parasitic array antenna in the E-plane for two load combinations. Inductor-capacitor (a) and Capacitor-Inductor (b).

The antenna is capable of radiating either with single beam or dual beam depending on the reactive load combination. Two typical reconfigurable radiation patterns in the E-plane for the load combinations (inductor-capacitor and capacitor-inductor) are plotted in Fig. 2. The main beam of the radiation pattern is switchable along θ = ±56° in the E-plane. The simulated antenna gain along θ = -56° and θ = +56° are 5.2 dBi and 5.5 dBi, respectively. The radiation pattern profiles are relatively stable across the entire frequency bandwidth.

Related publications:
[1] L. Petit, L. Dussopt and J.M. Laheurte, "MEMS-Switched Parasitic Antenna Array for Radiation Pattern Diversity," IEEE Trans. Antennas Propagat, vol. 54, no.9, pp. 2624-2631, Sept. 2006.
[2] S.S.V. Nair, L. Dussopt, A. Siligaris, "Design of reconfigurable 60_GHz On-Chip CMOS-SOI Pattern-Diversity Antenna," 7th European Conference on Antennas and Propagation (EUCAP), Gothenburg, Sweden, April 2013.

Lumped loading technique for printed antenna miniaturization

Research topics : miniature antennas

L. Rudant, C. Delaveaud

ABSTRACT: A miniaturization technique using capacitive loads is investigated in order to design an electrically-small antenna for compact wireless sensor nodes. A specific implementation is developed to build a prototype.

Wireless Sensors Networks (WSN) allow for the development of innovative sensing solutions of the environment. Sensors will be deployed in a variety of scenarios, ranging from environmental monitoring to health care, from the public to the private sector, etc. Prior to large-scale deployment, a large variety of problems still has to be solved. One critical issue in real WSN deployment is antenna miniaturization and integration inside compact electronic devices especially in UHF frequency bands. These frequency bands are attractive for good propagation properties and can contribute to limit energy consumption of wireless electronic devices.

This work discusses the design of a miniature antenna for easy integration in a compact sensor node operating at 868MHz [1]. The unavoidable tradeoff between antenna performances (operating bandwidth and radiation efficiency) and size reduction is smoothly relaxed due to the narrow operating bandwidth (868-870MHz). This narrow band characteristic asks for particular attention concerning the antenna design where accurate manufacturing process can be critical. As a consequence, a particular topology of electrically small antenna is studied.

The investigated antenna geometry is a compact form of Inverted-F Antenna (IFA). Basically, an IFA is a conductor line above a ground plane, one end is connected to the ground and the other end is open circuited. A loading capacitor C_l is introduced at the open end to shift down the resonance frequency of the IFA or to reduce the length of the conductor line if the resonant frequency is constant. A non-classical impedance configuration is used in this work to further reduce the antenna dimensions. Impedance matching is obtained below the parallel resonance which exhibits a high magnitude. Consequently, the impedance matching is obtained by giving a capacitive behavior of the antenna at low frequencies. For this, a second serial capacitor C_f is introduced on the feeding line.

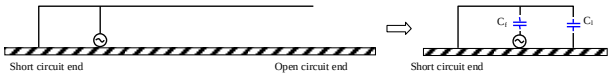

Figure 1: Antenna geometry description.

The antenna geometry and loading strategy have been investigated with 3D EM simulations. The loading parameters effects are observed based on resonator characteristics with respect to the impedance real part. In this way, the effect of each parameter can be distinguished and investigations give a better understanding of possible antenna optimization. The results show that extreme accuracy in C_l capacitor tuning is necessary to avoid out-of-band shift of the narrow operating bandwidth. The effect of C_f on the frequency resonance is less significant. The effect on quality factor is more complex and consequently an optimization of the loading capacitors C_l and C_f for impedance matching should be carried out with an iterative process.

In order to reduce the geometrical tolerance impact on capacitance tolerance, a coplanar capacitor configuration has been selected. The distance between the two metallic conductors etched on a single side of the antenna PCB is a key parameter which relaxes the capacitor tolerance with respect to manufacturing process. This particular antenna loading technique has been implemented in an antenna geometry designed to be integrated on the node demonstrator PCB. The node developed for the demonstration is mainly constituted of a PCB of 6cm×6cm (λ_0/5.8xλ_0/5.8, λ_0 being the operating wavelength) where the antenna is placed.

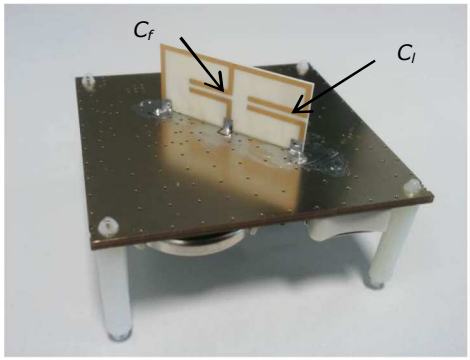

Figure 2: Antenna prototype on the node demonstrator.

The antenna prototype performances have been measured using a specific measurement set-up dedicated to electrically-small antennas. Measured peak gain versus frequency from both EM simulation and measurement are in a good agreement. The antenna has best performances in the ISM 868-870MHz band proving the accuracy of the antenna tuning and manufacturing.

A technique of lumped capacitive loading has been developed to design a miniature narrowband antenna for a demonstrator of sensor node. The analysis of the behavior of the antenna with respect to this technique leads to a specific implementation successfully used to construct a demonstrator.

Related publications:
[1] L. Rudant, C. Delaveaud, "Investigation of lumped loading technique for printed antenna miniaturization," International Workshop on Antenna Technology (iWAT), March 4-6, 2013, Karlsruhe, Germany.

Miniature antenna for micro-SD card

Research topics : miniature antennas, antenna integration

L. Huitema, C. Delaveaud, R. D'Errico

ABSTRACT: A miniature antenna for Micro SD card integration has been proposed. This antenna is intended to provide wireless connectivity between a smartphone having a micro SD card slot and other devices operating at 2.4 GHz. A prototype has been realized and measured by means of specific miniature antenna characterization methodology.

Wireless devices miniaturization asks for the reduction of antenna's dimensions, which becomes one of the most important challenges for antenna designers. As an example, a miniature antenna operating in the 2.4 GHz Industrial Scientific Medical (ISM) band has been designed to be integrated in a micro-SD card. This antenna is intended to provide wireless connectivity between a smartphone having a micro-SD card slot and medical devices, for therapeutic, sensing or telemetry applications.

The available volume for the antenna has been set to 11×7×1 mm^3 micro-SD extension, i.e. λ/12×λ/18×λ/125 at 2.4 GHz. The proposed antenna is a hybrid design between a folded T-shaped monopole and an inverted-F antenna. The antenna design, realized on FR4 substrate, is presented in Fig. 1.

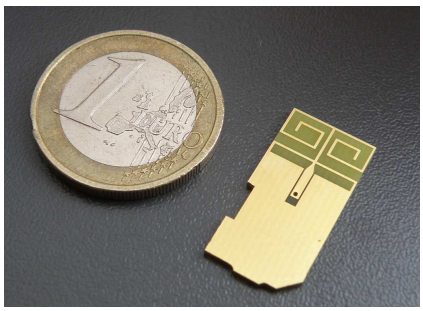

Figure 1: Micro SD antenna prototype.

Different miniaturization techniques have been combined to optimize the radiation performances in a limited antenna surface. The shorting lines to the ground plane, allow achieving a parallel resonance, which helps in optimizing the input antenna impedance, according to the lines' shape and length. As expected, the value of the resonant frequency is controlled by the folded radiating element length. The T-shaped folded monopole radiator allows an omnidirectional pattern while ensuring an impedance bandwidth enhancement thanks to the arms folding. The symmetrical antenna geometry is used to limit alteration on wished dipolar type radiation.

To measure the antenna properties, the 50Ω-discrete port has to be replaced with a practical feeding, i.e. in our case a coplanar waveguide printed on the FR4 substrate. To get rid of parasitic RF cable effect in antenna characterization, a specific measurement methodology, currently under development at CEA LETI, has been used to obtain the true impedance and radiation characteristics.

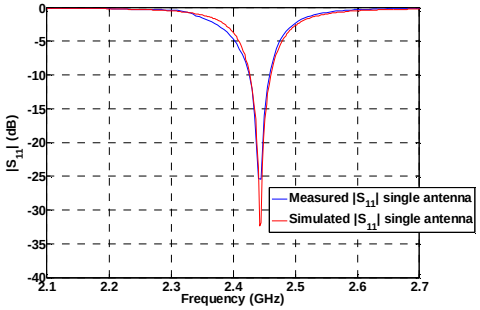

Figure 2: Reflection coefficient of the Micro-SD antenna.

The results show an excellent agreement between the simulation and measurements. The antenna prototype is matched over the 2.426 – 2.461 GHz frequency range, representing 1.43% of relative bandwidth at -10 dB.

The radiated performances have also been simulated and measured in the anechoic chamber at CEA LETI, showing that the total efficiency reaches 67% at the central frequency, whereas the maximum realized gain equals 0.2 dBi.

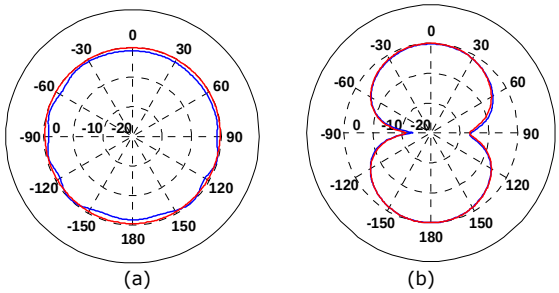

Figure 2: Radiation pattern of the Micro-SD antenna: azimuth (a) and elevation (b). Comparison between simulation (red) and measurement (blue).

The integration of the Micro-SD antenna in a smartphone has been investigated through 3D electromagnetic simulation. The 3D directivity pattern is disturbed and presents a slightly more directional behavior, with respect to the isolated antenna. On the other hand, a ground plane enlargement due to the presence of the smartphone PCB, yields to a larger radiation efficiency, which can be convenient for the application.

More recent studies are investigating the introduction of a variable capacitor in the antenna design in order to make this antenna frequency agile.

Related publications:
[1] L Huitema, C. Delaveaud, R. D'Errico, "Miniature antenna for micro SD card," 2013 7th European Conference on Antennas and Propagation (EuCAP), April 8-12, 2013, Gothenburg, Sweden.

Miniature directive antennas

Research topics : miniature antennas, directional antennas

M. Pigeon, C. Delaveaud, L. Rudant

ABSTRACT: This work aims to assess the feasibility of miniature directive antennas. It is based on an analysis of the physical limits of antenna directivity in general and in particular as a function of their compact dimensions. A state of the art is done to identify and classify techniques to increase the directivity of compact antennas.

The miniature antennas have been and remain widely studied. Limits of the performances of these antennas in terms of quality factor, gain (efficiency) or bandwidth have been the subject of numerous studies and publications. Radiation properties of miniature antennas are less discussed and are mainly characterized via radiation efficiency. As a result, investigation works have been carried to discuss the directivity properties of miniature antennas. The analysis is based on a complete state of the art of directive compact antennas dealing with theoretical limits and identified techniques to shape the radiation pattern of compact antennas.

The high directivity of the antenna has been studied in the mid of the last century and promising concepts have been discussed (often theoretically) under the term super directivity. From a theoretical point of view, spherical wave expansion has been used by different authors to establish a practical limit for the antenna directivity which remains mathematically infinite. By expressing the antenna directivity (D) as a linear combination of spherical wave modes, a limit for the maximal directivity when the wave functions are restricted to orders n ≤ N has been demonstrated. The same maximal directivity limit has been derived using the set of wave coefficients derived by the maximum directivity expansion of the two orthogonal polarization components.

$$D = N^2 + 2N$$

The qualitative evaluation of the field in the vicinity of the minimal sphere (radius r) that encloses the antenna suggests the relationship between the antenna size r, the spherical wave order N and the wave number β (Harrington).

$$N = \beta r$$

Although the relationship between the maximum directivity in one direction and the N order of spherical modes radiated seems absolute, the relationship linking the number of modes to the size of the antenna is questionable. Indeed, for electrically-small antenna sizes ($2r/\lambda << 1/\pi$), the maximum directivity becomes negative (dBi), which does not correspond to the theoretical definition of maximum directivity.

An extensive search of compact antenna solutions with high directivity was achieved. Among the different compact and directive antenna topologies identified in the literature, we suggest to regroup them into four categories: Antennas above reflector (Perfect Electrical Conductor or Artificial Magnetic Conductor), Huygens Source, Loaded antenna (resistor), Compact antenna array (multiple fed sources or coupled parasitic array). We propose to classify the different kinds of compact directive antennas according to their size using a graph (Fig. 1). The antenna size is expressed as 2r / λ. The directivity D is expressed in dBi and corresponds to the maximum directivity achieved by the antenna. This directivity is recorded directly in the articles, recalculated from the gain and efficiency or simulated when the information is not given. Specific attention has been given for antenna performance comparison. The definition of antenna size has been done in accordance with ground plane role and for large ground plane, a 3 dB reduction of directivity has been applied since antenna radiates in the half space.

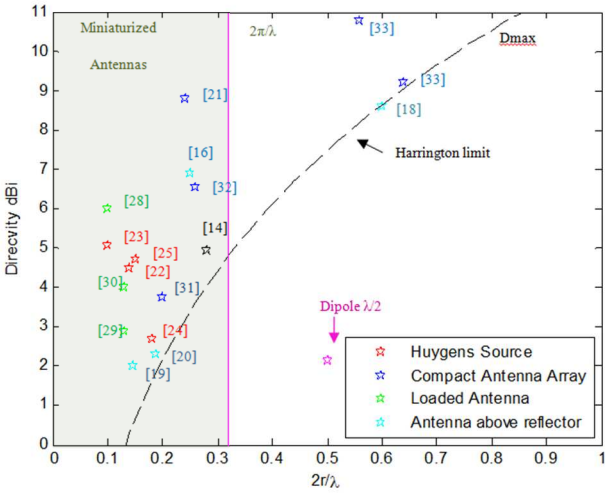

Figure 1: Chart comparing compact antenna performances with normal directivity of Harrington [2].

Considering the position of the various referenced works on the chart, numerous miniature directional antennas found in the literature are above the maximal normal limit of Harrington. They can be considered as super directive antennas. The smallest directive antennas are loaded antennas or Huygens sources. They presented limited performances (very low efficiency) and technological drawbacks. The most directive compact antennas are sources arrays. This type of solution is to be revisited with the contribution of new electronic and microelectronics technologies to design innovative miniature directive antennas.

Related publications:
[1] M. Pigeon, L. Rudant, C. Delaveaud, K. Belmkaddem, "Antennes miniatures superdirectives", Journées Nationales Microondes (JNM), May 15-17 2013, Paris, France.

Multi-dimensional channel modeling for UWB backscattering communications

Research topics : radio channel, Ultra-Wide Band, RFID

R. D'Errico, A. Sibille (Telecom ParisTech)

ABSTRACT: A multi-dimensional channel model of UWB indoor backscattering has been proposed for passive RFID applications enabling identification and localization. Starting from extensive measurement campaigns, the tag backscattering clutter, but also reader interference, have been evaluated.

Ultra-Wide Band (UWB) passive Radio Frequency Identification (RFID) is expected to provide information on identification and location of the objects in indoor environments. The design and performance evaluation of these systems demands for a complete channel model including backscattering (related to structural and antenna mode), clutter, but also reader interference. This results into a multi-dimensional channel, which depends not only on the environment, but also on the tag antenna considered. Moreover the channel modeling requires the inclusion of the polarization distribution information, since the tag can be arbitrarily oriented in realistic applications.

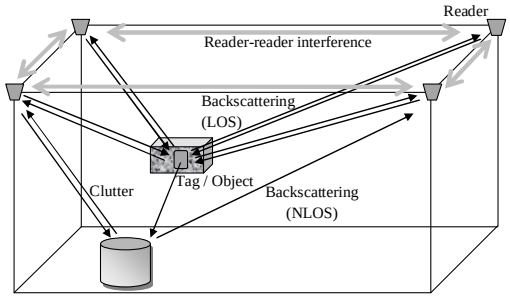

Figure 1: Indoor channel contribution in UWB backscattering-based systems [2].

UWB antenna backscattering propagation in indoor environments has been characterized and modeled at CEA LETI, using a full-polarization UWB channel measurement set-up [1]. The measured backscattered channel impulse responses (CIRs) of the two load conditions (open and short circuit) on the tag have been processed to isolate the antenna mode from the structural part, which includes the nominal structural antenna backscattering, the clutter and mutual coupling between reader antennas.

The model proposed was based on wideband indoor channel formulation, but with some specific double polarized features characterization of UWB antenna backscattering channel in different environments of interest for indoor applications. It was found that the cross-polarization distribution (XPD) follows a log-normal distribution whose mean value depends on both scenario and tag antenna. For instance, we show in Fig. 2 that XPD is higher in warehouse scenarios because of the greater polarization re-distribution due to the presence of several metallic scatterers. The full model parameters are reported in [1].

Since the tag detection is based on backscattering, a major source of disturbance in addition to the tag structural mode is clutter, which is due to all objects within a propagation distance from the readers. This effect has been modeled through specific channel measurements in the environments of interest. In practical applications with a UWB RFID tag, this means that different readers transmit at the same time, implying that a given reader will receive a strong interference signal from the others. In an additional set of measurements, the Signal to Interference plus Noise Ratio (SINR) between the tag BS signal and the LOS signal from a second reader antenna at 10 m distance was evaluated. The SINR is high up to 5 m distance, beyond which it gets very low. This effect is very simple to understand, as in one case (reader to reader) it is a one way propagation, while in the second, it is a two way propagation (reader to tag to reader), thus a doubled attenuation.

A generic channel model for a detection and location system of UWB RFID tags, incorporating several important effects with respect to the system performance has been obtained in [2]. The realistic behavior of tags on objects was approached by a statistical model of the backscattering gain, both for the antenna mode and the structural mode [3,4]. The general idea is to start from databases of tags and propagation characteristics and combine them together, then simplify the whole set of characteristics into a tractable tool, parameterized by high level descriptors of the propagation environment and the use case.

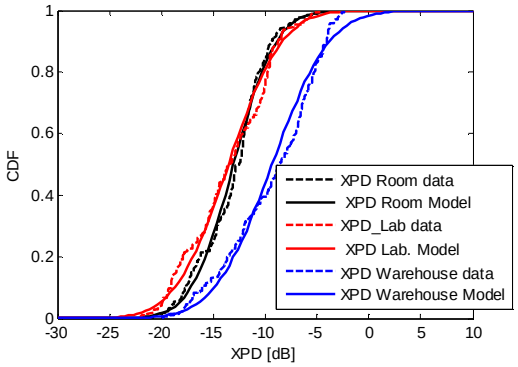

Figure 2: Cross-polarization distribution in UWB backscattering for different indoor scenarios [1].

Related publications:
[1] R. D'Errico, J. Keignart, L. Rudant, "Characterization of UWB backscattering propagation for passive tags identification and localization," 2013 7th European Conference on Antennas and Propagation (EuCAP), April 8-12, 2013, Gothenburg, Sweden.
[2] A. Sibille, Z. Mhanna, M. Sacko, R. Contreras, V. Casadei, R. D'Errico, "Channel modeling for backscattering based UWB tags in a RTLS system with multiple readers," 7th European Conference on Antennas and Propagation (EuCAP), April 8-12, 2013, Gothenburg, Sweden.
[3] A. Sibille, R. D'Errico, M. Mackowiak, "Statistical Modeling of Antennas Applied to Realistic Use Cases in Wireless Networks", Future Networks and Mobile summit (FuNeMS) (invited talk), July 3-5, 2013, Lisbon, Portugal.
[4] A. Sibille, R. D'Errico, Z. Mhanna and R. Contreras, "The Backscattering Channel in an UWB RFID System of Tags and Readers", European Workplace Innovation Network (EuWin) (invited talk), July 8-10, 2013, Bologna, Italy.

UHF-UWB tag antenna for passive RFID applications

Research topics : miniature antennas, Ultra-Wide Band, RFID

M. Pigeon, R. D'Errico and C. Delaveaud

ABSTRACT: A miniature tag antenna for hybrid UHF-UWB RFID applications has been designed. This new antenna co-localizes a small UHF slot and a UWB monopole antenna on the same substrate layer. The whole design leads to a multi-port antenna system whose dimensions are smaller than a credit card size.

In the last years, impulse-radio (IR) ultra-wide bandwidth (UWB) techniques have shown very promising results, which may meet the stringent requirements of passive tag localization needed for automatic identification (AutoID) and Real Time Location Systems (RTLS). Combining UWB (semi-) passive RFID with already existing Ultra High Frequency (UHF) technologies can be a possible solution to exploit energy harvesting or to implement a wake-up function in order to increase the battery life of a semi-passive tag. Tag antenna design is one of the most challenging issues to be solved in systems combining UWB and UHF passive RFID solutions, because of the need to co-localize two radiators operating in two different frequency bands in a limited volume. A co-localized tag antenna has been designed to operate in the RFID European band at 868 MHz and in the European UWB lower band between 3.1 and 4.8 GHz. In order to limit the size of the overall antenna system, the design strategy consisted in combining the structural properties of compact antennas. The proposed antenna is composed of a miniature UHF slot and a UWB planar disc monopole. Both antennas are on a single layer low cost FR4 dielectric substrate, 0.8mm thick. In particular the UHF slot is etched on the UWB monopole ground plane in order to reduce the tag dimensions. This slot presents folded arms which allow antenna miniaturization while the UWB circular monopole advantageously exploits the metallic part of the UHF slot antenna as a ground plane, to realize the "image" needed for an efficient wideband behavior. The UWB monopole is fed by a 50Ω coplanar waveguide, to place the ground plane in the same layer than the resonating part. The multi-port antenna is designed in order to be connected to two different chips addressing respectively the UHF and the UWB bands, which are placed on the non-metallic plane of the tag.

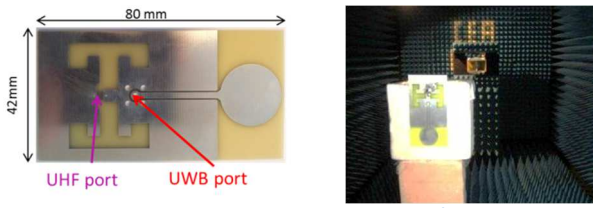

Figure 1: UHF-UWB Tag antenna prototype and measurements in CEA-LETI anechoic chamber.

The proposed antenna design is shown in Figure 1. Its overall size is 80×42×0.8 mm^3, i.e less than a credit card size. Each radiator is connected to its chip through vias in the dielectric substrate.

The UHF chip reference differential impedance is 4-j170 Ω. The measured bandwidth at -6dB of the UHF antenna is 855-880MHz when an open circuit is placed on the UWB antenna. For the UWB part, the antenna input matching band, with respect to -10 dB, is 2.7-4.8 GHz in simulation and 2.7-4.6 GHz in measurements when an open circuit is placed on the UHF antenna.

Antenna radiation measurements have been carried out in anechoic chamber. In order to reduce the RF cable parasitic effects, radiation measurements were performed by using an optical link. The maximum realized gain of the UHF antenna is 2dBi in the azimuth plane, while the average realized gain over the UWB band is 2.6 dBi.

Due to the limited size of the UHF antenna ground plane, the UHF slot radiates as an electric dipole. This mode creates strong currents on the ground plane. A strong coupling effect (-5 dB) between the two radiators is noticed in the UHF band around 868 MHz, while the coupling is very low (-30 dB) in the UWB frequencies (Figure 2). To complete the analysis, load modulation effects on antenna performance have been investigated. As the UHF antenna is connected to a chip acting as a backscattering modulator, an open circuit, a short circuit and a 50 Ω loads have been considered on the UWB port. UWB loading variations modify the UHF reflection coefficient as predicted by the coupling results. UHF antenna impedance matching band shifts from 857-870MHz to 866-882MHz when varying the UWB load from short circuit to 50 Ω. On the other hand, the load variation on the UHF antenna as a small effect on the UWB reflection coefficient and even for the worst case (open circuit), the UWB bandwidth is preserved. The antenna design fulfills the specifications in bandwidth, matching and radiation characteristics in their respective band.

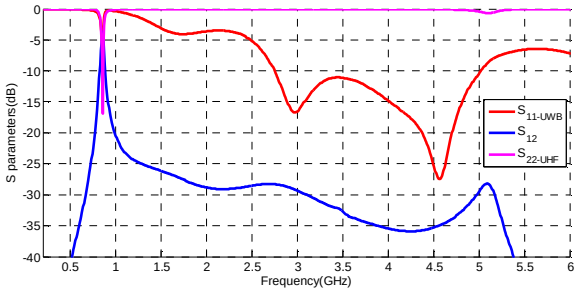

Figure 2: S parameters for the UWB (port 1) and UHF (port 2) antennas.

Related publications:
[1] R. Rosini, R. D'Errico, "Space-time correlation for on-to-Off Body channels at 2.45 GHz," 7th European Conference on Antennas and Propagation (EuCAP), April 8-12, 2013, Gothenburg, Sweden.
[2] M. Pigeon, R. D'Errico, C. Delaveaud, "UHF-UWB tag antenna for passive RFID applications," 7th European Conference on Antennas and Propagation (EuCAP), April 8-12, 2013, Gothenburg, Sweden.

Radio channel modeling for on-to-off-body communication

Research topics : radio channel, Body Area Networks

R. Rosini, R. D'Errico

ABSTRACT: Starting from a real-time dynamic measurement campaign performed at 2.45 GHz, off-body channel models taking into account the space and time correlation have been proposed. The study investigated the relationship between fading effects characterizing different links and the time correlation of a single channel. Several on-body node positions were considered and the results obtained with different antenna designs and in different measurement conditions are presented and compared.

Body-centric communications have been gaining a growing attention in recent years, due to their wide range of application possibilities. The main attention was initially paid to "on-body" transmissions, where the ends of the communication link are all located on the same human body. More recently, the interest moved to the study of communications between nodes on the body and some external devices, for example an Access Point (AP) in the off-body scenario (Fig.1).

CEA-LETI is working on the channel modeling for on-body, off-body and body-to-body communications mainly at 2.45 GHz. Previous work at CEA-LETI proposed an experimental radio channel model, given as composed of a channel gain and short-term fading contributions. The body effect on channel characteristics was also highlighted through a body shadowing component.

The off-body channel model was recently completed by the evaluation of the space and time correlation properties of the different links under investigation [1]. These aspects are of outmost importance for providing system designers with some useful guidelines. In a first place, space correlation aims at evaluating the relationship between fading effects of different links. Cooperation possibilities among nodes can be then investigated, considering the different channel behavior experienced by nodes placed in specific positions. It was calculated through the cross-correlation values obtained in dynamic conditions, for two antenna designs and for different measurement scenarios (i.e. Line of Sight (LOS) and Non Line of Sight (NLOS), where NLOS is the case where the human body completely shadows the direct communication path). LOS cross-correlation turns to be strictly dependent on the node positions, whereas in NLOS this dependency is reduced due to the shadowing effect of the body and it results in stronger correlations (Fig.2). Moreover, normally-polarized antennas yield to large cross-correlation values in NLOS conditions, as compared to tangentially oriented devices, due to the enhancement of creeping waves diffusion on the body.

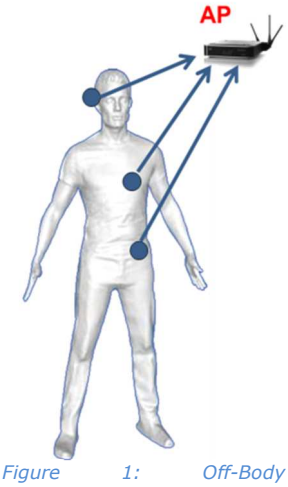

Figure 1: Off-Body Communications.

As for the time correlation, it is computed as the normalized channel autocorrelation function, and it defines its stability over time. Antenna type and measurement conditions have a strong impact on correlation properties. In particular, moving from LOS to NLOS results in faster channel decorrelation. Autocorrelation functions are less stable over time, presenting less smooth evolutions due the stronger fading effect characterizing the NLOS condition.

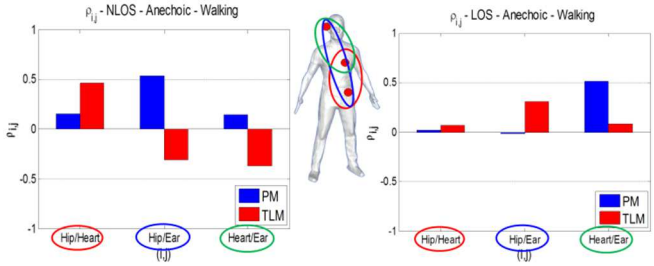

Figure 2: Cross-correlation values in walking conditions, for two antenna designs.

In additions the values obtained from the channel modeling were used as a benchmark for the validation of a simulation campaign, which aimed at assessing the impact of body dynamics on antennas radiation pattern [2]. Simulations were performed considering a node position and antennas characteristics similar to the one accounted for in the experimental campaign. Results show a good agreement between the trend for the simulated and the measured channel gain, with some dissimilarity due to the environment considered in the two cases, to local variations of nodes on-body position, to the movement performed by the users or reproduced via simulations, and to the different body physical characteristics.

Related publications:
[1] R. Rosini, R. D'Errico, "Space-time correlation for on-to-off body channels at 2.45 GHz," 2013 7th European Conference on Antennas and Propagation (EuCAP), April 8-12, 2013, Gothenburg, Sweden.
[2] M. Mackowiak,R. Rosini,R. D'Errico, L.M. Correia, "Comparing off-body dynamic channel model with real-time measurements," 2013 7th International Symposium on Medical Information and Communication Technology (ISMICT), March 6-8, 2013, Tokyo, Japan.

Adaptive, flexible and ultra-low-power MAC protocols for wireless body area networks: from specification to implementation

Research topics : MAC protocol, Body Area Networks, low-power communications

M. Maman, D. Miras, L. Ouvry

ABSTRACT: Wireless Body Area Networks (BAN) require an adaptive, dynamic and flexible Medium Access Control (MAC) to cope with a variety of requirements. This protocol enables to collect multiple real-time motional and emotional sensor informations at different places on the human body and to wirelessly transmit them towards dedicated devices or computers. As body posture highly affects MAC protocols performances, we proposed a protocol based on BATMAC that automatically detects the shadowing effect and quickly adapts the relaying scheduling to BAN changes. Our protocol makes a trade-off between the quality of service (QoS) and the energy consumption depending on the environment conditions and user activities and needs.

Wearable wireless technologies have raised interest in modern applications such as smart fabrics and interactive textile, robotics, gaming and health. The propagation channel associated with BANs is slowly varying considering the human motion and the connectivity of the network suffers from shadowing and fading variations due to the proximity of the human body and its environment. The vicinity of the human body is thus a challenging environment for the design of communication protocols for BAN. These protocols enable forwarding between distributed BAN sensors so that individual data transmitted by each is easily identified, received without error and transmitted to a central station for further processing and visualization.

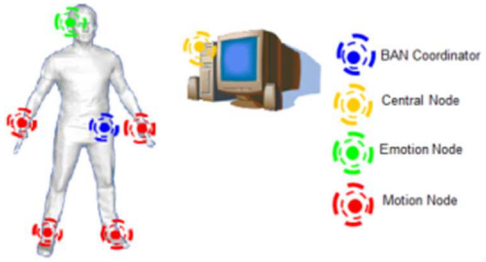

Figure 1: Description of a BAN.

Figure 1 illustrates an example of a BAN. The devices have different roles according to their functionalities and their energy capabilities. The BAN coordinator is in charge of forming and maintaining the network, maintaining synchronization and managing the channel access. The central node is the interface with the PC. Two sensor nodes are defined, the motion sensor integrated in textile and the audio sensor integrated in a headset.

BATMAC, a self-organizing, adaptive and flexible protocol, automatically adjusts the parameters of the IEEE 802.15.4 superframe, detects the shadowing effect and quickly adapts the relaying scheduling to BAN changes. This protocol has been implemented on a SoC combining a dedicated low-power 868-915 MHz radio optimized for BAN and a low-power 32-bit icyflex DSP core [1].

The implemented communication protocol stack is as follows. The Hardware Abstraction Layer (HAL) provides a programming interface between the protocol stack and the specific drivers. Separating the protocol stacks and the hardware has significantly simplified the management of the physical layer and facilitates the software reuse. The radio layer, controlled by the HAL, defines possible states and optimizes the current consumptions and the time necessary to switch to another mode. The MAC layer provides channel access control mechanisms to several communicating devices and is responsible for the association and disassociation of devices (network formation), the maintenance of the network and the management of the access to the radio channel. The Logical Link Control (LLC) layer can simultaneously manage several data flow to MAC layer and provides bandwidth and QoS. Each flow category is defined by one or several associated profiles. A profile is defined by some QoS parameters managing the MAC layer (e.g. the priority levels, the period used, the time to live, the maximum tolerable Packet Error Rate (PER), the packet rate and the acknowledgement, retransmission and relaying policies). When a packet has to be sent through the radio channel, the application creates a flow and selects its first profile with corresponding QoS. If a profile does not provide a sufficient QoS, the flow switches to another profile with better QoS but higher power consumption. Hence, thanks to several profiles defined in the LLC layer, the MAC layer becomes transparent for the application.

Table I gives the PER and Energy Consumption per useful Bit (EC/B) measured for several traffics and link budgets. The calculation of the EC/B considers the total amount of energy used to transmit a useful data i.e. the energy used by the coordinator, the relay and the originator.

Table I: PER and energy consumption for several traffics and link budgets.

PER / Consumption /Bit / Link Budget	Direct		Relaying		Direct with RTX		Relaying with RTX	
average value = -70dBm	6.3%	**512 nJ/bit**	0%	825 nJ/bit	5.5%	562 nJ/bit	0%	862 nJ/bit
average value = -75dBm	14%	**562 nJ/bit**	0%	837 nJ/bit	12.3%	612 nJ/bit	0%	875 nJ/bit
average value = -80dBm	26.7%	**675 nJ/bit**	0%	850 nJ/bit	23.6%	712 nJ/bit	0%	900 nJ/bit
average value = -85dBm	43.2%	887 nJ/bit	0%	**862 nJ/bit**	38.2%	912 nJ/bit	0%	950 nJ/bit
average value = -90dBm	61.1%	1325 nJ/bit	0%	**875 nJ/bit**	54.2%	1275 nJ/bit	0%	962 nJ/bit

We can note that the EC/B increases when relaying or retransmission functionalities are activated. The direct traffic has the best EC/B in the least restrictive environments but in the most restrictive environment, the relaying traffic becomes more efficient.

This protocol is a very interesting piece of technology with respect to existing/emerging BAN protocols since it provides all features to potentially map most of the identified applications in the BAN area while offering the right level of performance. It also provides innovative features like dynamic relaying and traffic flow arbitration to optimize QoS and/or battery lifetime depending on user needs.

Related publications:
[1] M. Maman, D. Miras and L. Ouvry, "Implementation of a self-organizing, adaptive, flexible and ultra low-power MAC protocol for Wireless Body Area Networks", in 24th Annual Int. Symp. on Personal, Indoor, and Mobile Radio Communications (PIRMC), Sept. 8-11, 2013, London, UK.

Heterogeneous wireless body area networks for joint coarse motion capture and navigation applications

Research topics : radio localization, body area networks, motion capture

J. Hamie, B. Denis

ABSTRACT: Positioning solutions adapted to heterogeneous Wireless Body Area Networks (WBANs) are proposed to jointly address indoor navigation and motion capture applications. On-body devices are localized at the building scale by combining peer-to-peer range measurements over intra-WBAN links and additional measurements from external anchors forming the building infrastructure. Following a 2-step approach, we first perform decentralized relative positioning at the body scale, before applying adequate transformations into the absolute global coordinates systems thanks to a few reference on-body nodes. A graph completion method is also considered to mitigate body shadowing effects and approximate erroneous or missing range measurements.

As an alternative to costly, geographically restricted, power greedy and/or drift-sensitive capture technologies, stand-alone wireless localization solutions (on and around the body) have been investigated recently, making direct and opportunistic use of the transmitted radio packets in low-power Body Area Networks (BAN), with tolerated low precision levels. They rely on cooperative peer-to-peer range measurements through e.g., Time Of Arrival (TOA) estimation over Impulse Radio-Ultra Wideband (IR-UWB) links or even Received Signal Strength Indicators (RSSI) over narrowband links. But the latter solutions also suffer from body shadowing and partial connectivity under pedestrian mobility, as well as poor relative on-body ranging precision.

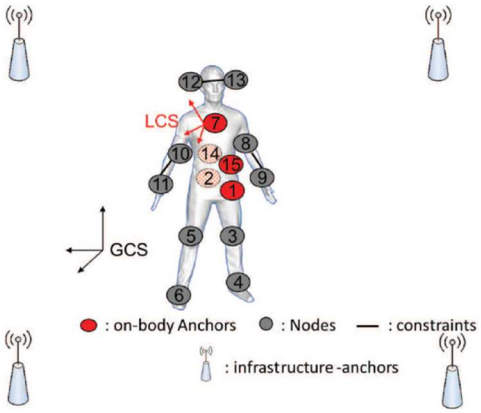

Figure 1: Typical heterogeneous WBAN deployment for the absolute localization of on-body nodes.

In [1], we proposed to combine relative motion capture (i.e. at the body scale) and absolute single-user navigation (i.e. at the building scale) capabilities within one single heterogeneous WBAN scenario. More particularly, we have considered using on-body links in a mesh intra-WBAN topology (e.g. slightly modified IEEE 802.15.6 standard), as well as off-body links (e.g. IEEE 802.15.4 or 15.4a standards) with respect to fixed elements of infrastructure, set as anchors (Fig. 1). The idea is that both components could be mutually beneficial, while preserving the finest precision of relative localization over large-scale trajectories, contrarily to our previous work, where the precision of relative localization at the body scale was degraded by the introduction of off-body links. Different options and scenarios have been compared in terms of location-dependent radio metrics (i.e. TOA, TDOA, RSSI), synchronization constraints and transmission ranges. We have also proposed a specific 2-step algorithm. The proposed solution first performs the relative localization of on-body nodes in a body-strapped Local Coordinates System (LCS) through decentralized positioning, before applying adequate transformations to express the estimated coordinates into an absolute Global Coordinates System (GCS) external to the body. We also take advantage of the presence of multiple on-body nodes to mitigate body obstructions with respect to external anchors through distance approximations based on neighborhood information and graph completion methods ("shortest path" approximations). Relying on realistic ranging error models [2], simulation results (Fig. 2) show that absolute on-body localization at the building scale could be almost as precise as relative on-body localization at the body-scale. Penalized nodes located at the body extremities, suffering from lower connectivity, poor geometric dilution of precision and higher accelerations (ID: 4, 6, 9 and 11) also benefit from a better robustness. Related use cases could concern coarse attitude detection and gesture-based remote control.

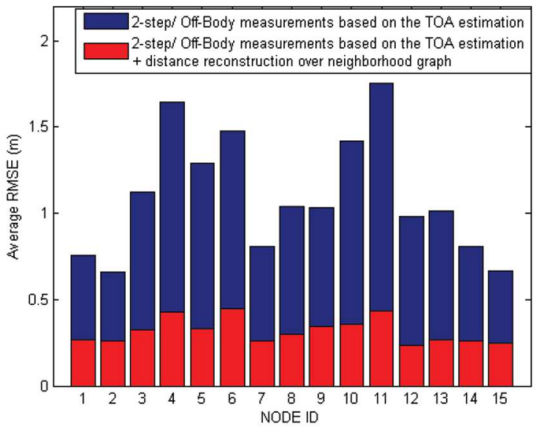

Figure 2: RMSE of estimated locations per on-body node (ID) with the two-step algorithm based on TOA over off-body links and distances approximation over neighborhood graph.

Related publications:
[1] J. Hamie, B. Denis, C. Richard, "Joint Motion Capture and Navigation in Heterogeneous Body Area Networks with Distance Estimation Over Neighborhood Graph", in proc. Workshop on Positioning, Navigation and Communication 2013, Dresden, March 2013.
[2] J. Hamie, B. Denis, R. D'Errico, C. Richard, "On-Body TOA-based Ranging Error Model for Motion Capture Applications within Wearable UWB Networks", in Journal of Ambient Intelligence and Humanized Computing, ACM/Springer, Dec. 2013.

Entropy harvesting from physical sensors

Research topics : secure communications, random numbers generation

C. Hennebert, C. Lauradoux (INRIA), H. Hossayni

ABSTRACT: Finding entropy sources is a major issue to design non-deterministic random generators for headless devices. Our goal is to evaluate a collection of physical sensors as potential sources of entropy. A challenge in the analysis of these sources is the estimation of min-entropy. We have followed the NIST recommendations to obtain pessimistic estimations from the dataset collected during our campaign of experiments. The most interesting sensors of our study are the accelerometer, the magnetometer, the vibration sensor and the internal clock. Contrary to previous results, we observe far less entropy than it was expected before. Other sensors which measure phenomena with high inertia such as temperature or air pressure provide very little entropy.

Non-deterministic random bit generators (NDRGB) play an important role on security as cryptographic keys, since seeds or padding are based on random numbers. The best way to generate a "true" random number consists in rolling a dice. But how to reproduce, or at least to approach, the result of a dice roll into a headless device?

Into such scarce devices that communicate wirelessly, random disorder could be observed in three types of sources: internal clock jitter, physical sensor noise, and wireless statistics. In this paper, we focus on the entropy that can be collected from the analogous physical sensors and the internal clock of the Zolertia Z1 node.

All standards in the literature, including RFC 4086, the German BSI report AIS 20 and AIS 31, and the NIST report SP800-133, emphasize the need to analyze the entropy sources. These standards provide statistic tools to analyze the output of the random bit generator and to evaluate if the numbers obtained after a cryptographic processing is independent and identically distributed (IID). But, the source analysis is omitted and the security of many systems can be ruined by this omission when an attacker is able to take the control of a source.

In a recent draft, the NIST has recommended several statistical tools to evaluate the quantity min-entropy on physical biased sources. We have followed the process recommended by the NIST and qualified the data sequence sensed in various experiments in order to quantify the amount of entropy brought by each source in a given condition.

To compare entropy sources, we need some metrics for security and efficiency. The Shannon entropy and the min-entropy are the main metrics used to evaluate the entropy. While the Shannon entropy (H(Y)) was the first metric used, it fails to measure the capability of an adversary. Min-entropy ($H_\infty(Y)$) appears as a better metric recommended by the NIST. The estimation of min-entropy differs if the probability distribution of the source data sequence S is known or not. If S is IID, the well-known standard tests cited above are applied. But the data coming from a physical sensing are never IID and always biased. For biased data sequence, five tests are used to compute statistics on the digitized samples and to provide informations on the data structure.

No assumption is done on the probability distribution associated to the source S. Each test reveals information on the unknown distribution given a statistical measurement. The entropy is evaluated by minimizing over this set of distribution. The five tests are:

- The Frequency Test Est1(Y) counts the occurrence of the most likely sample value.
- The Collision Test Est2(Y) estimates the probability of the most likely state in the dataset.
- The Partial Collection Test Est3(Y) estimates the entropy based on the diversity of the values produced as output.
- The Compression Test Est4(Y) builds a dictionary of values based on the Maurer Universal Statistic.
- The Markov Test Est5(Y) models the dependencies in the dataset.

The entropy estimators have been applied to many physical sources on data sequences acquired in various experimental conditions. Each data sequence is composed of, at most, one million samples. In the example details in figure 1, we can observe that the Shannon estimator over-estimates the entropy. The most pessimistic estimators are the partial collection test and the compression test. The frequency test and the classical min-entropy test leads to close min-entropy values.

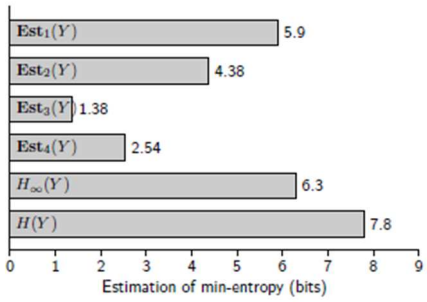

Figure 1: Different entropy measurements for the vibration sensor excited at 30Hz.

Our study has highlighted that the best candidate to produce entropy are the vibration sensor, the magnetic sensor and the internal clock. The accelerometer provides a significant amount of entropy when only one axis is considered at each sample acquisition because its three axes are correlated.

Related publications:
[1] C. Hennebert, C. Lauradoux and H. Hossayni, "Entropy Harvesting from Physical Sensors", 6th ACM Conference on Security and Privacy in Wireless and Mobile Networks (WiSec'2013), April 2013, Budapest, Hungary.

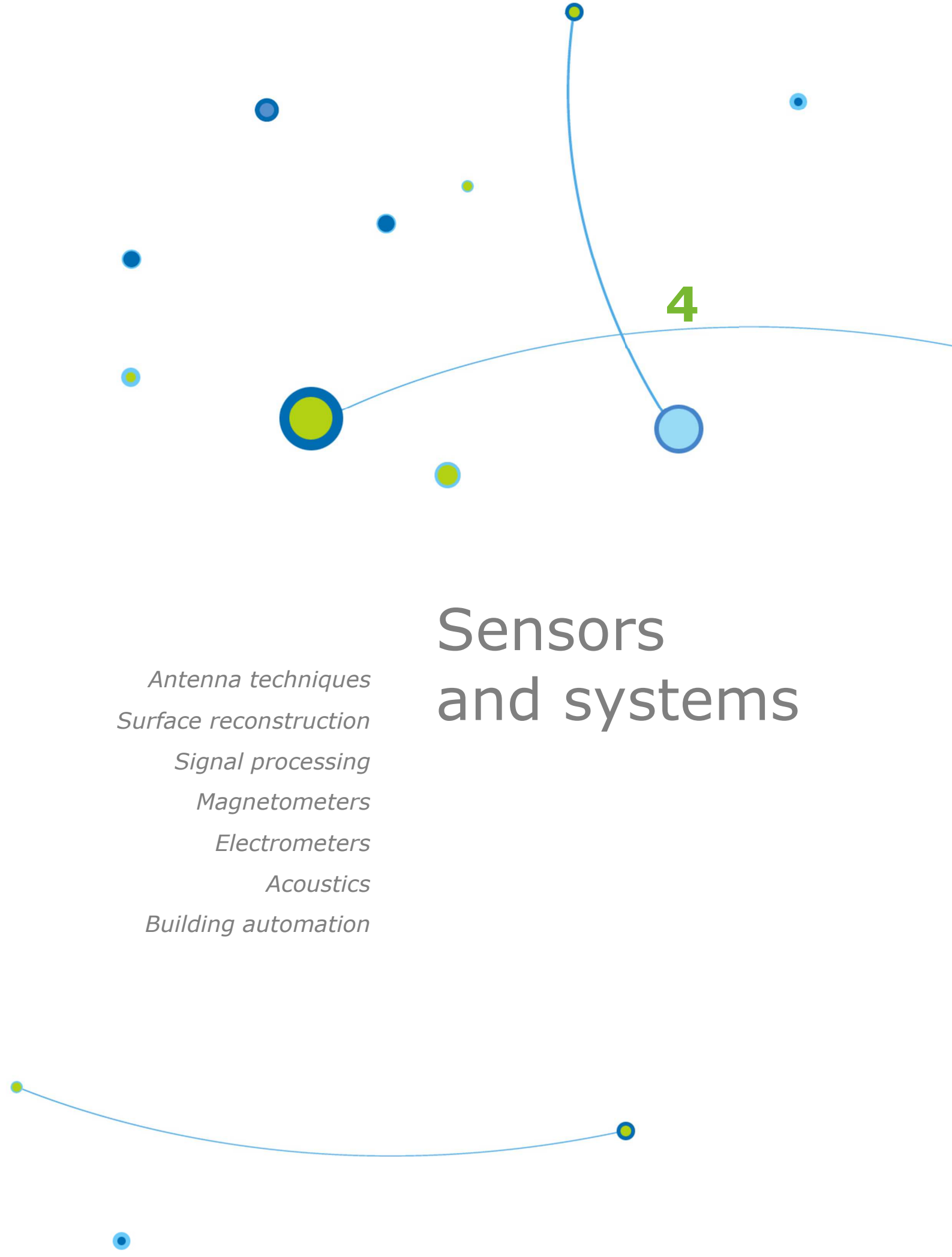

4

Sensors and systems

Antenna techniques

Surface reconstruction

Signal processing

Magnetometers

Electrometers

Acoustics

Building automation

Optically modulated scatterer probe for in-situ antenna monitoring

Research topics : antennas characterization, retro-modulated scattering

L. Ghattas, S. Bories, D. Picard (Supelec), P. Pouliguen (DGA)

ABSTRACT: This paper proposes to evaluate the benefit of an in-situ measurement system for detecting and compensating the disturbance of antenna radiation due to unexpected close obstacle scattering. A model combining 3D electromagnetic simulations and system level simulations allows analyzing quantitatively the effect of a biased calibration in the presence of near scatterers. Two major requirements have to be considered in order to provide perturbation-free measurements. First, the monitoring system should be in the near field of the antenna. Meanwhile, its presence should not perturbate the nominal radiation of the antenna. The optically Modulated Scatterer technique (OMS) is selected. A formulation to optimize the dimensioning of a probe array is also presented.

Antenna arrays operate at their peak performance when they are well calibrated at the factory. When deployed in a real environment, they might be subject to unpredictable disturbances. That's why recalibration after operational deployment is required but is usually not done due to practical difficulties. It is therefore necessary to develop an 'in-situ' measurement system for detecting the real-time perturbations introduced by potential obstacles in the reactive near field region affecting its radiation pattern.

In order to highlight the benefit of an 'in-situ' measurement system, the application of Direction Finding (DF) is studied. A model combining 3D electromagnetic simulations, a complete receiver model and a MUSIC direction of arrival algorithm (Fig. 1) is developed.

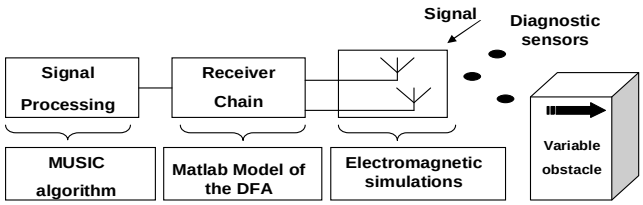

Figure 1: Model of the Direction Finding system and signal processing channel.

To assess the impact of near scatterers on the performance of antennas, the DF accuracy is calculated for a configuration where an obstacle not considered in the first calibration is present. Degradation greater than 20 dB on the performance of DF is observed especially when the antenna is close to the scatterer [1].

When the near field is perturbed by an obstacle, the proposed monitoring system detects the field components shift thanks to an indirect approach [1]. It consists in marking the field at each probe location using a modulated scatterer. The selected Optically Modulated Scatterer (OMS) technique has two major advantages: insensitivity to scattering and non-invasiveness measurements since no wired RF cable neither DC bias wires is required between the probe and the receiver. Fig. 2 shows the bistatic configuration of the OMS technique. The OMS probe is composed of a small dipole loaded by a photodiode. The load of the probe is changed by a low frequency modulation signal carried by optical fiber and switching the photodiode between two states ON and OFF. As a result, the modulated component of the voltage at the output terminals of the receiving antenna is related to the complex amplitude at the probe position. The spectrum of the received signal contains a carrier at the measurement frequency and harmonic spectral lines due to modulation.

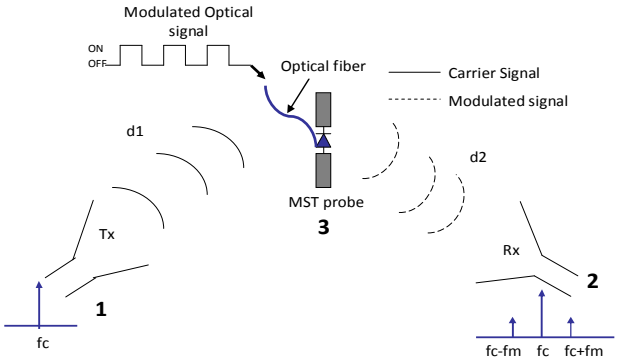

Figure 2: Bistatic configuration of the OMS technique.

Since the OMS probes should be placed in the near field of the antenna and as there is no formula to compute the link budget in the near field, a new formulation to compute the modulated backscattered power in the near field of the antenna is developed in [2].

Eq. 1 shows the Fourier coefficients for the first sideband of the complex voltage at the receiving antenna port.

$$V_{n,\sin} = \begin{cases} \frac{4}{n\pi} Z_{rs} Z_{st} \left(\frac{1}{Z_{ss} + Z_{OFF}} - \frac{1}{Z_{ss} + Z_{ON}} \right) I_t & n \text{ odd} \\ 0 & n \text{ even} \end{cases}$$

$$V_{n,\cos} = 0$$

Where Z_{rs} describes the mutual impedance between the AUT and the OMS probe, Z_{ts} the mutual impedance between the transmitter and the OMS probe, Z_{ss} the probe impedance and Z_{ON}, Z_{OFF} represent the photodiode impedance in the ON and OFF states respectively.

This formulation allows optimizing the design of probes in order to meet a compromise between low invasiveness and high sensitivity. The sensitivity can be improved by adding a matching network to the probe [2] without degrading severely the frequency bandwidth of the system.

Related publications:
[1] L. Ghattas, S. Bories, D. Picard, P. Pouliguen and P.Poteir, "Benefit of a moniotring system in-situ for direction finding antennas", Antenna Measurement Techniques Association (AMTA) 35th annual meeting, Columbus, Ohio, October 6-11, 2013.
[2] L. Ghattas, S. Bories, M. Hirvonen, and D. Picard, "Broadband optically modulated scatterer probe for near field measurements," Antenna Measurement Techniques Association (AMTA) 35th annual meeting, Columbus, Ohio, October 6-11, 2013.

Low-cost GNSS antennas phase center variations characterization for UAV attitude determination applications

Research topics : antennas characterization, phase calibration

S. Bories, Y. Méhut, Ch. Delaveaud

ABSTRACT: A mass market GNSS antenna calibration method is evaluated, with a special focus on the significant errors due to phase variations of the receiving antennas. Measurements in an anechoic chamber are processed with an algorithm used to compute the mean Phase Center (PC) and its associated Phase Center Variation (PCV) for all angular directions. PC and PCV are then computed when four antennas are placed near the command unit of an unmanned aerial vehicle (UAV). The impact of this structure is evaluated thanks to PCV maps. Two low-cost COTS antennas PCV maps are compared with regards to their geometry.

Accuracy in attitude, position and velocity at a low cost is required in a great number of real-time applications such as vehicle guidance and tracking. The European project called LOGAM aims to design and develop a truly low-cost attitude determination and navigation system, which would be initially embedded in a rotary-wing UAV. This navigation system is primarily based on non-dedicated mass market GNSS (single frequency) receivers and antennas, and is aided by MEMS inertial sensors.

As far as carrier-phase computation is concerned, the relative position of multiple antennas placed on any platform can be determined with enough precision to estimate the attitude angles of such a vehicle using the sub-centimetric carrier phase precision of GNSS signals [1]. The overall performance of the system is determined by its ability to measure phase differences between signals received from the four antennas (of which phase center variations are compensated) forming 2 or 3 baselines, the length of which being respectively 50 cm and 71 cm. Note that PCV compensation is especially important when the close environment individually affects the phase behavior of each of the four antennas. Then, for each antenna, this PCV calibration is taken into account during the double difference carrier phase algorithm in order to accurately estimate the UAV attitude angles.

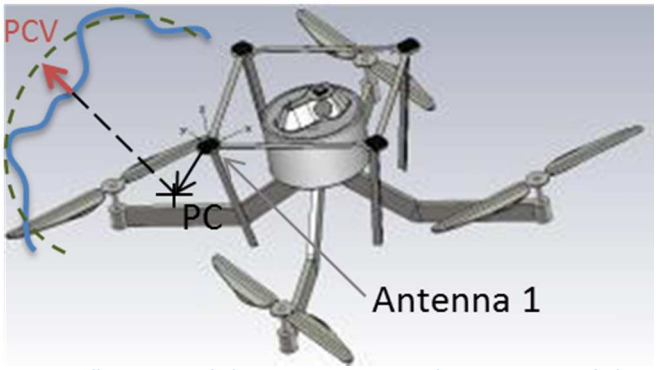

Figure 1: Illustration of the PCV concept on the Antenna 1 of the UAV with the ideal (spherical) phase front (grey dash) and real phase front (blue).

As illustrated in Figure 1, the PCV (Phase Center Variation) is nothing more than the residual difference between the ideal spherical phase pattern and the measured one [2]. Note that the origin of the coordinate system is the center of rotation defining both the azimuth and elevation angles.

Due to its large ground plane the Bullet III antenna has a very "clean" phase pattern, in which one can find both the rotational symmetry and the typical elevation behavior. Its PCV varies in the range ±4 mm. Conversely, the phase pattern of the Titan III antenna is quite clearly affected by the small size of its ground plane. Its cable configuration also impacts the phase pattern with regards to the azimuth axis. Its PCV values are comprised between -6 and 8 mm which is roughly twice the excursion obtained for the Bullet III.

Based on the characterization of ten samples of the Titan III antenna (different serial numbers), the mean PCV and the related standard deviation have been estimated. For the upward hemisphere directions, the standard deviation for the ten PCV maps is always lower than 3 mm. This reproducibility analysis ensures that only one indoor calibration campaign is needed to calibrate one particular antenna type.

Once the four antennas are installed on the top of the UAV body, PCV are measured in the 20-m long CEA anechoic chamber. PCV maps show an important degradation (PCV range between -20 and +25 mm) (Fig. 2); that is 4 times the PCV range for isolated antenna. The accurate calibration of such complex PCV behavior is dedicated to a given geometrical configuration. To mitigate this high sensitivity, antennas can be raised up by about 10 cm above the top of the UAV structure. As a result the PCV range is divided by a factor of two (with a PCV range between 0 and 10 mm) at the cost of a limited extra height for the UAV configuration.

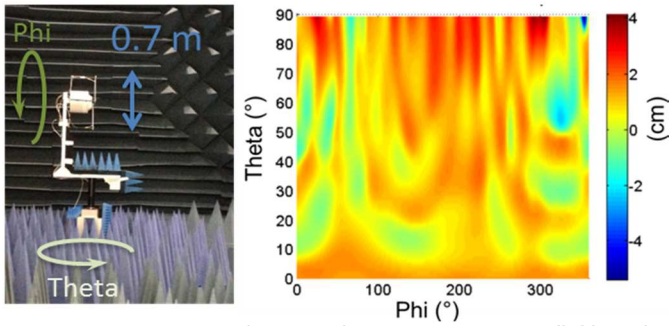

Figure 2: Antennas on the UAV during measurement (left) and simulated PCV (cm) calibration map of the antenna 1 within the UAV configuration (right).

Related publications:
[1] G. Falco, E. López, F. Zacchello, S. Bories, "Double Difference Carrier Phase Tightly-coupled and Low-cost GNSS/INS System for UAV Applications", ION GNSS+ meeting, Sept. 16-20, 2013, Nashville, Tennessee.
[2] S. Bories, Y. Méhut and Ch. Delaveaud, "Low-cost GNSS Antennas Phase Center Variations Characterization for UAV Attitude Determination Applications", Antenna Measurement Techniques Association (AMTA) 35th annual meeting, Columbus, Ohio, October 6-11, 2013.

Geometric models for the reconstruction of instrumented shapes from inertial sensors

Research topics : shape capture, geometric modeling

M. Huard, N Saguin-Sprynski

ABSTRACT: For several years, CEA-LETI developed Morphosense, a physical ribbon-like device instrumented with attitude sensors. The combined use of accelerometers and magnetometers allows Morphosense to provide its spatial orientation along the curve followed by the ribbon. Several methods of interpolation of these tangential data have been developed, with which one can reconstruct the shape of the ribbon. We focus here on two ways of development: first, we develop new methods for curve reconstruction; then, we use these methods for quasi developable surfaces from geodesic curves for the case where geodesics are planar curves.

The aim of this work is to reconstruct the curve followed by the Morphosense by the means of an interpolation method. This interpolation problem presents two distinctive and challenging features. First, the knots of sensors only provide their orientation: we do not know their absolute location in space. Therefore, the problem is not to be confused with a classic Hermite interpolation one. On the other hand, we also want to find a solution for which the segments between two adjacent knots will match the actual known length of the ribbon between them. These lengths are to be taken into account as constraints of the interpolation problem.

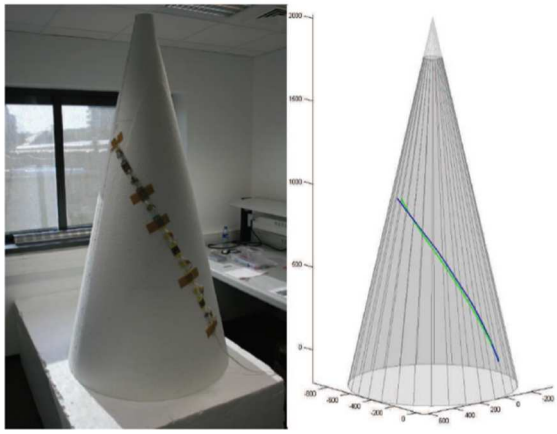

Figure 1: Curve reconstruction from a ribbon of sensors via this method of PH, and experimentation.

The problem has already been addressed by the means of an arc-length parameterization, which allows having a control on the length of the interpolated curve. These methods amount to interpolate the hodograph (derivative) of the curve on the unit sphere. They perform quite well, though such a parameterization is constraining and precision is lost when the spherical splines must be integrated numerically to obtain the interpolated curve. We follow another approach here, using C2 spatial Pythagorean-Hodograph quintic spline curves [1]. The algebraic structure incorporated in the hodograph of PH curves offers many useful computational advantages over ordinary polynomial parametric curves. For example, they possess rational offset curves, and are well suited for real-time CNC interpolator algorithms, used to drive computer-controlled machines along curved paths with a prescribed speed variation. Most importantly for our problem, there exists an exact, closed-form expression for their arc lengths, which will prove crucial for the control of the length of our reconstructed curves.

In the context of our application, it leads to more precise, physically coherent solutions for the reconstruction problems. Since the length highly influences the shape of interpolated curves, it could also be a useful design tool for CAGD. When the length of the target curve is known, it also allows an enhanced reconstruction precision in case of a weak sampling of the curve.

Next, let us talk about the surface reconstruction from a set of curves. Following our previous work on the reconstruction of surfaces from the Morphosense ribbons, we introduce geometric models of the surfaces so as to perform a more precise reconstruction depending on the type of surface we want to reconstruct. We focus on methods where quasi developable surfaces are defined from geodesic boundary curves. Here, for a significant amount of objects, these boundaries can be planar (each curve is in a plan). Then constraints for defining a surface where these curves are geodesics are simplified, and we can find the shape solution [2].

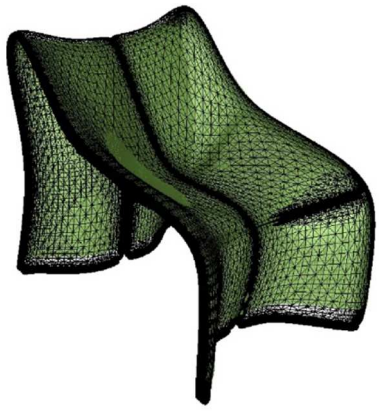

Figure 2: Results of surface reconstruction from boundaries planar geodesics curves.

Related publications:
[1] M. Huard, R. Farouki, N. Sprynski, L. Biard, "Splines PH quintiques pour l'interpolation C2 sous contraintes de longueur" GTMG 2013, March 27-28, 2013, Marseille, France.
[2] M. Huard, "Modélisation géométrique et reconstruction de formes équipées de capteurs d'orientation", PhD thesis, University of Grenoble, France, 2013.

New algorithm for footstep localization using seismic sensors in an indoor environment

Research topics : localization, signal processing

R. Bahroun, O. Michel , F. Frassati , M. Carmona , J.L. Lacoume

ABSTRACT: Seismic sensors are considered for footstep localization in indoor environments. A classical localization technique is to measure time differences of arrival (TDOA) from the signal source by multiple receivers. However, classical algorithms assume a constant propagation velocity as a function of the source position, which is not the case in, a bounded medium such as a concrete slab (encountered in indoor environment) where the propagation is usually dispersive and damped. Considering a Kelvin–Voigt damping model, we introduce the notion of perceived propagation velocity, which decreases with the source-sensor distance. A new localization algorithm is proposed and evaluated based on simulation and experimental data.

The floor of an indoor environment is assimilated to a thin damped isotropic plate. If we consider a plate of thickness h, of infinite extent in the xy plane, the governing equation for the bending motion of a thin damped Kelvin–Voigt model plate is:

$$\rho h \frac{\partial^2}{\partial t^2} u(x,y,t) + D\left(1 + \vartheta \frac{\partial}{\partial t}\right) \Delta^2 u(x,y,t) = f$$

where u is the transversal displacement, $D = Eh^3/(12(1-\sigma^2))$ is the bending stiffness, E is the Young's modulus, σ is the Poisson ratio, ρ is the mass density, Δ is the Laplacian, and f describes the external forces applied on the plate.

We established jointly by stationary phase calculation and numerical simulations of propagated waves, that the perceived velocity (namely the ratio between source-sensor distance d to travel time t of the wave), take the following power law form:

$$c_p = \frac{d}{t} = \frac{d}{\left[\frac{\vartheta}{16a^2} d^4\right]^{1/3}} = \left[\frac{16a^2}{\vartheta d}\right]^{1/3}.$$

where "a" is a mechanical characteristic of the concrete slab. Figure 1 plots the envelope of the displacement amplitude as a function of time and source-sensor distance and shows that the wave slows down as it propagates.

This fact implies that traditional hyperbolic localization methods based on Time Difference of Arrival (TDOA) of the wave between sensor pairs would be inaccurate because the propagation speed of waves cannot be considered as constant. Only the order of arrival of a wave on a sensor set is preserved: the closer the sensor is from the vibration source, the sooner it will receive the wave.

Based on this physical dispersive behavior of flexural waves, we propose a new localization algorithm based on the Sign of Time Difference of Arrival (SOTDOA) of the wave on a pair of sensors.

We compare it with simulations and real life accelerometer signals and show that the new SOTDOA algorithm presents a better RMS localization error than TDOA localization under different constant velocity values (red SOTDOA; green TDOA c=500m/s, black TDOA c=1000m/s, blue TDOA c =1500 m/s, pink C=2000m/s) (Figure 2). With this new robust, calibration less, easy to implement method we reach localization accuracy lower than 1 meter on a 50m² room.

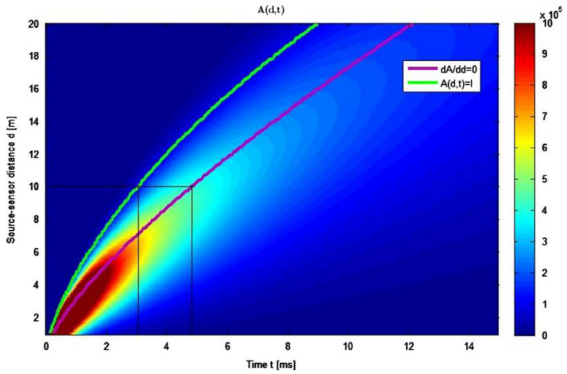

Figure 1: Displacement amplitude as a function of time and source-sensor distance.

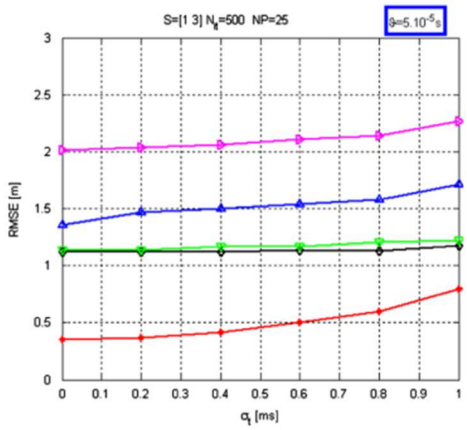

Figure 2: RMS localization error under different constant velocity values (red SOTDOA; green TDOA c=500m/s, black TDOA c=1000m/s, blue TDOA c =1500 m/s, pink C=2000m/s).

Related publications:
[1] R. Bahroun, O. Michel, F. Frassati, M.Carmona, J.L. Lacoume, " New algorithm for footstep localization using seismic sensors", Journal of Sound and Vibrations (2013), http://dx.doi.org/10.1016/j.jsv.2013.10.004i.

Tactile surface characterization using an artificial finger including a 3D force MEMS sensor

Research topics : metrology, MEMS sensors, signal processing

C. Godin, L. Olmos, F. de Boissieu, B. Guilhamat

ABSTRACT: Based on a piezo-resistive three-axial force micro-sensor developed by CEA-Leti, we have built an artificial tactile device dedicated to surface analysis. We showed its ability to discriminate several surfaces and to estimate their physical parameters.

CEA-Leti has developed a very sensitive miniature 3D force sensor which mimics mechanoreceptors of human tactile system [1]. Using this sensor we have developed an artificial tactile system for surface analysis [2]. The system (fig. 2) is made of an artificial fingertip including and protecting the sensor [3] (fig. 1), its acquisition system and two motors and their controllers. External force sensors made by cantilevers associated with inductive sensors are used for calibration and validation purposes (fig. 3).

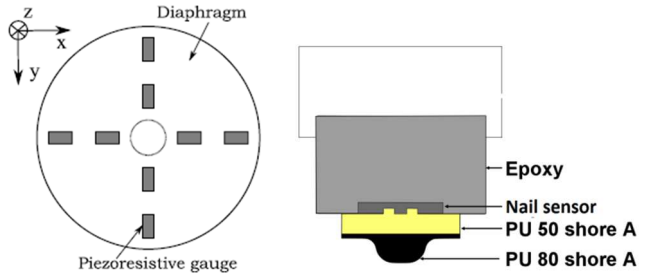

Figure 1: Schematic representation of the sensor (left) and the artificial fingertip (right).

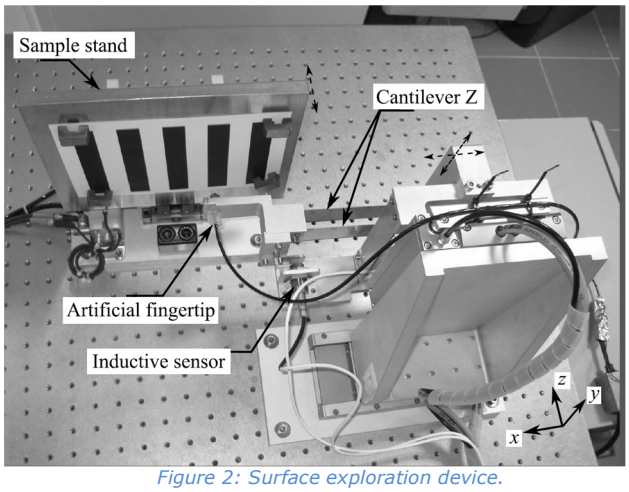

Figure 2: Surface exploration device.

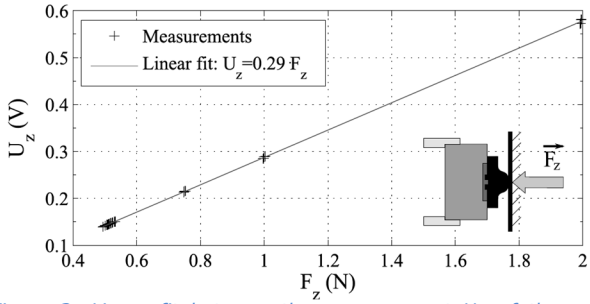

Figure 3: Linear fit between the measurement Ux of the artificial fingertip and the external force sensor measurement Fx using a cantilever and the inductive sensor.

In order to evaluate the ability of the system to discriminate several surfaces, we have chosen 10 papers having different tactile properties but very similar topology. The papers are : printer paper (dry, very fine grain), special paper (hairy, adherent, soft), special paper (smooth, soft), tracing paper (dry, plastified, fine grain), drawing paper (dry, coarse grain), blotting paper (fibrous, dry, important roughness), newspaper (smooth, dry, fibrous), coated paper (very smooth, plastified), drawing paper (dry, medium grain size), photo paper (smooth, sticky). Each paper is explored several times. The signal acquired for each exploration is used as a sample of a database for supervised classification purpose. The rate of correct classification is 92.8±0.9% for learning set, 89±3% for validation set, and 88±5% for test set.

Another application is the estimation of physical or sensorial properties of the surfaces. We have shown that it is possible to estimate the roughness of the surface as well as the friction coefficient between the surface and the finger using the 3 dimensional capability of the sensor [4]. We have also proposed a methodology for estimating several surface parameters [5].

In future work we will consider the use of the sensor to enhance the manipulation of objects by robotic hands. This is one other major application field of artificial tactile systems.

Related Publications :
[1] N. Alcheikh, C. Coutier, S. Giroud, C. Poulain, and P. Rey, "Characterization and modeling of a piezoresistive three-axial force micro sensor," Sens. Actuators Phys., vol. 201, pp. 188–192, Oct. 2013.
[2] M. Boukallel, H. Yousef, C. Godin, and C. Coutier, "Flexible Tactile Sensors for Multidigital Dexterous In-Hand Manipulation," in Flexible Robotics, M. Grossard, N. Chaillet, and S. Régnier, Eds. John Wiley & Sons, Inc., 2013, pp. 181–242.
[3] F. de Boissieu and B. Guilhamat, "Device for the touch-sensitive characterisation of a surface texture," US201211808003-Dec-2009.
[4] L. Olmos and C. Godin, "Method for estimating a roughness of a surface," US201331250227-Nov-2013.
[5] F. de Boissieu and C. Godin, "Tactile surface texture characterization method," US201210954105-Nov-2009.

Forward model computation of magnetostatic fields inside electric vehicles

Research topics : magnetism, electric vehicle

A. Vassilev, (O. Pinaud, O. Chadebec, LL. Rouve, JM. Guichon - G2ELAB)

ABSTRACT: The magnetostatic field inside a simplified electric vehicle-like geometry is analyzed. The developed model allows the evaluation of the shielding effect of the magnetic chassis and frame. It also proposes an equivalent model for the power battery and cables. The study of different configurations leads to the field reduction inside the car.

Vehicle electrification is widely promoted to address environmental issues and reduce the reliance on fossil fuels. However, electric vehicles require a significant number of electrical devices within a quite small space (electric motor, power electronics, power battery, power cables, etc.). As a consequence, electromagnetic fields due to these components may appear inside the cabin. This work is dedicated to the identification and evaluation by simulation of the electromagnetic field generated by batteries and cables [1].

A 3-door-utility electric vehicle from end 90's (Fig. 1) has been chosen for this study.

Figure 1: Studied 3-door-utility electric vehicle.

A numerical model has been built (Fig. 2). The geometry and the mesh are created in Flux3D software. The problem is solved with an integral formulation developed in G2ELab software Locapi, better suited than FEM to compute accurately the magnetic field in air regions.

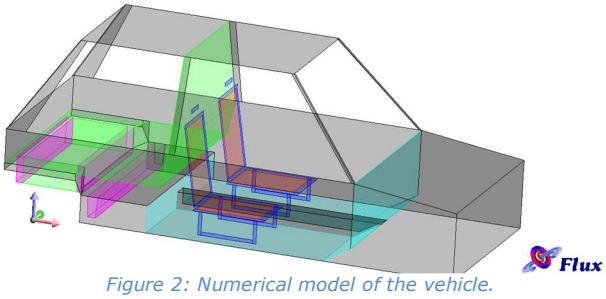

Figure 2: Numerical model of the vehicle.

The model has been used to simulate the induced magnetization due to the earth magnetic field and the magnetic field created by currents inside the power battery and associated cables. The results show a good agreement compared to the measurements (Fig. 3).

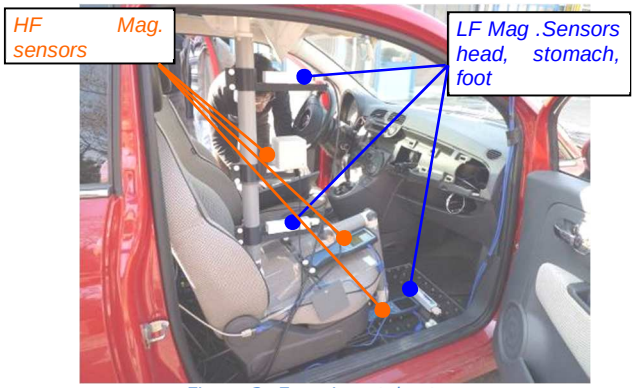

Figure 3: Experimental set-up.

This validated model allows studying new configurations to reduce the magnetic field. We show that a simple cabling modification should drastically reduce (by a factor six) the magnetic field (red curve in Fig. 4). Electrical current cells distribution has also been modified to minimize their contribution thanks to electrical loops management. The field is once more reduced by a factor of three (green curve).

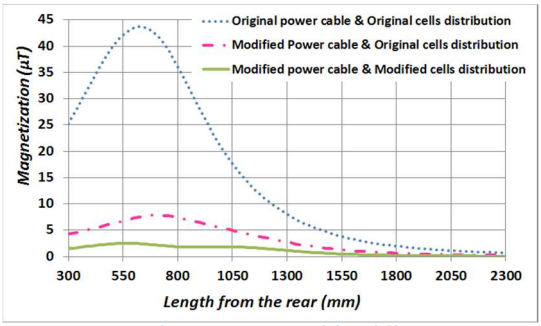

Figure 4: Magnetic induction generated by different versions of the rear battery pack in which 100A flows at 160mm above the battery casing.

This study is a first important step in the characterization and modeling of magnetic fields inside electric vehicles for exposure or CEM purposes. In further works, it may be applied to any new structure that develops strong currents and special attention should be paid to the modeling of higher frequency ranges.

Related publications:
[1] O. Pinaud, O. Chadebec, LL. Rouve, JM. Guichon, A. Vassilev, "Forward Model Computation of Magnetostatic Fields inside Electric Vehicles", 19th Int. Conf. on the Computation of Electromagnetic Fields (COMPUMAG), June 30-July 4, 2013, Budapest, Hungary.

Towards a miniature atomic scalar magnetometer using a liquid-crystal polarization rotator

Research topics : atomic magnetometers

J. Rutkowski, W. Fourcault, F. Bertrand, U. Rossini, S. Gétin, S. Le Calvez, T. Jager, E. Herth, C. Gorecki, M. Le Prado, J-M. Léger and S. Morales

ABSTRACT: This paper reviews the progress made in the miniaturization of an isotropic space-qualified optically pumped magnetometer. Sensor isotropy is provided by a liquid crystal polarization rotator that sets the linear pumping beam polarization at 90° with respect to the ambient magnetic field. This non-magnetic rotator allows a continuous polarization rotation from 0° to more than 300° with response times compatible with mobile or space applications. The miniature helium-4 sensor reaches a sensitivity of 10 pT/√Hz in a bandwidth from DC to 100 Hz.

CEA-LETI & CNES have successfully designed and manufactured an isotropic space-qualified ^{4}He magnetometer for the SWARM mission with a 1 pT/√Hz resolution (DC-100Hz) and an accuracy better than 45 pT [1]. Here, we summarize the path to the downscaling of this macroscopic magnetometer and early performances of the miniature isotropic ^{4}He magnetometer [2].

1. Sensitivity and scaling rules for ^{4}He pressure

The sensitivity of ^{4}He magnetometer is directly impacted by the gas pressure, discharge parameters, size of the cell. The optimal gas pressure is that which maximizes the product of the density and relaxation time of the triplet ^{4}He metastable atoms: the latter are destroyed upon diffusion to the wall and by collisions with neutrals atoms, electrons and pairs of metastables.

The relative importance of these processes has been modeled depending on gas pressure and size of the cell. Simulations have shown that optimal ^{4}He pressure of the miniature gas cell (100 mm^3) has to be increased by a factor 40 in comparison with the SWARM macroscopic cell (32 cm^3) Theoretical predictions are in agreement with experimental data.

2. Atomic magnetometer accuracy

The resonance signal amplitude depends on the angle between the laser linear polarization $\vec{E}$ and the magnetic field $\vec{B}_0$. Isotropic magnetometers can be obtained by servo-controlling the angle $(\vec{E};\vec{B}_0)$ at 90°. The SWARM isotropic magnetometer uses a piezoelectric motor to rotate the laser linear polarization. This system is however difficult to downscale and it is not perfectly non-magnetic.

A well-adapted solution to the miniaturization is to replace the motor by a liquid crystal polarization rotator (figure 1). In this configuration, the polarization axis is controlled by an AC square electric voltage [0.5 Vrms ; 5 Vrms], whose frequency [1 kHz ; 10 kHz] is larger than the bandwidth of the sensor. A polarization extinction ratio (PER) of the laser beam around 20dB was measured at the output of the rotator. This feature is essential to limit heading errors. Moreover, the rotator structure has no moving parts, it can benefit from low cost and reproducible MEMS processing and it is perfectly non-magnetic which enables a positioning very close to the ^{4}He cell. It allows a continuous polarization rotation from 0 to more than 300° with response times compatible with mobile or space applications.

3. Miniature magnetometer performances

A sensitivity of 10pT/√Hz has been obtained with glass-blown cells (100 mm^3). The atomic magnetometer resolution is not affected by the presence of the polarization rotator (figure 2).

The next steps of this downscaling approach are the characterization of the accuracy of this demonstrator, and then the integration of our micro-fabricated glass-silicon-glass cells so that smaller ^{4}He atomic magnetometer will be obtained.

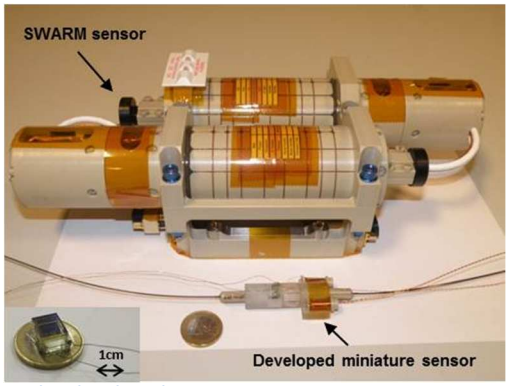

Figure 1: The developed miniature magnetometer compared to the macroscopic version and the developed polarization rotator.

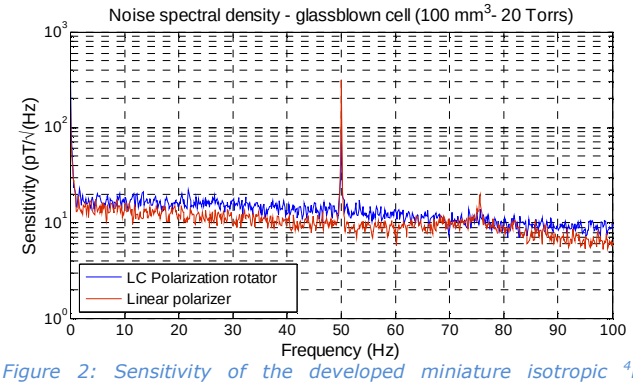

Figure 2: Sensitivity of the developed miniature isotropic ^{4}He magnetometer with and without the LC polarization rotator.

Related publications:
[1] T. Jager, J.M. Leger, F. Bertrand, I. Fratter, J.C. Lalaurie, "SWARM absolute scalar magnetometer accuracy: analyses and measurements results", 2010 IEEE sensors, Nov. 1-4, 2010, Waikoloa, HI, USA.
[2] J. Rutkowski et al., "Towards a miniature atomic scalar magnetometer using liquid crystal polarization rotator", 17th Int. Conf. on Solid-State Sensors, Actuators and Microsystems (Transducers), June 16-20, 2013, Barcelona, Spain.

The SWARM absolute scalar magnetometer

Research topics : atomic magnetometers

T. Jager, J.M. Léger, F. Bertrand, W. Fourcault, S. Morales, A. Boness

ABSTRACT: The Absolute Scalar Magnetometer (ASM), proposed by CEA-Leti and CNES with the scientific support from IPGP, was selected by ESA in 2005 as the SWARM magnetic reference. Thanks to a new dedicated design, the ASM offers the best precision and absolute accuracy ever attained in space, with similar performances all along the orbit. This paper presents the new features, capabilities and performances of this instrument as well as the latest status.

The Swarm mission, conducted by the European Space Agency (ESA), will provide the best ever survey of the Earth's magnetic field and its temporal evolution. This will be achieved by a constellation of three satellites. The ASM operating principle is based on the atomic spectroscopy of the helium 4 metastable state. It makes use of the Zeeman's effect to transduce the magnetic field into a frequency, the signal being amplified by optical pumping [1-2]. A picture of the realized ASM instrument is given in Figure 1 with one ASM sensor assembly including two sensors (full cold redundancy scheme) and one ASM electronics (DPU). The corresponding satellite instruments locations are also depicted in Figure 1.

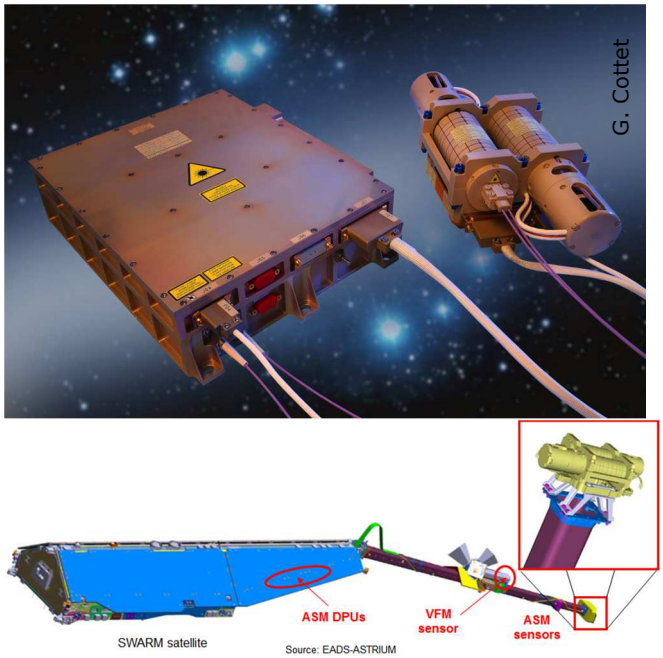

Figure 1: ASM sensor assembly with a ASM DPU, and corresponding satellite integration location.

The ASM delivers high resolution scalar measurements (cf Figure 2, with a scalar resolution of 1 pT/√Hz over a DC-100 Hz bandwidth) at 1 Hz for the in-flight calibration of the SWARM Vector Field Magnetometer (VFM) over the 4 year mission. It can also be operated at a much higher sampling rate (burst mode at 250 Hz). The ASM overall scalar precision is less than 45 pT (1 σ), which is well under the 300 pT specified by the mission for the global ASM accuracy.

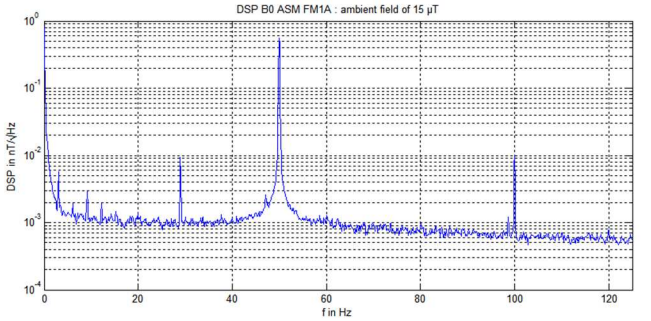

Figure 2: ASM FM1A scalar resolution performance.

In addition, thanks to an innovative architecture, the ASM is able to carry out continuous vector measurements, hence delivering simultaneously both the magnitude and direction of the ambient magnetic field measured at the same point, which is a premiere on a single instrument. While the main advantage of this vector capability lies in the lack of offsets or drifts, its precision is by design significantly lower than the scalar's. This capacity will be used in flight on an experimental basis, the nominal SWARM vector data being delivered by the VFM.

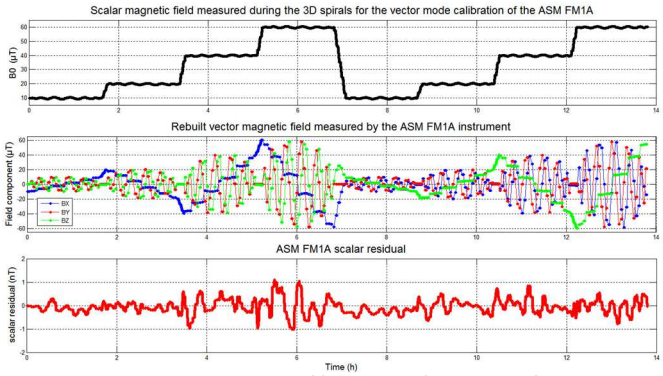

Figure 3: ASM FM1A vector calibration and vector performances.

The six ASM instruments have been further integrated on the three SWARM satellites (full cold redundancy). The launch campaign has then been successfully conducted in Plesetsk (Russia) in October 2013. It was followed by the launch performed with a Rockot launcher on 22/11/2013. First ASM in-orbit performance results are in full agreement with the demonstrated on-ground characteristics. All ASM level 1B products will be validated during the first months following the launch, in close partnership between CEA-Leti, CNES and IPGP.

Related publications:
[1] T. Jager, J.M. Léger, F. Bertrand, I. Fratter, J.C. Lalaurie, "SWARM Absolute Scalar Magnetometer accuracy: analyses and measurement results", 2010 IEEE sensors, Nov. 1-4, 2010, Waikoloa, HI, USA.
[2] I. Fratter, J.M. Léger, F. Bertrand, T. Jager, G. Hulot and X. Lalanne, "The SWARM Absolute Scalar Magnetometer", The XIIth Scientific Assembly of the International Association of Geomagnetism and Aeronomy (IAGA), August 26-31, 2013, Merida, Yucatan, Mexico.

Modeling of an atomic electrometer for marine applications

Research topics : atomic sensors, electrometers

M. Baicry, M. Le Prado, C. Lefrou, L.-L. Rouve (G2ELAB)

ABSTRACT: For the last ten years, strong efforts were devoted to atomic magnetometer miniaturization and allowed a reduction of their volume by two orders of magnitude. The sensitive part of a magnetometer is now only a few cm^3 large with a noise below 10 pT/√Hz. Leti is designing a compact electrometer based on these small and efficient sensors. This electrometer could be used for oil and gas exploration, homeland security and detection of corrosion.

At the early 2000s, atomic clocks have been miniaturized thanks to military funding, which goal was to provide to each infantryman a mean to have a rapid access to data. Atomic magnetometers based on the same building blocks took advantage of these developments to reduce their volume by more than two orders of magnitude while keeping a noise lower than 10 $pT/\sqrt{Hz}$ [1].

Leti is designing a compact electrometer benefiting of the recent atomic magnetometers breakthroughs. It is composed by two electrodes electrically linked with coils. The electric field $\vec{E}$ induces a current that generates a magnetic field inside the coils and is measured thanks to the atomic magnetometer (figure 1). Two magnetometers and two coils, wired in opposite ways, are used to distinguish the ambient magnetic field $\overrightarrow{B_0}$ from the one induced by coils $\overrightarrow{B_C}$, proportional to one $\vec{E}$ component.

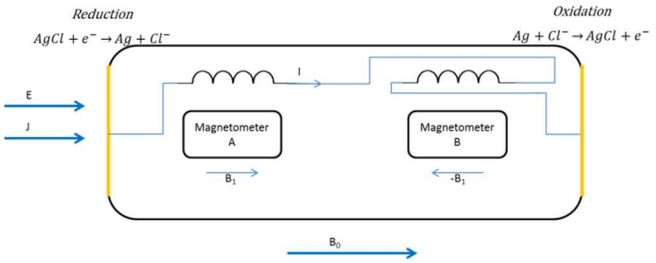

Figure 1: Electrometer operating principle.

Leti has built a model of the whole electrometer to quantify the contribution of each of the sub-elements to the magnetic field generated by the coils: the resistivity of the saltwater $\rho_W = 0.25\,\Omega m$, the surface impedance of the Ag/AgCl electrode $Z_e = 0.036\,\Omega m^2$ and the resistance of the copper coils R_c, depending on the diameter of the wire and of the number of loops, are taken into account. Figure 2 illustrates the impact of the resistance of the electrometer relatively to the saltwater one for identical volumes on the sensor transfer function. Various lengths L and radius r are considered for the sensor that is supposed cylindrical.

The results clearly show that the sensitivity of the electrometer is improved when its resistance is lower than the resistance of the equivalent volume of saltwater. In this configuration, the electrometer canalizes the currents that are therefore higher inside the coils. This phenomenon is accentuated on long electrometers.

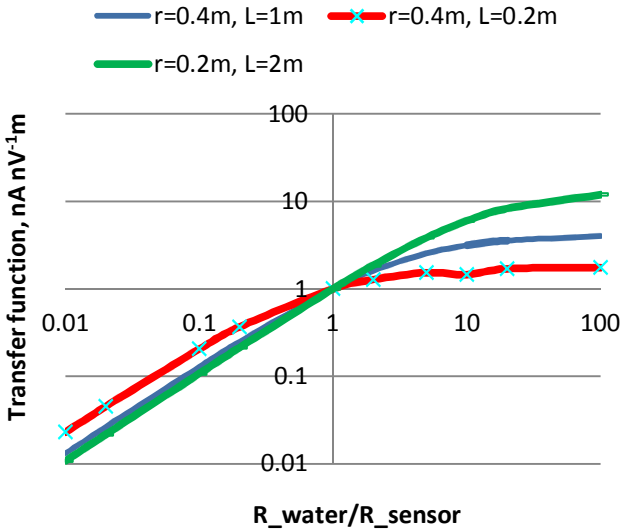

Figure 2: Sensor transfer function.

Another trend, not visible in figure 2, is that the magnetic field generated by the coil improves with the number of loops. However, the resistance R_c is also increased, which reduces the current collected by the electrometer. A tradeoff has to be found onto the design of the coils of the electrometer to have the highest transfer function.

The model of the whole electrometer has to be validated with an experimentation that is still in preparation. Then we will design the electrodes, the coils and adapt the atomic magnetometer to achieve a noise of 1 $nVm^{-1}Hz^{-1/2}$ with the smallest electrometer volume.

The miniaturization of the electrometer will ease its utilization in seas and their deployment in arrays. It will be particularly relevant for oil exploration, homeland security or corrosion studies.

Related publications :
[1] M. Baicry, C. Lefrou, M. Le Prado, L.L. Rouve, E. Chainet, R Nogueira "Electromètre marin à mesure de courant" Journées d'électrochimie 2013, 8-12 juillet 2013, Paris, France.
[2] J. Rutkowski, W. Fourcault, F. Bertrand, U. Rossini, S. Gétin, O. Lartigue, S. Le Calvez, T. Jager, M. Le Prado, J.M. Leger and S. Morales "Towards a miniature atomic scalar magnetometer using a liquid crystal polarization rotator" The 17th Int. Conf. on Solid-State Sensors, Actuators and Microsystems (Transducers 2013), June 16-20, 2013, Barcelona, Spain, pp. 705-708.

High-resolution acoustic imaging

Research topics : acoustic transducers, nano sensors

N. Sridi, A. Ghis, M. Delaunay (CEA/DSM/INAC)

ABSTRACT: Acoustic probing and imaging using micrometric transducing area matrixes is a relevant tool for chemical, biological and material sciences as it will allow for compact, in situ, non destructive and ultrahigh resolution observation. The actual challenge is to demonstrate the feasibility of such a device, considering nano-membrane material and implementation, mechanical behavior of micrometric vibrating areas, readout electronic and overall packaging. Most of the relevant concepts have now been demonstrated or about to be passed.

The applicative field of high resolution acoustic probing spreads from biology to material science, for any purpose requiring a micrometer resolution, for in situ non-destructive testing, in fluid or polyphasic media.

Micrometer is the suitable range for biological cell observation. Cellular dynamic could be monitored in-vitro by passive pressure imaging, or chemical species may be identified in-vivo by micrometric cMUTS (Capacitive Micromachined Ultrasonic Transducers) fixed onto an endoscope.

For high resolution acoustic imaging, specific cMUTs featuring a micrometric size and a resonance frequency in the GHz range are required.

Efficient specific modeling needed:
The key part of these cMUts is a suspended membrane with a micrometric surface. Analytical study emphasizes the importance of having a nanometric thickness to obtain a detectable electrical signal.

Because of this extreme thinness, the physical laws for continuous media and bulk material properties are not sufficient to reliably predict the mechanical membrane behavior when excited in vibration. Moreover, the implementation of such nanosized objects is highly dependent on the technological processes involved.

This is why we developed a characterization protocol for nanomembranes after technological integration into device - or preliminary dummy devices. This protocol allows for extracting the mechanical parameters related to the considered membrane embodiment and provides for experimental modeling data and final device optimization.

Experimental parameters for modeling:
Because of the micrometric size of the area of the membrane, optical observations are not eligible. The proposed protocol consists then in AFM measurements of the deflection of the membrane profile under electrostatic pressure. Moreover, we compared with usual AFM measurements in force mode, and experienced that the sets of values collected when applying a punctual force do not figure the actual behavior of the membrane when excited by an averaging surface pressure, namely when the membrane suspended area is polystructured.
Material experimental exploration:
Several materials have been tested, from their specific technological implementation to characterization. We then elected silicon and Diamond Like Carbon (DLC) as high performing materials for realizing the vibrating membranes of integrated micrometric cMUTS.

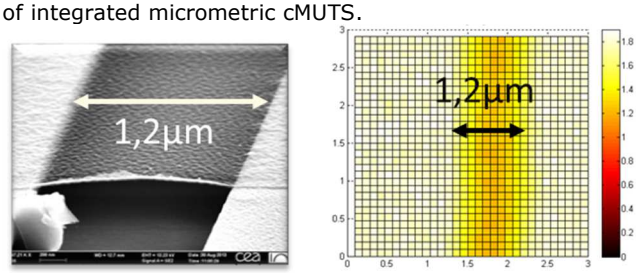

Figure 1: DLC (2nm) +Ni (2nm) bilayer membrane suspended above a 1µm large trench. DLC is Ni coated for conductance.
Left : SEM picture, right : cartography of the constant rigidity; the white zones are measurements taken on the bank, and the center part on the suspended membrane.
DLC thickness from 2nm to 5nm has been experienced. Measured bending rigidities range from 36 fN.m to 113fN.m. Displacement of several nanometers have been observed with a few Volts DC biasing

Device relevance demonstration:
To demonstrate the feasibility of the device and the relevance of the targeted experiments in the various application fields identified, each of the elementary cMUTS is to be embedded in a circuit together with a subpixel electronic. Preliminary modeling has confirmed the efficiency of the displacement detection.

Next step of the proof of concept demonstration path is the fabrication of the circuit providing the subpixels readout electronics.

Related publications:
[1] N. Sridi, B. Lebental, J. Azevedo, J-C. P. Gabriel, and A. Ghis. "Electrostatic method to estimate the mechanical properties of suspended membranes applied to nickel-coated graphene oxide", Applied Physics Letters 103, 051907 (2013); doi: 10.1063/1.4817301.
[2] N. Sridi, "Etude de membranes ultrafines pour l'intégration de transducteurs acoustiques ultrasonores", Thèse de Doctorat de l'Université de Grenoble, 16 oct. 2013.

Architecture for self-organizing, cooperative and robust building automation systems

Research topics : building management systems, sensor networks

C. Guyon-Gardeux, S. Lesceq, F. Pacull, L.-F. Ducreux, S. Thior, O. Yaakoubi

ABSTRACT: This paper presents an overview of the architecture for self-organizing, co-operative and robust Building Automation Systems (BAS) proposed by the EC funded FP7 SCUBA project. According to the current situation in monitoring and control systems, seven typical use cases were defined in the project and will be demonstrated and evaluated on pilot sites. From these use cases, the project designed an architecture relying on six main modules that realize the design, commissioning and operation of self-organizing, co-operative and robust BAS.

Building automation uses a large number of different systems such as heating, ventilation, air-conditioning (HVAC), lighting, access control, fire, safety and security systems. They usually co-exist alongside each other with little co-operation within and among heterogeneous systems which hampers the increasing demand to operate the whole system optimally.

The SCUBA project aims to address this lack of cooperation by proposing a self-organizing and self-adaptive architecture to form the basis for co-operative and robust Building Automation Systems.

Typical use cases encountered by building actors such as system integrators, facility managers and business applicants were defined [1]:

- Control system design
- Control system commissioning
- Rooms repartitioning
- Fault adaptation
- Coordination and external control
- Emergency situation handling

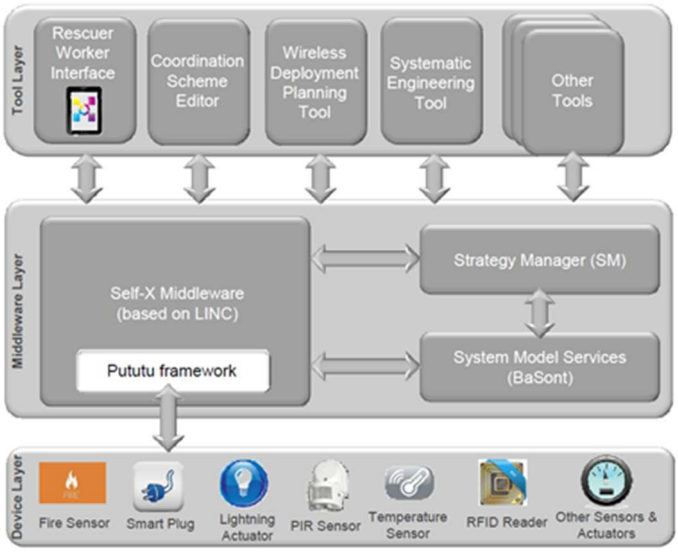

Figure 1: The SCUBA architecture.

To cover all these use cases, SCUBA project follows a systematic approach that covers the whole building system life cycle from design, to commissioning, operation and recommissioning. It leads to design an architecture relying on six main modules (Figure 1).

This architecture addresses the interoperability problem with a Systematic Engineering Tool that helps users in selecting interoperable devices. The issue of indoor signal propagation for wireless devices is addressed by the Wireless Deployment Planning tool that optimizes the number and position of wireless devices to ensure reliable communications between sensors, actuators and backend systems.

System commissioning is supported by the Self-organization Middleware LINC [2] that utilizes design knowledge from an ontology-based model database, the BaSont. The Coordination Scheme Editor permits to define scenarios involving different sensor/actuator technologies as they are not easily handled by the Systematic Engineering Tool. Extensions of existing systems are supported by reengineering approaches that are currently developed to feed system knowledge back into the design. The Middleware can be connected to different protocols and functions as an automatic gateway. The self-organization of the device layer improves the reliability of the system as it preserves its decentralized communication. All modules provide self-documenting web services that allow the easy implementation of additional services. One such service is the Strategy Manager that harmonizes different building operation strategies and handles emergencies in the system. Another service is a Rescue Worker Interface that assists emergency wardens and rescue workers when an emergency event is detected.

To validate that SCUBA delivered components fully address projects requirements and in order to demonstrate how valuable these features are from a system integrator or facility manager perspective, several experimental sites will be equipped with a SCUBA based prototype of a building automation system.

Wireless sensors deployments have already been done on an experimental site and validate the quality improvements achieved by the Wireless Deployment Planning Tool [3].

Related publications:
[1] F. Bernier, J. Ploennigs, D. Pesch, S. Lesecq, T.Basten, M. Bouekeur, D. Denteneer, F. Oltmanns, A. Mc Gibney, S. Rea, F. Bonnard, F. Pacull, C. Guyon-Gardeux, L.-F. Ducreux, S. Thior, M. Hendriks, S. Fedor, M. Lehmann, Mai Tuan Linh, "Architecture for Self-organizing, Cooperative and Robust Building Automation Systems", 39th Annual Conf. of the IEEE Industrial Electronics Society (IECON), Nov. 10-13, 2013, Vienna, Austria.
[2] F. Pacull, L.-F. Ducreux, S. Thior, H. Moner, D. Pusceddu, O. Yaakoubi, C. Guyon-Gardeux, S. Fedor, S. Lesecq, M. Boubekeur, D. Pesch, "Self-Organisation for Building Automation Systems: Middleware LINC as an Integration Tool", 39th Annual Conf. of the IEEE Industrial Electronics Society (IECON), Nov. 10-13, 2013, Vienna, Austria.
[3] A. McGibney, S. Lesecq, C. Guyon-Gardeux, S. R. Thior, D. Pusceddu, L.F. Ducreux, F. Pacull, " Wireless Sensor Networks for Building Monitoring : Deployment Challenges, Tools and Experience", Fifth Workshop on Real-World Wireless Sensor Networks (REALWSN), Sept. 19-20, 2013, Como lake, Italy.

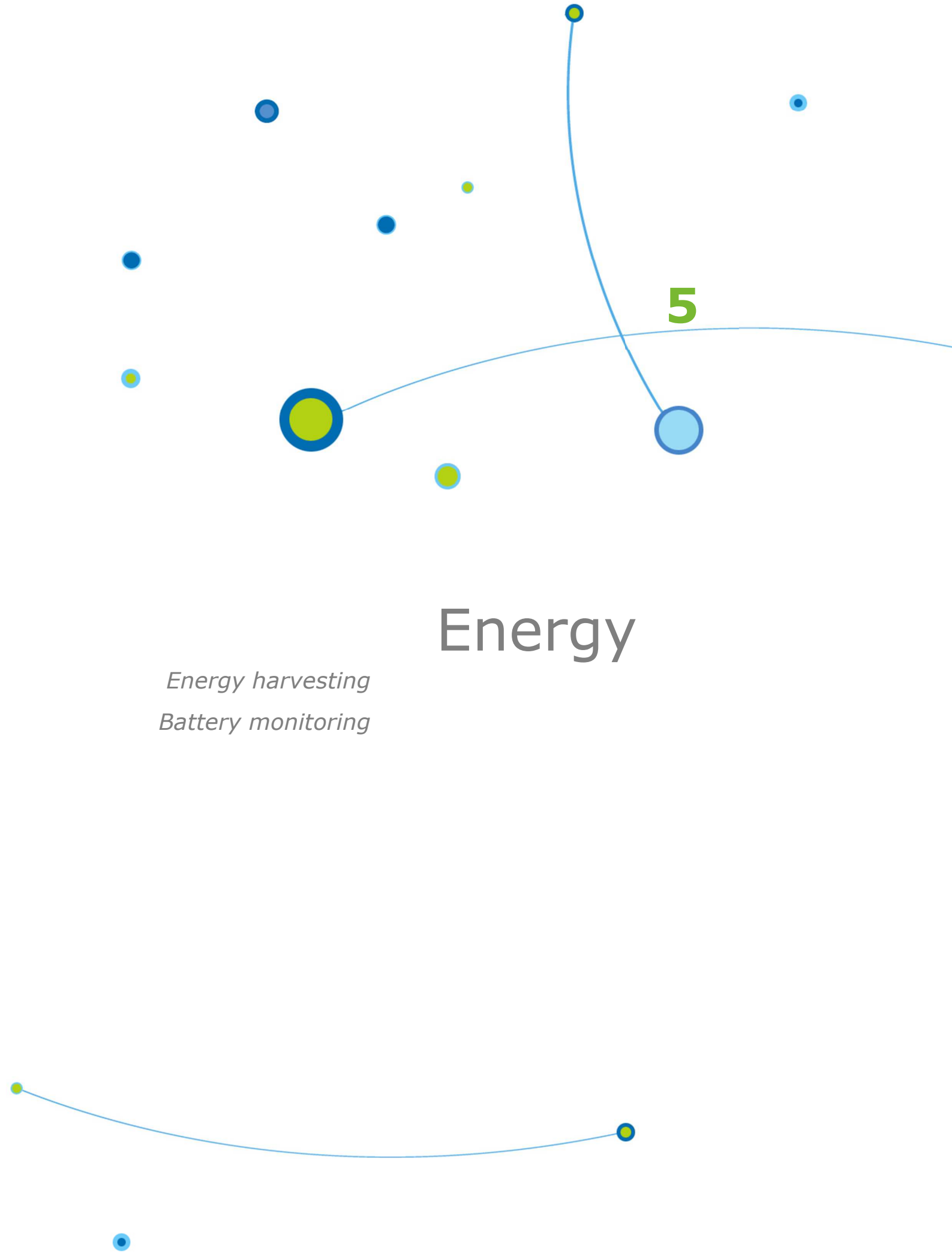

5

Energy

Energy harvesting

Battery monitoring

Self-starting power management circuits for piezoelectric and electret-based electrostatic mechanical energy harvesters

Research topics : energy harvesting, power management, electrets

S. Boisseau, P. Gasnier, M. Gallardo, G. Despesse

ABSTRACT: This paper reports on a power management circuit, fabricated with discrete components only and used to harvest energy from piezoelectric and electret-based mechanical harvesters. It is able to self-start and to power battery-free Wireless Sensor Nodes (WSNs) "from scratch" (without any initial energy). This circuit is based on two energy paths (non-optimized passive/optimized active). Its power consumption is in the 500nA-1µA range which enables to harvest energy in the 10µW-500µW range.

The output power of piezoelectric and electret-based mechanical energy harvesters (EH) is generally in the 10µW-100µW range and their high AC output voltages are not compatible with standard electronic circuits requirements (3V-DC supply source needed). As a consequence, a power management circuit (PMC) is essential to turn the EH raw output into a viable supply source for WSNs.

On one hand, Passive PMCs (e.g. diode bridge rectifier + storage capacitor) do not require power to operate but they suffer from a non-optimal energy extraction. On the other hand, Active PMCs have high conversion efficiencies, but they unfortunately require power to operate (e.g. a rechargeable battery). The problem arises when using battery-less systems, starting "from scratch" (without any initial energy): the active PMC cannot be powered and cannot control the power converter used to efficiently extract the energy from the EH. The PMC we propose solves this problem. It is based on both passive and active PMC and its architecture is depicted in figure 1.

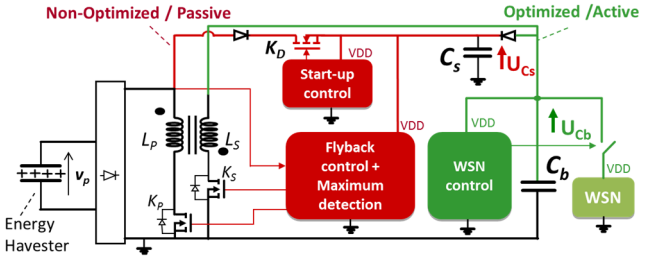

Figure 1: Architecture of the autonomous and self-starting PMC.

In this circuit, two capacitors are used: (i) C_s which powers the control circuit and (ii) C_b which supplies the WSN. A flyback converter implementing an efficient technique (called SECE) has been chosen as the active PMC: all the energy stored into the EH capacitance is transferred to C_b through the coupled inductors when the EH's voltage reaches a maximum. The passive part is based on a depletion-mode MOSFET (dMOS) K_D which is employed to bypass the flyback converter during the startup, in order to charge C_s. This way, this circuit is able to start and to switch from the passive to the active mode according to U_{Cs} (the voltage across C_s). A Schmitt trigger uses a dMOS as a voltage limiter and controls the startup with an ultra-low power consumption not exceeding 100nA. The control circuit is made of a RC differentiator (R_D-C_D) and a comparator (fig. 2a) to detect the zero crossings of V_p's derivative, i.e. its maximums.

Three delay cells (figure 2b) generate the control times T_1 and T_3 for K_p and K_s. The circuit has been made from standard electronic components and its power consumption is comprised between 500nA@3V and 1µA@3V.

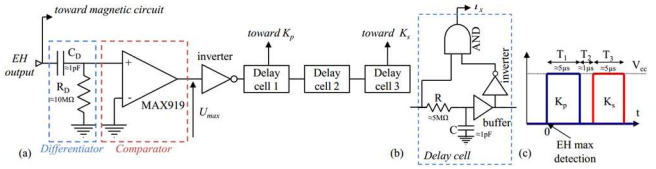

Figure 2: RC differentiator (R_D-C_D) comparator to detect the maximum voltage (a), delays cells to control the flyback (b) and control times (c).

The power consumption of the complete PMC is in the 1.5µW-3µW range. Its operation has been validated with a simple electret-based vibration EH oscillating at 35Hz and harvesting 23µW (fig. 3a). Moreover, a simple piezoelectric EH (fig. 3b) deformed by hand at 7Hz and harvesting about 100µW has also been used to validate our PMC. Fig. 3a and 3b show a complete operation of the PMC and a WSN operation.

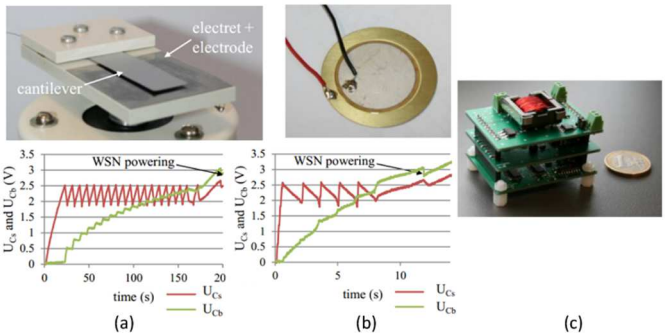

Figure 3: U_{Cb} as a function of the time and WSN measurement for an electret-based energy harvester (a) and a simple piezoelectric energy harvester (b); discrete harvesting system (c).

This new PMC (Fig. 3c) is completely autonomous and can be made from standard and low cost off-the-shelf components. The proposed architecture is able to turn most of piezoelectric and electret-based mechanical EH into viable supply sources for battery-free WSN. An ASIC, based on the same architecture, has finally been designed, fabricated and validated [2].

Related publications:
[1] S. Boisseau, P. Gasnier, M. Gallardo and G. Despesse, "Self-starting power management circuits for piezoelectric and electret-based electrostatic mechanical energy harvesters", 13th Int. Conf. on Micro and Nanotechnology for Power Generation and Energy Conversion Applications (POWERMEMS), Dec. 3-6, 2013, London, UK.
[2] P. Gasnier, J. Willemin, S. Boisseau, G. Despesse, C. Condemine, G. Gouvernet and J-J. Chaillout, "An autonomous piezoelectric energy harvesting IC based on a synchronous multi-shots technique", 39th European solid-State circuits Conf. (ESSCIRC), Sept. 16-20, 2013, Bucharest, Romania.

An autonomous piezoelectric energy harvesting IC based on a synchronous multi-shot technique

Research topics : energy harvesting, power management

P. Gasnier, J. Willemin, S. Boisseau, C. Condemine, S. Robinet

ABSTRACT: This work presents a fully autonomous Integrated Circuit (IC) that efficiently converts the raw output of mechanical Energy Harvesters (EH) into a 3V supply source compatible with WSNs. The IC has been fabricated in the standard voltage AMS0.35 CMOS technology. It autonomously harvests energy from 10 µW to 500 µW and operates with high output voltage harvesters (from 3 to 200 V). It performs an efficient energy extraction thanks to an off-chip inductive element and a precise control strategy. Furthermore, the system self-starts and does not need any battery to operate.

In dusty or dark environments submitted to shocks, stresses or vibrations, where solar energy is unreliable or non-existent, mechanical energy harvesting is a relevant candidate to power Wireless Sensor Nodes (WSN). The piezoelectric principle is relevant to convert mechanical energy into electricity: in addition to its low cost and its availability, it offers a high power density at micro and macro scales and low mechanical frequencies. The output power of piezoelectric harvesters is generally in the 10 µW to 1 mW range and their high AC output voltages are not compatible with standard electronic circuits' requirements.

As a consequence, a power management circuit (PMC) is essential to turn the piezoelectric raw output into a viable supply source for WSNs. Synchronous Electric Charge Extraction (SECE) is a technique which enhances the energy extraction compared to a full-bridge rectifier and a smoothing capacitor. SECE consists in entirely discharging the piezoelectric harvester in a coil when its voltage reaches a maximum. The architecture of the PMC is depicted in Fig. 1**Erreur ! Source du renvoi introuvable.**. It is based on an IC surrounded by discrete components. The system uses two energy paths and two storage capacitors. The Flyback is employed to perform SECE (by precisely controlling K_p and K_s when the piezoelectric voltage reaches a maximum).

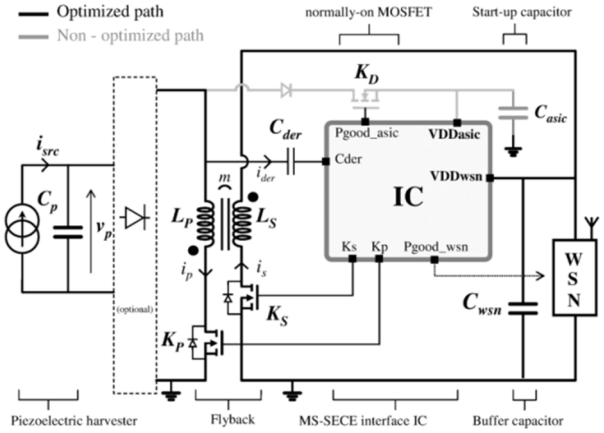

Figure 1: Power management IC surrounded by off-chip components.

Moreover, the PMC described herein implements a new SECE technique called MS-SECE ("Multi-Shot" SECE). Instead of a single energy transfer (SECE), the piezoelectric harvester is discharged in N successive energy transfers.

This novel technique enables to reduce the volume of the power circuit or improve the efficiency of the energy transfer compared to SECE, by reducing conduction losses.

The IC (Fig 2a) has been fabricated in the 3.3V AMS0.35 CMOS technology. The IC, surrounded by a few off-chip components, self-starts and operates with capacitors as storage elements. Thanks to the off-chip Flyback topology, it is not limited in terms of piezoelectric voltages.

Figure 2b shows some results of the chip efficiency for various maximum piezoelectric voltage and mechanical frequencies. It is shown that MS-SECE increases the efficiency of the energy transfer by 15% and up to 25% compared to SECE. The chip also enables to use small inductive components to discharge a considerable quantity of energy without reaching the saturation induction.

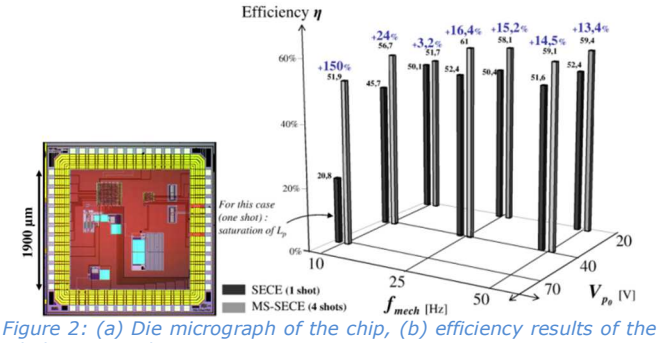

Figure 2: (a) Die micrograph of the chip, (b) efficiency results of the whole system shown in Figure 1.

This IC, designed in a low voltage and low cost technology, consumes 1 µW @ 5 Hz. This IC, along with the MS-SECE technique, paves the way towards size reduction of power converters for piezoelectric harvesters while using efficient harvesting techniques: its overall volume is expected to be less than 1 cm^3 (Fig. 3).

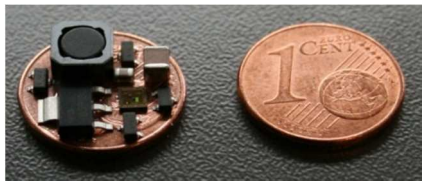

Figure 3: the whole system next to a one cent euro coin.

Related publications :
[1] P. Gasnier, J. Willemin, S. Boisseau, G. Despesse, C. Condemine, G. Gouvernet and J-J. Chaillout, "An autonomous piezoelectric energy harvesting IC based on a synchronous multi-shots technique", 39th European solid-State circuits Conf. (ESSCIRC), Sept. 16-20, 2013, Bucharest, Romania.
[2] S. Boisseau, P. Gasnier, M. Gallardo and G. Despesse, " Self-starting power management circuits for piezoelectric and electret-based electrostatic mechanical energy harvesters", 13th Int. Conf. on Micro and Nanotechnology for Power Generation and Energy Conversion Applications (POWERMEMS), Dec. 3-6, 2013, London, UK.

Stable DRIE-patterned electrets for electrostatic vibration energy harvesters

Research topics : energy harvesting, electrets

S. Boisseau, J.J. Chaillout, A.B. Duret, J.S. Danel, J.B. Legras, G. Despesse

ABSTRACT: This paper presents a new manufacturing process aimed at making stable patterned electrets for electrostatic vibration energy harvesters. Based on a preliminary DRIE step, these electrets have shown an excellent stability as no charge decay has been observed in 450 days at room temperature. They also withstand high temperatures (200°C), short-term X-rays and strong magnetic fields.

Among ambient energy sources, vibrations have aroused an increasing interest of scientists and industrials. Many devices have been developed, exploiting three main kinds of electromechanical converters: piezoelectric materials, coil-magnet and variable capacitors (electrostatic devices).

This paper focuses on electret-based electrostatic devices (figure 1a). Electrets are electrically charged dielectrics that can keep their charges for years; they have long been used in electrostatic vibration energy harvesters (VEH), enabling a direct mechanical-to-electrical conversion.

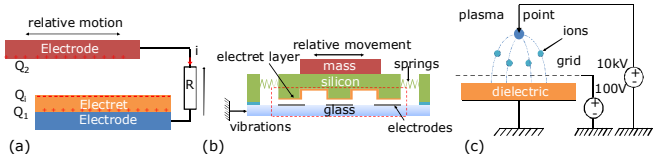

Figure 1: Electret-based converter (a), electret-based vibration energy harvester (b) and corona charging process(c).

An electret-based VEH is introduced in figure 1b. The vibrations and the exploitation of a mass-spring resonance lead to a relative movement of the upper plate compared to the lower one. Capacitance changes and charge influence variations convert this relative movement into electricity. One of the most critical challenges of these devices is the charge stability of electrets. Actually, dielectrics are not perfect insulators and some charge conduction phenomena may appear: electrets lose their charges and VEH do not work any longer. Charge stability of full-plate electrets has been proven for long; charge stability of patterned electrets is clearly more difficult, but is yet required to harvest energy from low amplitude vibrations.

The solution we propose is different from the state of the art and consists in searching for an equivalent full-plate behavior for patterned electrets by using a DRIE preliminary step so as to get a continuous layer of electret (figure 2a) following crenels on silicon wafers. The process (figure 2b) starts with a standard silicon wafer. After a lithography step, the wafer is etched by DRIE. It is then cleaned and oxidized at 1100°C to get a 1µm-thick SiO_2 layer. A 100nm-thick LPCVD Si_3N_4 layer on the front face and a 100nm-thick Aluminum layer on the rear face are then deposited. The wafer undergoes a thermal treatment and is protected by a ~10nm-thick HMDS layer. Finally, the wafer is charged by a corona discharge (figure 1c). Figure 2 presents SEM images of these patterned electrets: a global view in figure 2c, a zoom of the constitutive layers in figure 2e and the continuity of the layers in figure 2d. Figures 2g and 2h also show the uniformity of charges by comparing a non-charged area to a charged one (charged areas are brighter than non-charged ones in SEM).

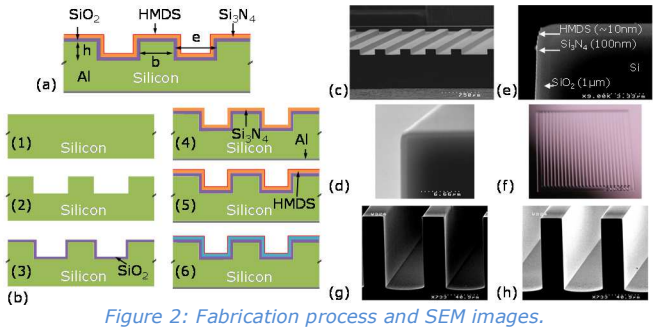

Figure 2: Fabrication process and SEM images.

A full-wafer corona charger (figure 3a) has been developed to uniformly charge 200-mm wafers at one time (figure 3b) and the high stability of these electrets has been shown with a 1-year measurement campaign (figure 3c): no charge decay has been observed on electrets charged up to 120V.

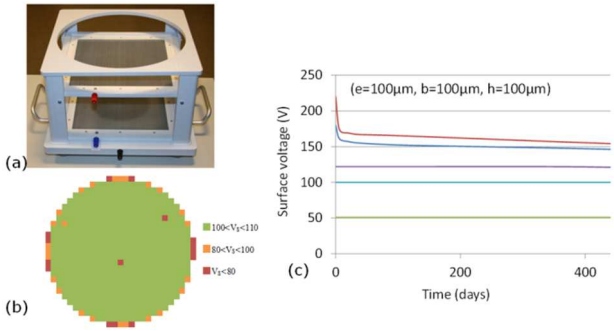

Figure 3: Full-wafer corona charger(a), uniformity of charges on a 200-mm wafer (b) and stability of DRIE-patterned electrets in 400 days (c).

Electrets' stability has also been validated with various patterning spaces from 25µm to 400µm: 2% was the maximum surface voltage decay observed with electrets initially charged at 100V. Finally, it has been shown that these electrets can withstand high temperatures (200°C), short-term X-rays and strong magnetic fields without showing any charge decay, proving their compatibility with medical exams such as MRI or X-Rays.

We have proven the benefit of this manufacturing process to develop stable patterned electrets; X-rays and strong magnetic fields compatibility validates the viability of DRIE-patterned electrets to develop autonomous medical implants powered for example by heartbeats or by human movements.

Related publications:
[1] S. Boisseau et al., "Electrostatic conversion for vibration energy harvesting", Small Scale Energy Harvesting, Intech, 2011.
[2] S. Boisseau et al., "New DRIE-Patterned Electrets for Vibration Energy Harvesting", Proc. European Energy Conference, 2012.
[3] S. Boisseau et al., "Stable DRIE-patterned SiO2/Si3N4 electrets", 17th International Conference on Solid-State Sensors, Actuators and Microsystems . (Transducers), June 16-20, 2013, Barcelona, Spain.

Bimetal-and-electret-based thermal energy harvesters – application to a battery-free wireless sensor node

Research topics : energy harvesting, electrets

S. Boisseau, M. Gallardo, A.B. Duret, S. Monfray (ST), A. Arnaud (ST), T. Skotnicki (ST)

ABSTRACT: We report on a breakthrough concept to turn thermal gradients into electricity by using a curved bimetallic strip coupled to an electret-based converter and involving a two-step conversion: thermal gradients are firstly turned into mechanical oscillations, finally converted into electricity. The output power per device on a 60°C hot source is in the 5µW range. Then, by parallelizing ten devices, we managed to power a battery-free Wireless Sensor Node (WSN) from scratch by using a self-starting power management circuit.

In this paper are presented innovative thermal energy harvesters (TEH) turning heat fluxes into electricity in a two-step conversion, involving (i) a curved bimetallic strip as a first thermal-to-mechanical converter turning thermal gradients into mechanical oscillations which are eventually (ii) converted into electricity by an electret-based electrostatic transducer.

Curved bimetallic strips are made of two metals with different coefficients of thermal expansion (CTE) that are joined together (fig. 1a) and have long been used as thermal actuators able to turn temperature changes into sudden mechanical movements (snapping), involving buckling effects. Curved bimetallic strips are then capable of switching between two mechanical states according to the temperature and with a hysteretic behavior (snapping and snapping back). Then, when they are inserted in a cavity with a hot lower plate and a cold upper plate, curved bimetallic strips turn the thermal gradient into mechanical oscillations (fig. 1a,b).

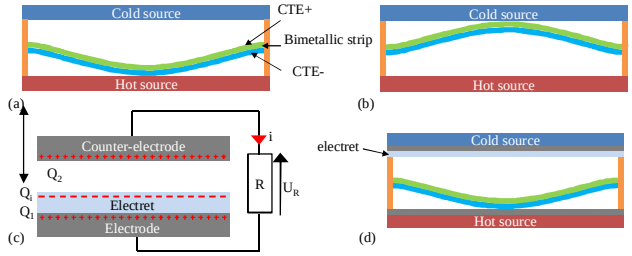

Figure 1: bimetal-based heat engine - lower state (a) and upper state (b), electret-based converter (c) and bimetal-and-electret-based thermal energy harvester(d).

Mechanical oscillations are finally turned into electricity by an electret-based converter (fig. 1c). The basic concept gathering the two successive converters is presented in fig. 1d.

A small hot point and a heat sink have been added in order to increase the thermal gradient between the two plates (fig. 2a,b). Prototypes have been manufactured from 2cmx1cmx115µm curved bimetallic strips snapping at 50°C and snapping back at 47°C (fig. 2c). When the device is placed on a hot source at 60°C, the bimetallic strip starts to oscillate and to harvest energy. The output voltages reach hundreds of volts (fig. 2d); the snapping frequency is in the 2-4Hz range and the output power is about 5µW. Due to their constitutive materials, these new thermal energy harvesters are compatible with mass-manufacturing and low-cost concepts.

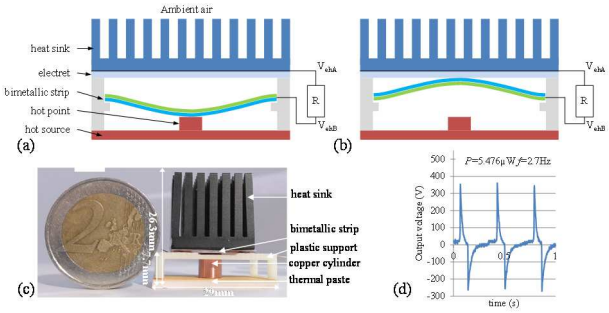

Figure 2: Thermal energy harvester lower state (a), upper state (b), prototype (c) and output voltage (d).

TEH have been parallelized and combined to a power management circuit (fig. 3a) implementing a Synchronous Electric Charge Extraction: the energy stored in TEH capacitances is transferred to a buffer through coupled inductors when one of the TEH reaches its maximum output voltage. The available output power at the end of the process is ≈10µW with 10 bimetallic strips in parallel..

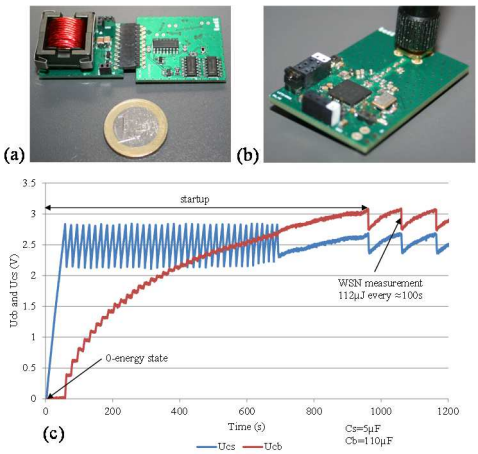

Figure 3: discrete power management circuit (a), Wireless Sensor Node (b), WSN measurement from a 0-energy state (c).

This power enabled to supply a Wireless Sensor Node (figure 3b) intermittently from scratch and without battery (figure 3c), which definitely validates the suitability of bimetal-based thermal energy harvesters for WSN.

Related publications:
[1] S. Boisseau et al., "Semi-flexible bimetal-based thermal energy harvesters", Smart Materials and Structures, 22, 025021, 2013.
[2] A. Arnaud et al., "Piezoelectric and electrostatic bimetal-based thermal energy harvesters", 13th Int. Conf. on Micro and Nanotechnology for Power Generation and Energy Conversion Applications (POWERMEMS), Dec. 3-6, 2013, London, UK.
[3] S. Boisseau et al.," Self-starting power management circuits for piezoelectric and electret-based electrostatic mechanical energy harvesters ", 13th Int. Conf. on Micro and Nanotechnology for Power Generation and Energy Conversion Applications (POWERMEMS), Dec. 3-6, 2013, London, UK.

Detection and localization of electric arcs in large batteries

Research topics : battery monitoring systems, acoustics

V. Cattin, P. Perichon, J. Dahmani, B. Schwartzmann, V. Heiries

ABSTRACT: A system for early detection and localization of electric arcs in an electric vehicle battery has been developed. The detection principle is based on the arc acoustic emission. The identification of the electric arc acoustic signature as well as disturbances in the environment has first been realized. We have then been focused on the propagation of acoustic waves emitted by the arc in the battery confined environment. We proposed a detection method based on correlation whose performance was evaluated. Finally, a localization system based on signal time-difference-of-arrival estimation and triangulation is described and assessed.

The battery of an electric vehicle (EV) is made of several modules consisting of several battery cells arranged in series and in parallel. This type of arrangement leads to a high number of internal connections which may be damaged or broken. A break at the connection may cause electric arcs that can be maintained because of DC current flowing into the battery. These arcs can cause overheating and even thermal runaway in the battery. Thereby, the aim of our study is to detect these arcs from their beginning and prevent possible accident. Because of the many disturbing transient signals present on the voltage and the current measurements made on the battery, we propose an innovative method based on the acoustic emission of electric arcs. The specificity of the acoustic arc signal is characterized by a transient signature with a decreasing envelope. Therefore, the sensors used for the detection must be microphones having an excellent coupling with the air and a large flat bandwidth.

The studied detection method consists in measuring the similarity between the signal received by the sensor and a model of the arc. So, the first step is to model the arc signal: we used an Auto-Regressive Moving Average (ARMA) model which describes well amortized oscillating signals. We then detect the presence of the arc by correlating the time signal measured by the sensors with this model.

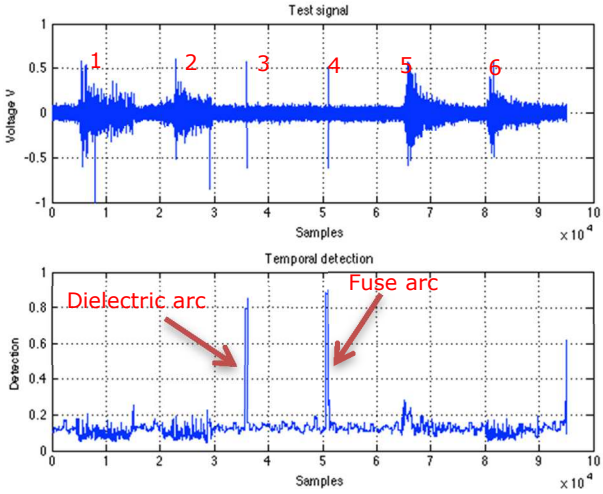

Figure 1: Test signal (above) and normalized time detection curve (below) for the detection by correlation.

Detection is then performed by applying a threshold on the correlation results obtained. This threshold is selected in order to obtain the desired probabilities of good detection and false alarm. We plot on figure 1 an example of a simulated signal including two arcs and other disturbances measured on the EV. We apply the above detection method on this signal and the detection curve is computed.

Further on, in order to increase the efficiency during maintenance and fixing of the battery after the electric arc outbreak detection, it could be highly valuable to get the arc localization information.

In this perspective, a localization method based on a typical triangulation process has been studied [1]. We have focused our work on a two-dimension plan localization problem. Three acoustic sensors with known exact positions are arranged at the edge of the area of interest. The acoustic signal emitted by the arc is received by the three sensors, and the position of the electric arc is computed by a typical Time Difference Of Arrival (TDOA) approach.

A study on the impact of the sensors configuration on the position estimation accuracy has been carried out.

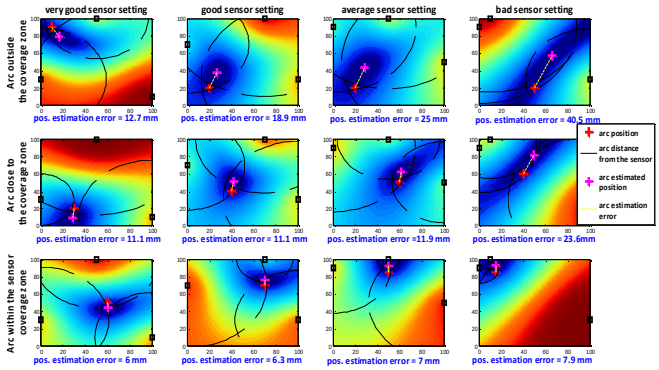

Figure 2: Arc acoustic signal in the three sensors' configuration.

The result in terms of arc localization accuracy is showed on Figure 2. The colored curves pictured on this figure represent the cost function to be minimized in the TDOA localization inversion problem.

It can be noticed that the localization accuracy decreases as the arc is moved away from the sensors coverage area, and that the localization performance is strongly impacted by the sensors configuration. More particularly, when a bad sensors setting is considered, the cost function to be minimized in the TDOA localization inversion problem exhibits a much larger minimum zone (blue zone) leading to high biases in the estimation results.

Related publications:
[1] V. Cattin, P. Perichon, J. Dahmani, B. Schwartzmann, V. Heiries, "Detection of Electric Arcs in Large Batteries", IEEE Electric Vehicle Symposium 27, November 17-20, 2013, Barcelona, Spain.

Broadband identification of the electrical impedance for the improvement of on-board battery diagnostic

Research topics : battery monitoring systems, impedance tracking

R. Al Nazer, V. Cattin, M. Montaru (CEA-LITEN), M. Ranieri (CEA-LITEN), P. Granjon (GIPSA-Lab)

ABSTRACT: Electrical impedance measurements provide useful informations about the characteristics of a Li-ion battery. In order to address embedded applications, broadband excitation signals are proposed for impedance measurements. To evaluate the performance of this method, a set of experiments is compared with electrochemical impedance spectroscopy (EIS) results on a well-known reference impedance and on a Li-ion battery. Interest for the improvement of on-board aging estimation is studied.

Non-parametric identification estimates the frequency response function $H(\lambda)$ of a linear and time invariant (LTI) system from input x[n] and noisy output measurements z[n] without the use of any model. The unknown additive measurement noise is supposed uncorrelated with the input and therefore with the output. Under this last assumption and using the input auto-spectral and input-output cross-spectral power densities ($\hat{S}_{xx}$ and $\hat{S}_{zx}$), we can write:

$$\hat{H}(\lambda)=\frac{\hat{S}_{zx}(\lambda)}{\hat{S}_{xx}(\lambda)} \quad \text{if} \quad \hat{S}_{xx}(\lambda)\neq 0 \qquad \text{(Eq 1)}$$

An electronic board (Fig. 1) has been developed to generate squared patterns on a battery cell inside the battery management system (BMS).

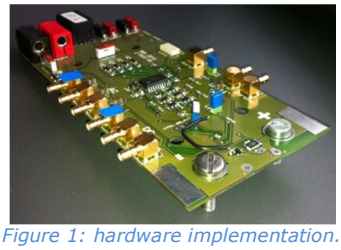

Figure 1: hardware implementation.

A Pseudo Random Binary Sequence (PRBS) (Fig. 2) is used as an excitation signal and compared to classical electrochemical impedance spectroscopy (EIS).

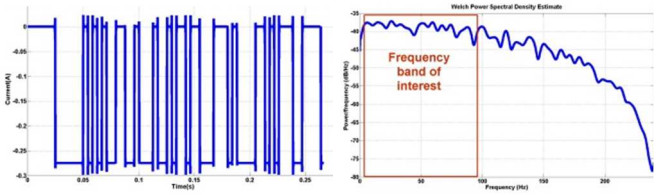

Figure 2: PRBS time signal (left) and its spectrum (right).

A simple R-C circuit is used as a reference. The selected frequency band of interest leads to the identification of a part of its Nyquist diagram (Fig. 3). The theoretical impedance is considered to be the analytical impedance expression. The classical EIS estimation gives high accuracy results. Broadband identification provides a bias result due to differences in connection, with low variability which is interesting for impedance tracking in BMS.

The PRBS is used as the input current for experimental validation on a Li-ion battery (Fig. 4). As the corresponding estimated coherence is close to 1 all over the specified frequency band, the battery can be considered as a LTI system under these operating conditions and its electrical impedance will be correctly estimated. The variability of the estimated impedance on different realizations is very small all over the frequency band.

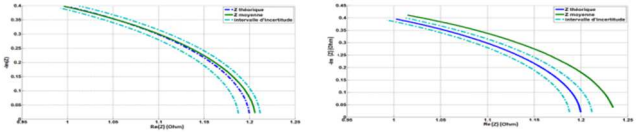

Figure 3: EIS (left) and PRBS (right) results on a well-known reference impedance.

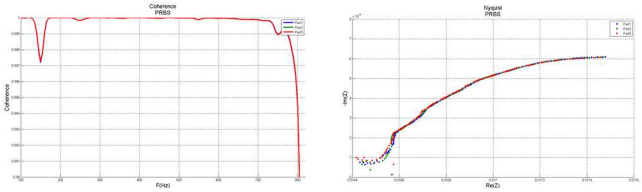

Figure 4: Estimated coherence (left) and Nyquist diagram (right).

Experimental identification results with PRBS in the frequency band of 13Hz-320Hz show a low variability. Using a simulator of the studied battery, we quantify the effect of a variation of the state of health (SOH) on the battery impedance value (with a simplified resistive model). The dispersion of experimental results is lower than this effect. It yields that the proposed method provides useful information for the SOH tracking even for new batteries (SOH=100%) and low SOH variation (1%).

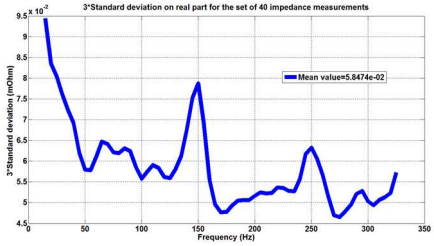

Figure 5: Standard deviation of PRBS results over the frequency band.

The broadband identification method is suitable to provide the tracking of the SOH with a high accuracy for HEVs and EVs application. A recursive version of the identification process has been developed for future implementation in the BMS.

Related publications:
[1] R. Al Nazer, V. Cattin, P. Granjon, M. Montaru, M. Ranieri, " Broadband identification of the battery electrical impedance for HEVs", IEEE Transactions on Vehicular Technology, vol. 62, no. 7, pp. 2896-2905, Sept. 2013.
[2] R. Al Nazer, P. Granjon, V. Cattin, M. Montaru, M. Ranieri, " Classical EIS vs Broadband Identification Comparison based on a well-known reference impedance ", IEEE Electric Vehicle Symposium 27, November 17-20, 2013,Barcelona, Spain.

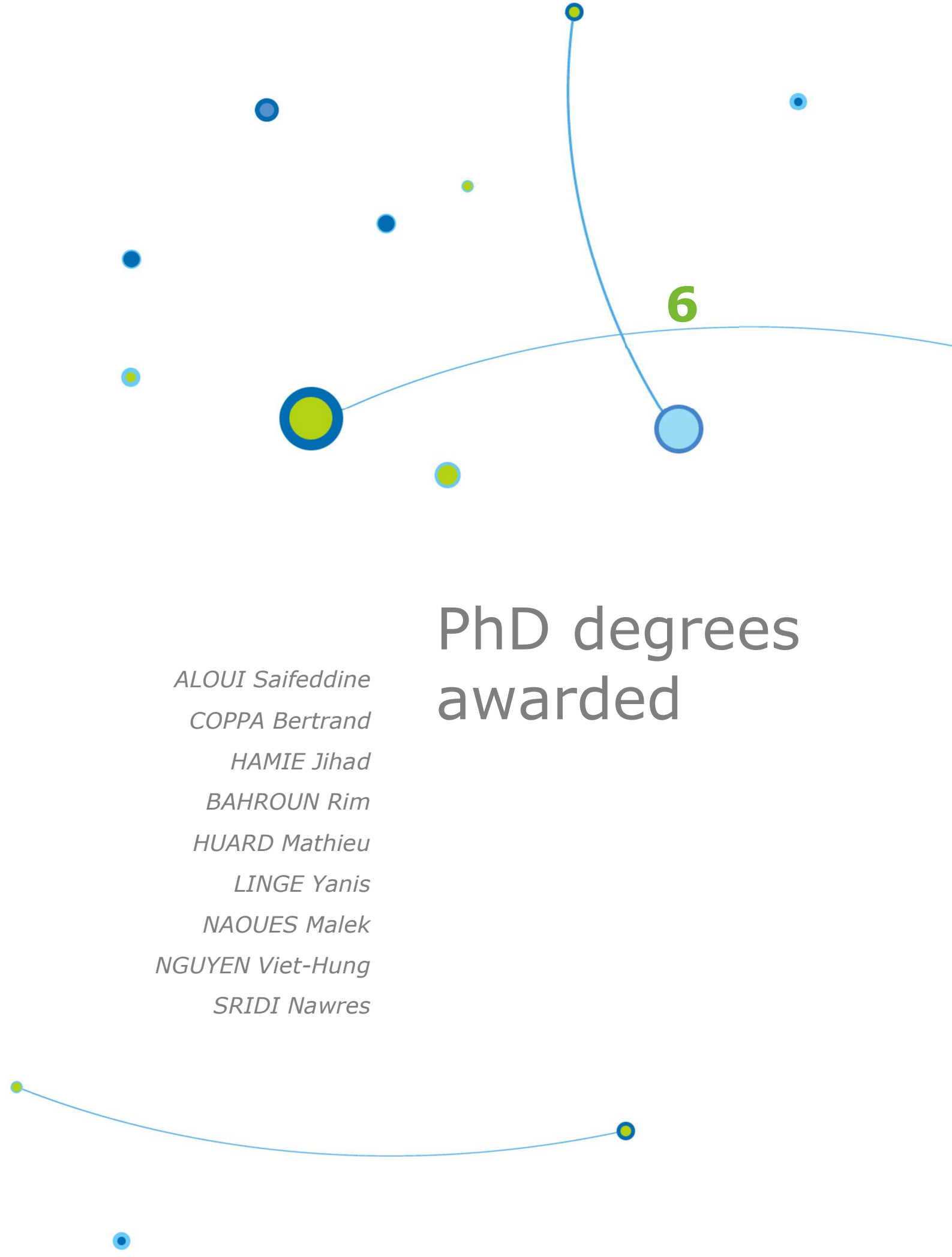

PhD degrees awarded

ALOUI Saifeddine

COPPA Bertrand

HAMIE Jihad

BAHROUN Rim

HUARD Mathieu

LINGE Yanis

NAOUES Malek

NGUYEN Viet-Hung

SRIDI Nawres

PhD degrees awarded in 2013

Aloui Saifeddine
University of Grenoble

Motion capture by distance measurements in a heterogeneous body network

Ambulatory motion capture is of great interest for applications such as monitoring elderly people, sport performances monitoring, functional rehabilitation, etc. These applications require the movement not to be constrained by an external system and to be performed in different environments, including outdoor; they require also lightweight and low cost equipments, and truly ambulatory operation without complex process of calibration.
Current systems based on exoskeleton can not be used in such applications as elderly monitoring due to the weight and the constrained movements. Other systems based on inertial sensors, often combined with magnetic field sensors, are lighter but suffer from drifts and need periodic calibration.
The objective of this thesis is to develop a motion capture system for an articulated chain to be used in many application fields (rehabilitation, sport, leisure, etc.); this system shall be low-cost, real-time, and truly ambulatory without specific infrastructure. We focus on intra-corporal measurements. Thus, all sensors are placed on the body and no external device is used. In addition to a final demonstrator to validate the proposed approach, we also developed tools to evaluate the system in terms of technology, number and position of sensors, but also to evaluate different algorithms for data fusion. To do this, we used the Cramer-Rao lower bound.
The subject is multidisciplinary. It addressed aspects of modeling and design of fully ambulatory hybrid systems. It studied estimation algorithms adapted to the field of motion capture of a whole body by considering the problem of observability of the state and taking into account the biomechanical constraints. Thus, with an appropriate processing, the pose of a subject can be reconstructed in real time from intra-body measurements.

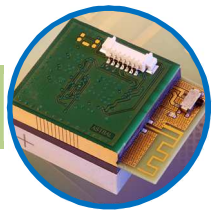

Coppa Bertrand
University of Grenoble

Implementing some applications of sparse coding

Sparse coding allows retrieving a signal from some linear projections of it, provided that the signal can be analyzed in a sparse manner, which means using only a few coefficients and a known dictionary. Coding is simple, while complexity is devoted to reconstruction.
Sparse coding is studied and explained in detail, followed by some theoretical results and simulations, in order to understand which performances can be expected from the approach. Then, we address three main problems.
First, a system allowing signal coding from a binary matrix is investigated and designed. We analyze the advantages of that approach. The second question concern the determination of the dictionary used to sparsely describe the signal, using learning methods. Finally, we discuss the feasibility of the classification of different signals of a family directly from the sparse coding, avoiding the need to reconstruct the signal by itself.

PhD degrees awarded in 2013

Hamie Jihad
University of Nice-Sophia Antipolis

Contributions to cooperative localization techniques within mobile wireless body area networks

Wireless Body Area Networks (WBAN) cover a large number of needs in various application fields (healthcare, security, sports or entertainment…). Such networks are now also considered for radiolocation functionalities. Under mesh or quasi-mesh topologies, mobile on-body nodes can indeed be located within a cooperative fashion, considering peer-to-peer range measurements based on e.g., Impulse Radio - Ultra Wideband (IR-UWB) Time of Arrival (TOA) estimates or narrow-band Received Signal Strength Indicators (RSSI) at 2.4 GHz. This radiolocation add-on represents an enabling feature for coarse but large-scale Motion Capture (MoCap) (e.g. as an alternative to video acquisition systems) and/or for robust group navigation applications in GPS-denied environments.
This PhD work explored new cooperative localization mechanisms, which could benefit jointly from on-body links at the body scale, body-to-body links between mobile equipped users, or off-body links with respect to the infrastructure. First, single-link ranging error models were proposed based on real WBAN channel measurements. Then, constrained decentralized positioning algorithms were put forward for relative MoCap purposes at the body scale, coping with on-body nodes' asynchronism to reduce system latency and exploiting the presence of constant-length radio links for better accuracy. Scheduling and censoring rules were also shown to limit the harmful influence of peripheral nodes. These algorithms were subsequently extended for absolute MoCap applications at the building scale, incorporating off-body links in a heterogeneous wireless framework. Then, both individual and collective kinds of navigation were addressed, comparing different location estimation and cooperative strategies. For the two MoCap and navigation scenarios of interest, low-complexity solutions exploiting deployment diversity were proved to combat error propagation and strong range biases due to body shadowing. The latter solutions rely on on-body nodes' spatial dispersion or neighbourhood graph to approximate the corrupted range measurements. Finally, experiments based on real IR-UWB radio platforms validated in part the previous proposals, while highlighting practical limitations.

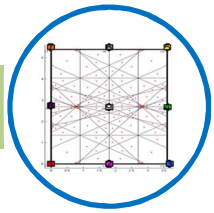

Bahroun Rim
University of Grenoble; University of Tunis El Manar

Indoor footstep localization using seismic waves

For many applications, it is important to obtain location information about a resident in an indoor environment. The vibration signature of the human footstep on a floor creates an elastic wave induced by the walking motions. Our goal in this study is to localize footsteps using seismic sensors that are fixed on the floor in the indoor environment. Firstly, we studied the existing techniques of seismic source localization. The complexity of the elastic wave's propagation in a building led to exclude these techniques. Then, we established a theoretical and experimental study of seismic wave propagation in a concrete slab. It appears that the only reliable information in such an environment is the conservation of the order of arrival of signals to the sensors. So, we deduced an algorithm of footstep localization based on the signs of time differences of signals arrival. This approach has been the subject of many numerical and experimental validations. In the end, an extension of this approach was developed to allow dynamic localization of a person with an accuracy of the order of some tens of centimeters.

PhD degrees awarded in 2013

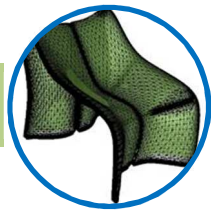

Huard Mathieu
University of Grenoble

Geometric modeling and reconstruction of surfaces equipped with inertial sensors

Embedded systems equipped with micro-sensors (magnetometers, accelerometers...) from which it is possible to retrieve informations about their spatial orientation allow for innovative applications in the field of shape acquisition and reconstruction. The problem of reconstructing surfaces from unstructured orientation data is ill-posed. However, previous works done in CEA-Leti came up with a valid reconstruction protocol. The Morphosense ribbon, a flexible ribbon instrumented with micro-sensors, is at the core of a number of curve reconstruction algorithms. When laid on a physical surface, Morphosense ribbons allow the acquisition and reconstruction of a network of curves on the surface used for the reconstruction of the entire surface.
We first propose new algorithms for curve reconstruction, which integrate the orientation informations provided by the sensors, as well as the mechanical properties of the ribbon forcing it to follow geodesic curves. From this point of view, the curve reconstruction can be considered optimal. We then study a set of methods for the reconstruction of surfaces using a network of ribbon curves. Such a network generally leads to problems linked to the closure of the network and estimation of missing data on the surface outside the network of curves.
In order to propose practical solutions for the reconstruction, hypotheses either on the surface models or the topology of the network of curves are required. The set of methods developed in this work allow formulating a global process for the reconstruction of surfaces, with flexible algorithms adapting to the different practical situations, so as to propose a solution both simple and accurate in each case. The validation of our results in the case of real sensors data provided by the Morphosense ribbons also led us to develop a metrological device. Finally, the general context of reconstruction from orientation data studied here raises original theoretical problems, to which we tried to answer with innovative solutions through interpolation and optimization algorithms.

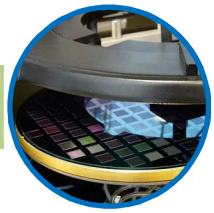

Linge Yanis
University of Grenoble

Cryptographic and statistical side-channel analysis

The main subject of this manuscript is the side channel attacks. These attacks investigate the variation of device emanations to retrieve a secret key. These emanations can be the power consumption, the electromagnetic radiation, etc. Most of the time, those attacks use statistical methods to examine the relationship between the emanations and some leakage models supposed by the attacker. Three main axes are developed here.
First, we have implemented many side channel attacks on GPGPU using the API OpenCL. These implementations are more effective than the classical ones, so an attacker can exploit more data.
Then, in order to provide a new side channel attack, we have suggested the use of a new dependency measurement proposed by Reshef et al., the MIC. The MIC is more advantageous than the mutual information, because its computation does not depend of a kernel choice nor a windows size. So, its use in side channel analysis is simple, even if the time complexity is large.
Finally, we have introduced a new attack based on the joint distribution of the input and the output of a cryptographic sub-function. If the distribution depends on the key used in the function, we can retrieve the secret key. This attack can be efficient even in presence of some countermeasures because it does not require the knowledge of either plain text or cipher text.

PhD degrees awarded in 2013

Naoues Malek
University of Carthage-Sup'Com; Supélec-Rennes

Common operator management in multi-standard terminals architectures

In today's telecommunication systems, communication standards are typically implemented separately using dedicated instantiations which are difficult to upgrade. To overcome these issues, Software Defined Radio (SDR) describes a software-reconfigurable multi-standard and multiband radio, capable of supporting multiple transmission standards in a single platform. A multi-standard digital communication chain uses typical signal processing operations (modulation, channel coding, equalization, etc.) which can be identified and explored to take advantage of their commonalities in order to enhance power efficiency and area occupation.
In this work, a parameterization approach, the common operator (CO) technique, is considered to build a generic terminal supporting a large range of communication standards. Its main principle is to identify common elements based on smaller structures widely used across signal processing functions. It aims at being less standard dependent and therefore more flexible and scalable for a wide range of standards. It is also well adapted to cope with silicon technology process variability.
The present work deals with two widely used algorithms in wireless communication systems, Viterbi decoding and Fast Fourier Transform (FFT), which require a significant computational complexity. Implementing them in a multi-standard context through a common architecture poses significant architectural constraints since it should allow variable FFT size and variable Viterbi constraint length.
In this thesis, we focus on the design of a flexible processor to manage the CO and take advantage from structural similarities between FFT and Viterbi trellis. A flexible FFT/Viterbi processor was proposed and implemented on FPGA and compared to dedicated hardware implementations. The results show a considerable gain in flexibility, obtained with no complexity overhead since the complexity is even decreased by more than 30% in some configurations.

Nguyen Viet Hung
University of Rennes I

Miniaturized and reconfigurable antennas using dielectric and ferroelectric oxydes and oxynitrides thin films

Given the requirements for a large number of new services in latest generation of hand held devices and in order to meet their dimensional constraints, new concepts of smart antennas are considered in many research works. Among several solutions mentioned in the literature, the technique of loading the antenna with tunable material is particularly interesting because it combines the effects of miniaturization and tunability.
The studies in this thesis focus on the integration of La-Ti-O-N and BST thin films in antenna design for miniaturization and frequency agility. A study of dielectric properties (permittivity, loss tangent and tunability) of La-Ti-ON thin films was realized. These properties are found to be dependent on the structural characteristics of the thin films, which derived from the nature of the substrate and the deposition conditions. In the meantime, another study for the integration of these materials in radiating structures to achieve agility in frequency was carried out. Demonstrations of miniaturized and reconfigurable antennas based on La-Ti- ON and BST thin films were fabricated and characterized.

PhD degrees awarded in 2013

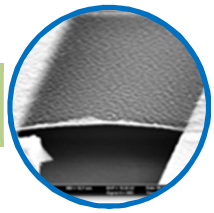

Sridi Nawres
University of Grenoble

Ultrathin membranes implementation for ultrasonic transducers integration

This thesis addresses the miniaturization of micromachined ultrasonic transducers (cMUTs). This type of device has been used for decades in the field of ultrasound imaging for the non-destructive testing of structures for example. The quest of a highly resolved imaging requires the use of cMUTs with a resonance frequency in the order of GHz and with a micrometer size. The main part of these cMUts is a suspended membrane with a micrometric surface. An analytical study, based on the mechanical behavior of thin plates, is used for the design of the suspended membranes. This study emphasizes the importance of having a nanometric thickness to obtain a detectable electrical signal. Several materials, namely carbon nanotubes, graphene, graphene oxide, DLC (diamond like carbon) and silicon have been implemented in this study to make micron-size suspended membranes with a nanometric thickness. Technological processes specific to each of these materials have been designed. Suspended membranes with thicknesses ranging from 2 to 15 nm and widths ranging from 1 to 2 microns were made.
A novel characterization method has been established to evaluate the mechanical properties of our membranes. A measurement protocol has been developed to measure the displacement of the suspended membrane under an electrostatic field. Amplitudes reaching ten nanometers were measured. More generally, this study provides a solid proof of the feasibility of suspended micrometer-sized membranes with an electrically detectable signal.

Greetings

Editorial committee
Laurent Dussopt
François Vacherand
Dominique Noguet
Sébastien Dauvé

Coordination LETI
Hélène Vatouyas

Photos
© CEA-LETI /G. Cottet

Contacts

Roland Blanpain
Head of Systems & Solutions Integration Division
roland.blanpain@cea.fr

François Vacherand
Deputy manager Systems & Solutions Integration Division
francois.vacherand@cea.fr

Céline Soubeyrat
Program Manager
céline.soubeyrat@cea.fr

Jean-Michel Léger
Program Manager
jean-michel.leger@cea.fr

Dominique Noguet
Head of Telecoms and security Lab.
dominique.noguet@cea.fr

Sébastien Dauve
Head of Sensors and Systems Lab.
sebastien.dauve@cea.fr

Tiana Delhome
Head of Innovation Lab.
tiana.delhome@cea.fr

CEA - Leti - DSIS
CEA Grenoble
17, rue des Martyrs
F-38054 GRENOBLE Cedex 9
Tel. (+33) 4 38 78 48 20
www.leti.fr